1960-08-01

Effect and shape and depth on wave forced oscillations of submerged moored objects.

Verrett, Eugene Gerald

Massachusetts Institute of Technology

EFFECT OF SHAPE AND DEPTH ON WAVE FORCED OSCILLATIONS OF SUBMERGED MOORED OBJECTS

EUGENE G. VERRETT

M 21

EFFECT OF SHAPE AND DEPTH ON WAVE FORCED OSCILLATIONS OF SUBMERGED MOORED OBJECTS

BY

EUGENE GERALD VERRETT

SUBMITTED IN PARTIAL FULFILLMENT OF THE REQUIREMENTS FOR THE DEGREE OF NAVAL ENGINEER AND THE DEGREE OF MASTER OF SCIENCE IN NAVAL ARCHITECTURE AND MARINE ENGINEERING

at the

MASSACHUSETTS INSTITUTE OF TECHNOLOGY
August 1960

PROFESSOR DONALD R. F. HARLEMAN

THESIS SUPERVISOR

EFFECT OF SHAPE AND DEPTH ON WAVE FORCED OSCILLATIONS OF SUBMERGED MOORED OBJECTS

by

EUGENE GERALD VERRETT
B.S. U.S. COAST GUARD ACADEMY
1952

SUBMITTED IN PARTIAL FULFILLMENT OF THE

REQUIREMENTS FOR THE DEGREE OF NAVAL

ENGINEER AND THE DEGREE OF MASTER OF

SCIENCE IN NAVAL ARCHITECTURE AND MARINE

ENGINEERING

at the

MASSACHUSETTS INSTITUTE OF TECHNOLOGY

August 1960

ABSTRACT

EFFECT OF SHAPE AND DEPTH ON WAVE FORCED OSCILLATIONS
OF SUBMERGED MOORED OBJECTS

by

EUGENE GERALD VERRETT

Submitted to the Department of Naval Architecture and Marine Engineering on August 31, 1960 in partial fulfillment of the requirements for the Master of Science degree in Naval Architecture and Marine Engineering

It has been established by W. C. Shapiro (Sc D Thesis M.I.T. Cambridge, Mass., August 1958) that buoyant moored objects subjected to wave forces will obey the equation of motion for forced vibrations with square law damping. This equation may be expressed as:

$$M\ddot{x} + C_2 \dot{x}^2 + Kx = Pom \cos \omega t$$

An approximate solution for this non-linear equation has been presented by Jacobsen and it is this solution which was the basis for predicting hydrodynamic forces on the test model used in this study. The model is best described as a streamlined body of revolution, ellipsoidally shaped but not possessing fore and aft symmetry.

Experimental results obtained in the 90 ft wave tank of the M.I.T. Hydrodynamics Laboratory confirmed that the approximate solution to the non-linear equation did adequately describe the behavior of the object under the influence of wave forces.

As a result of the investigation it was possible to compare the hydrodynamic response of the test model to that of a spherical shape which was the model for Shapiro's analysis of the problem.

The comparison revealed that for such shapes of equal volume in similar wave and mooring conditions, the streamlined body would experience on the order of 23% smaller hydrodynamic force than the sphere.

This can be attributed, in large measure, to the greater drag resistance of the streamlined shape as the mooring radius of oscillation is reduced. The

radius of oscillation is defined as the distance from the center of gravity of the body to the common point at which the mooring lines are fixed to the bottom. In forced oscillatory motion it is the drag, or resistance, which provides damping in the system. While the streamlined body has less steady state drag resistance than the sphere, in oscillatory moored motion the situation is reversed. Early fluid separation and consequent energy loss in the case of the oscillating streamlined body is believed to be the primary reason for this increase in drag.

A second objective of the study was to determine the result of varying centerline depth of the body and to determine if an optimum depth for shallow water mooring could be established. No optimum depth was found, but there was a depth of centerline submergence at which maximum force magnification occurred. This depth should be avoided. It was found that the deepest possible depth would be most desirable although a necessary limitation would be to require that the object be moored high enough so that it did not strike bottom during the most violent oscillatory motion anticipated.

The experimental procedure was to subject the model to wave forced oscillations at centerline depths of 1.40, 3.45 and 6.49 diameters varying model weight through successive increments at each depth in order to produce variable natural frequencies.

The most interesting aspect of this study proved to be the variation in the coefficient of drag for the oscillating submerged body as the radius of oscillation was changed. The results indicated that an accurate determination of drag for this condition is essential to insure sound predictions for its behavior in wave forced oscillation. Further study is suggested to improve the method of evaluating the coefficient of drag as a function of the radius of oscillation of a submerged body.

Thesis Supervisor: Dr. Donald R. F. Harleman

Title: Associate Professor of Hydraulics

TABLE OF CONTENTS

LIST OF FIGURES

LIST OF FIGURES

LIST OF TABLES

ACKNOWLEDGEMENT

The author wishes to express his gratitude to Dr. Donald R. F. Harleman, Associate Professor of Hydraulics and Dr. Robert G. Dean, Assistant Professor of Hydraulic Engineering of the Civil Engineering Department, who gave their time and perceptive advice generously whenever needed.

The author also wishes to thank his associates and friends, Lieutenant Charles D. Roushorn, RCN, who assisted in a portion of the experimental work and who offered advice and encouragement throughout the preparation of the report, and to Lieutenant William C. Sargent, RCN, who prepared a number of the illustrations for the work.

LIST OF SYMBOLS

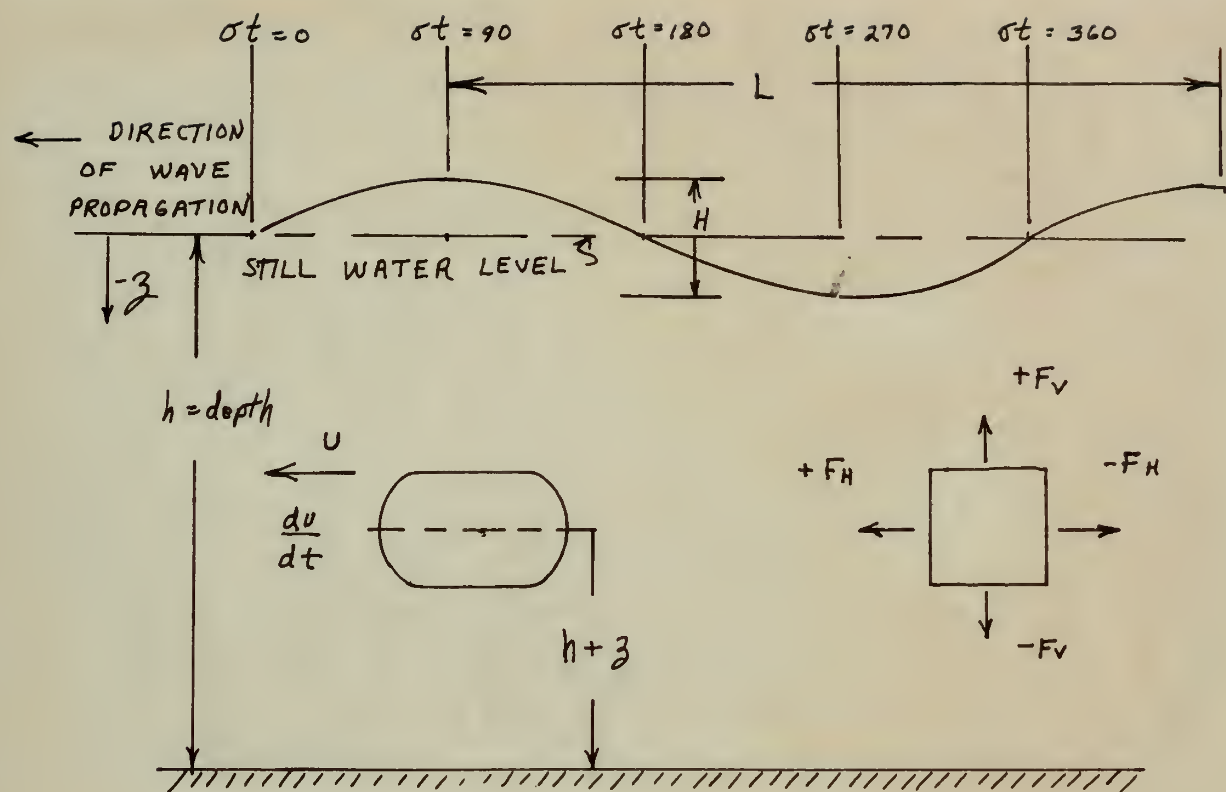

FIGURE I. DEFINITION SKETCH

A = Parameter defined by equation (25)

a_r = radial acceleration, ft/sec^2

B = parameter defined by equation (26)

C = parameter defined by equation (33)

C_D = drag coefficient

C_M = inertia coefficient

c = damping coefficient

C_c = critical damping coefficient

C_2 = square law damping coefficient

D = diameter, ft.

$-_D$ = subscript "D" referring to drag component

F = force lbs.

F_c = centrifugal force, lbs.

F_{v_s} = slacking force, lbs.

f = wave frequency or forcing frequency, cps

f_n = natural frequency, cps

f_d = damped natural frequency, cps

g = acceleration of gravity, 32.2 ft/sec^2

H = wave height, ft.

$-_H$ = subscript "H" referring to horizontal component

h = total depth of water

I = moment of inertia, slug ft^2

I_{oo} = moment of inertia about object center of gravity, slugs ft^2

I' = virtual mass moment of inertia, slug ft.^{2}

$-_I$ = subscript "I" referring to inertia component

K = added mass coefficient

k = spring constant, lbs/ft.

L = wave length, ft.

ℓ = moored radius of oscillation

M = mass of displaced fluid, slugs

M_s = slacking Moment, ft. lbs.

m = mass of test object, slugs

$---_m$ = subscript "m" referring to maximum value

N = net buoyancy, lbs.

N_R = Reynolds number

n_2, N_2 = square law damping factor

$---_o$ = subscript "o" referring to rigidly restrained conditions

P = driving force, lbs.

p = pressure, lbs/ft^2

q = damped natural frequency, radians /sec

T = wave period, sec

t = time, sec

u = horizontal component of particle velocity, ft/sec

Vol = volume, ft^3

$-_v$ = subscript "V" referring to vertical component

v = vertical component of particle velocity, ft/sec

x = coordinate parallel to direction of wave propagation positive in direction of wave propagation, ft.

3, z = coordinate perpendicular to direction of wave propagation negative in direction downward from water free surface, ft.

δ (delta) = logarithmic decrement, damped free vibrations

ν (nu) = kinematic viscosity, ft^2/sec

π (pi) = 3.141....

ρ (rho) = density, slugs $/ft^3$

σ (sigma) = wave angular frequency, radians /sec

$\mathcal{T}$ (Tau) = torque, ft lbs.

ϕ (phi) = phase shift angle, degrees

ψ (psi) = mooring line angle, degrees

ω (omega) = radian frequency = $2\pi f$, radians/sec

I. INTRODUCTION

1. Purpose of Study

This study was undertaken to determine the effect of shape and center-line depth on the dynamics of a moored submerged object in water waves, a problem which falls into the general class of forced vibrations dynamics.

A single moored buoyant object of streamlined shape not possessing force and aft symmetry was considered in this investigation. The object will hereinafter be referred to as an ellipsoidal shape. The mooring configuration consisted of two essentially inelastic lines attached at either end of the body which uniquely prescribed the path of motion in a plane parallel to the direction of wave propogation.

The motion of the object is due to a periodic wave force which is opposed by the inertia force of the object, the combination of buoyancy and mooring system force, which acts as a spring (restoring force), and by viscous effects of the fluid.

As in all vibration problems the most important dynamic parameter is the ratio of forcing frequency to the natural frequency. The natural frequency of the body when displaced from the equilibrium position in still water, and then released, is a function of various characteristics of the object and its mooring system. When the ratio of forcing frequency to natural frequency is near unity the system is said to be in resonance. In the problem under consideration it was found that the mooring forces and object motions depended to a large extent on the ratio of the wave frequency to the natural frequency of the moored object.

I. INTRODUCTION

1. Purpose of Study

This study was undertaken to determine the effect of shape and center-line depth on the dynamics of a moored submerged object in water waves, a problem which falls into the general class of forced vibrations dynamics.

A single moored buoyant object of streamlined shape not possessing fore and aft symmetry was considered in this investigation. The object will hereinafter be referred to as an ellipsoidal shape. The mooring configuration consisted of two essentially inelastic lines attached at either end of the body which uniquely prescribed the path of motion in a plane parallel to the direction of wave propagation.

The motion of the object is due to a periodic wave force which is opposed by the inertia force of the object, the combination of buoyancy and mooring system force, which acts as a spring (restoring force), and by viscous effects of the fluid.

As in all vibration problems the most important dynamic parameter is the ratio of forcing frequency to the natural frequency. The natural frequency of the body when displaced from the equilibrium position in still water, and then released, is a function of various characteristics of the object and its mooring system. When the ratio of forcing frequency to natural frequency is near unity the system is said to be in resonance. In the problem under consideration it was found that the mooring forces and object motions depended to a large extent on the ratio of the wave frequency to the natural frequency of the moored object.

This investigation was carried forth as an extension of a previous study conducted at the Hydrodynamics Laboratory of M.I.T. [1] in which a precise analysis of a spherical shape was presented. As a result of the present study it is possible to compare the hydrodynamic effects of wave forces on a spherical and ellipsoidal shape with equivalent volumes.

An additional parameter introduced in the problem has been the variation of centerline depth of the ellipsoidal shape. This was accomplished by changing the length of the mooring lines. The length of the mooring line plays an important role in determining the damping coefficient of the system. In addition the rigidly restrained force on the body is a function of centerline depth.

This facet of the study was of interest in order to establish an optimum depth, with respect to hydrodynamic forces, at which to locate the body.

2. Method of Investigation

One objective of the experimental program was to determine the effect on mooring line forces and object motions due to variations in the ratio of the wave frequency to the natural frequency of the object and thus to obtain results which could be compared with corresponding quantities found previously for a spherical shape. A single wave of desired characteristics was employed and variation of the frequency ratio was realized by changing the weight of the object. Submergence of the object was changed by varying the length of the mooring lines in order to accomplish the second objective of the program, determination of the effect of centerline depth on force magnification.

In order to obtain a measure of the mooring line force magnification with respect to the rigidly restrained force on the object in the same wave field, the object was held stationary and the horizontal and vertical wave form components were measured by electrical transducers recorded on a Sanborn oscillograph.

3. Scope of Study

The significant dimensions of the test program are shown in Figure 2 and Table I.

TABLE I TEST CONDITIONS

Wave and Submergence Characteristics

Runs	Height Ft.	Length Ft.	Period Sec.	Freq Cps	Centerline Depth	Wave Freq / Nat Freq
1-12	0.289	14.45	2.00	0.500	0.291 ft	0.833-2.78
13.23	0.289	14.45	2.00	0.500	0.720 ft	0.707-3.00
24.35	0.289	14.45	2.00	0.500	1.352 ft	0.548-1.69

The wave steepness for these tests is $H/L = 0.02$
This wave was selected in order to serve as a basis for comparison with the analysis carried out by Shapiro (1). The small steepness allows the use of the first approximation expressions for the wave kinematics due to Airy which, according to Marlow (2) are valid up to a wave steepness of 0.03.

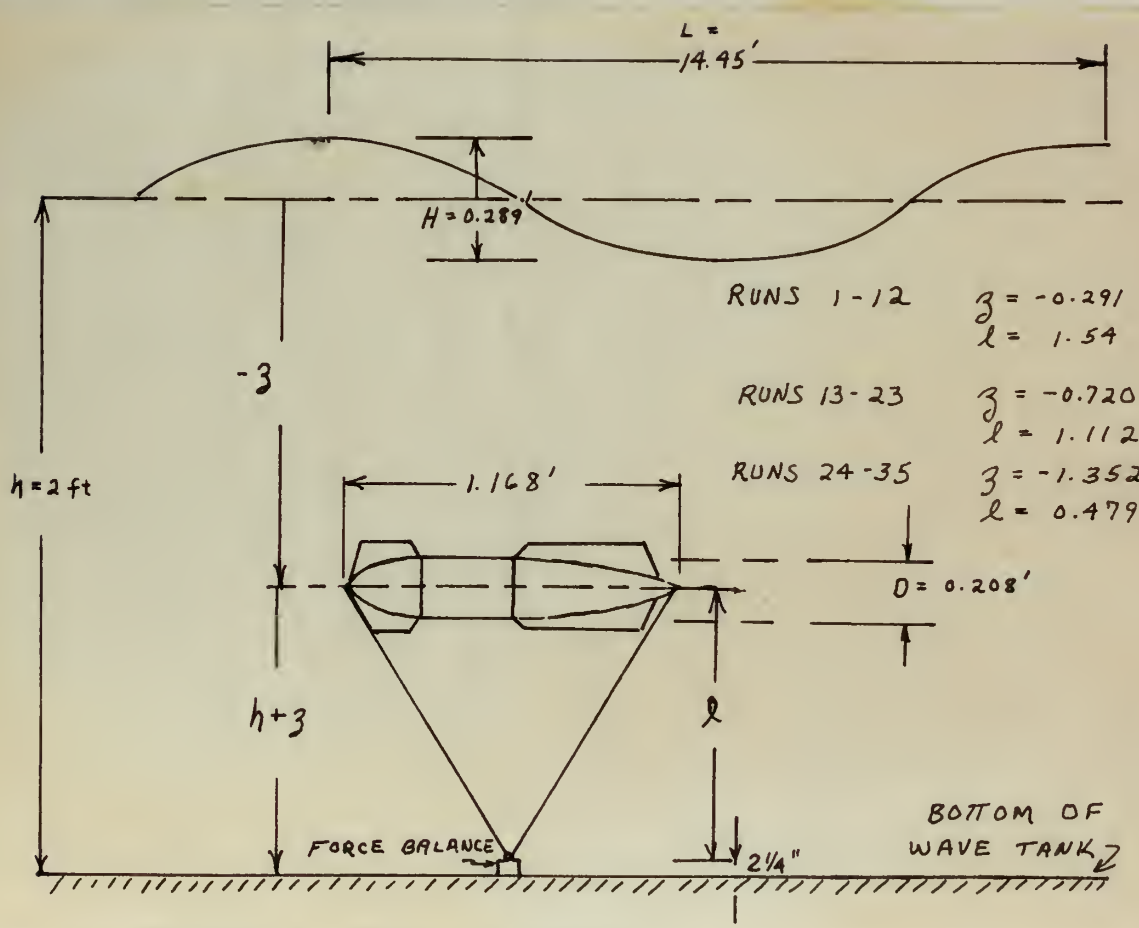

FIGURE 2. TEST CONDITIONS

II THEORETICAL CONSIDERATIONS

1. Introduction

The theoretical development will, to a certain extent, parallel the development given by Shapiro (1). This is due to the fact that the physical systems and forces studied differ only with respect to shape, weight and centerline submergence of the object. The forces involved will be governed by the same fundamental laws of hydromechanics and vibrations.

2. Wave Motion Theory

The hydrodynamic forces on the object are the result of the water particle velocities and accelerations in the wave system, hence it is appropriate to consider the theoretical equations which will define these quantities.

In the experimental procedure a wave of H/L ratio 0.02 was employed which can be successfully treated (2) according to Airy's solution (3) for the small amplitude wave. The resulting equations for velocity and acceleration components, expressed in the notation of Figure 1 are:

$$u = \frac{\pi H}{T} \frac{\cosh \frac{2\pi}{L}(h + z)}{\sinh \frac{2\pi}{L} h} \sin \sigma t = U_m \sin \sigma t \qquad (1)$$

$$v = \frac{\pi H}{T} \frac{\sinh \frac{2\pi}{L}(h + z)}{\sinh \frac{2\pi}{L} h} \cos \sigma t = V_m \cos \sigma t \qquad (2)$$

II THEORETICAL CONSIDERATIONS

1. Introduction

The theoretical development will, to a certain extent, parallel the development given by Shapiro (1). This is due to the fact that the physical systems and forces studied differ only with respect to shape, weight and centerline submergence of the object. The forces involved will be governed by the same fundamental laws of hydromechanics and vibrations.

2. Wave Motion Theory

The hydrodynamic forces on the object are the result of the water particle velocities and accelerations in the wave system, hence it is appropriate to consider the theoretical equations which will define these quantities.

In the experimental procedure a wave of H/L ratio 0.02 was employed which can be successfully treated (2) according to Airy's solution (3) for the small amplitude wave. The resulting equations for velocity and acceleration components, expressed in the notation of Figure 1 are:

$$u = \frac{\pi H}{T} \; \frac{\text{Cosh} \frac{2\pi}{L}(h+z)}{\text{Sinh} \frac{2\pi}{L} h} \sin \sigma t = U_m \text{Sin}\, \sigma t \qquad (1)$$

$$v = \frac{\pi H}{T} \; \frac{\text{Sinh} \frac{2\pi}{L}(h+z)}{\text{Sinh} \frac{2\pi}{L} h} \cos \sigma t = V_m \cos \sigma t \qquad (2)$$

$$\frac{du}{dt} = \frac{2\pi^2 H}{T^2} \frac{\cosh 2\pi/L(h+z)}{\sinh \frac{2\pi h}{L}} \cos\sigma t = \frac{du}{dt_m} \cos\sigma t \tag{3}$$

$$\frac{dv}{dt} = -\frac{2\pi^2 H}{T^2} \frac{\sinh 2\pi/L(h+z)}{\sinh \frac{2\pi h}{L}} \sin\sigma t = -\frac{dv}{dt_m} \sin\sigma t \tag{4}$$

The speed of wave form propagation or celerity is -

$$\text{Celerity} = \frac{L}{T} = \left[\frac{g L}{2\pi} \tanh \frac{2\pi h}{L}\right]^{\frac{1}{2}}$$

3. Wave Forces

The force exerted on a submerged rigidly restrained body is the result of inertial, gravitational and viscous effects. The inertial effect results from unsteady water particle motion described by the above equations. In addition there is a hydrodynamic drag force on the body which is the sum of surface and form drag and is due to the velocity of the fluid.

For the purpose of analysis the total wave force may be separated into inertia and drag components with the sum being the total force, as given by O'Brien and Morison (4).

$$F_T = F_I + F_D \tag{6}$$

In this expression the inertia force can be shown, by potential flow theory, to have the following form -

$$F_I = C_m \rho \text{ Vol } \frac{du}{dt} \tag{7}$$

where the mass term ρ Vol is the displaced volume of water and the coefficient C_m includes the virtual mass effect and gravitational effects due to the pressure gradient occurring in surface waves.

$$\frac{du}{dt} = \frac{2\pi^2 H}{T^2} \frac{\cosh \frac{2\pi}{L}(d + z)}{\sinh \frac{2\pi d}{L}} \cos \sigma t = \frac{du}{dt_m} \cos \sigma t \qquad (3)$$

$$\frac{dv}{dt} = -\frac{2\pi^2 H}{T^2} \frac{\sinh \frac{2\pi}{L}(d + z)}{\sinh \frac{2\pi d}{L}} \sin \sigma t = -\frac{dv}{dt_m} \sin \sigma t \qquad (4)$$

The speed of wave form propagation or celerity is -

$$\text{Celerity} = \frac{L}{T} = \left[\frac{g L}{2\pi} \tanh \frac{2\pi d}{L}\right]^{\frac{1}{2}}$$

2. Wave Forces

The force exerted on a submerged rigidly restrained body is the result of inertial, gravitational and viscous effects. The inertial effect results from unsteady water particle motion described by the above equations. In addition there is a hydrodynamic drag force on the body which is the sum of surface and form drag and is due to the velocity of the fluid.

For the purpose of analysis the total wave force may be separated into inertia and drag components with the sum being the total force, as given by O'Brien and Morison (4).

$$F_T = F_I + F_D \qquad (6)$$

In this expression the inertia force can be shown, by potential flow theory, to have the following form -

$$F_I = C_M \rho \, \text{Vol} \frac{du}{dt} \qquad (7)$$

where the mass term ρ Vol is the displaced volume of water and the coefficient C_M includes the virtual mass effect and gravitational effects due to the pressure gradient occurring in surface waves.

The drag force is given by

$$F_D = C_D \, \rho/2 \text{ Area } |U| \; U \qquad (8)$$

where C_D is a function of shape and Reynolds number and area is the projected area of the body on a plane normal to the velocity.

Equation (6) may be rewritten in terms of the wave particle velocity and acceleration expressions:

$$F_{Total} = C_M \, \rho \text{ Vol } \frac{du}{dt_m} \cos \sigma t \quad C_D \, \rho/2 \text{ Area } U_m^2 \; |\sin \sigma t| \sin \sigma t \qquad (9)$$

where C_m and C_D are assumed constant over a wave cycle.

Equation (9) may be employed to evaluate C_D and C_m using experimental results, but consideration must be given to the relation between object and wave characteristics. This may be expressed as a dimenionless group known as the period parameter, $\frac{U_m T}{D}$.

Keulegan and Carpenter (5) found that C_m and C_D are functions of the period parameter. At values of period parameter less than 15 inertia forces predominate while at high values of $\frac{U_m T}{D}$ drag forces predominate and the steady state value of the drag coefficient will apply.

The period parameters involved in this series of tests are listed in Table II. They indicate that inertia forces may be expected to dominate

The drag force is given by

$$F_D = C_D \rho/2 \text{ Area } |u| \, u \tag{8}$$

where C_D is a function of shape and Reynolds number and area is the projected area of the body on a plane normal to the velocity.

Equation (6) may be rewritten in terms of the wave particle velocity and acceleration expressions:

$$F_{total} = C_M \rho \text{ Vol } \left(\frac{du}{dt}\right)_m \cos \sigma t + C_D \rho/2 \text{ Area } U_m^2 \, |\sin \sigma t| \sin \sigma t \tag{9}$$

where C_M and C_D are assumed constant over a wave cycle.

Equation (9) may be employed to evaluate C_D and C_M using experimental results, but consideration must be given to the relation between object and wave characteristics. This may be expressed as a dimensionless group known as the period parameter, $\frac{U_m T}{D}$.

Keulegan and Carpenter (5) found that C_M and C_D are functions of the period parameter. At values of period parameter less than 15 inertia forces predominate while at high values of $\frac{U_m T}{D}$ drag forces predominate and the steady state value of the drag coefficient will apply.

The period parameters involved in this series of tests are listed in Table II. They indicate that inertia forces may be expected to dominate the total force on the object. It may be expected, therefore, that the inertia coefficient found by equation (9) will be in close agreement with the coefficient given by potential flow theory while the drag coefficient may be expected to differ from the steady state value. For the object shape involved in this study the potential flow theory coefficient of inertia will be of interest. Landweber (6) gives the longitudinal inertia coefficient for a number of streamlined bodies not possessing fore and aft symmetry. By interpolation between two of these having almost identical proportions to the body which is the subject of this report, the longitudinal inertia coefficient is found as

$$K_{(a/b\,=\,5.6)} = 0.053 \qquad (C_M = 1.053)$$

This agrees, within 6%, to the inertia coefficient for an equivalent ellipsoid which is also given by Landweber

$$K \text{ ellipsoid } (a/b = 5.6) = 0.050 \qquad (C_M = 1.050)$$

The steady state drag coefficient for an object of similar shape at the effective Reynolds numbers involved in the test runs (as given in Table III) may be found by extrapolation, from Rouse (7).

$$C_{D_{\text{Airship Hull}}} \quad (\text{Re } 2 \times 10^3 - 4 \times 10^4) \doteq 0.10 - .08$$

This value, however, may be expected to be in sharp disagreement with the value found from equation (9) due to the low value of period parameter. As will be shown, a better approximation for the drag coefficient is available through consideration of the free vibration characteristics of the object.

The method of employing equation (9) is to set $\sigma t \doteq 90^\circ$ and 270°, where $F_{HI} \doteq 0$, in order to evaluate C_D and set $\sigma t = 0^\circ$ and 180°, where $F_{HD} = 0$ in order to evaluate C_m. The separate terms of equation (9) and their component sums F_{HO} and F_{VO} are plotted over a wave cycle in Figure 3.

the total force on the object. It may be expected, therefore, that the inertia coefficient found by equation (9) will be in close agreement with the coefficient given by potential flow theory while the drag coefficient may be expected to differ from the steady state value. For the object shape involved in this study the potential flow theory coefficient of inertia will be of interest. Landweber (6) gives the longitudinal inertia coefficient for a number of streamlined bodies not possessing fore and aft symmetry. By interpolation between two of these having almost identical proportions to the body which is the subject of this report, the longitudinal inertia coefficient is found as

$$K_{(a/b\ =\ 5.6)} = 0.053 \qquad (C_M = 1.053)$$

This agrees, within 6%, to the inertia coefficient for an equivalent ellipsoid which is also given by Landweber

$$K\ \text{ellipsoid}\ (a/b = 5.6) = 0.050 \qquad (C_M = 1.050)$$

The steady state drag coefficient for an object of similar shape at the effective Reynolds numbers involved in the test runs (as given in Table III) may be found by extrapolation, from Rouse (7).

$$C_{D\,\text{Airship Hull}} \quad (R = 2 \times 10^3 - 4 \times 10^4) = 0.10 - .08$$

This value, however, may be expected to be in sharp disagreement with the value found from equation (9) due to the low value of period parameter. As will be shown, a better approximation for the drag coefficient is available through consideration of the free vibration characteristics of the object.

The method of employing equation (9) is to set $\sigma t = 90^\circ$ and 270°, where $F_{HI} = 0$, in order to evaluate C_D and set $\sigma t = 0^\circ$ and 180°, where $F_{HD} = 0$ in order to evaluate C_M. The separate terms of equation (9) and their component sums F_{HD} and F_{HI} are plotted over a wave cycle in Figure 3.

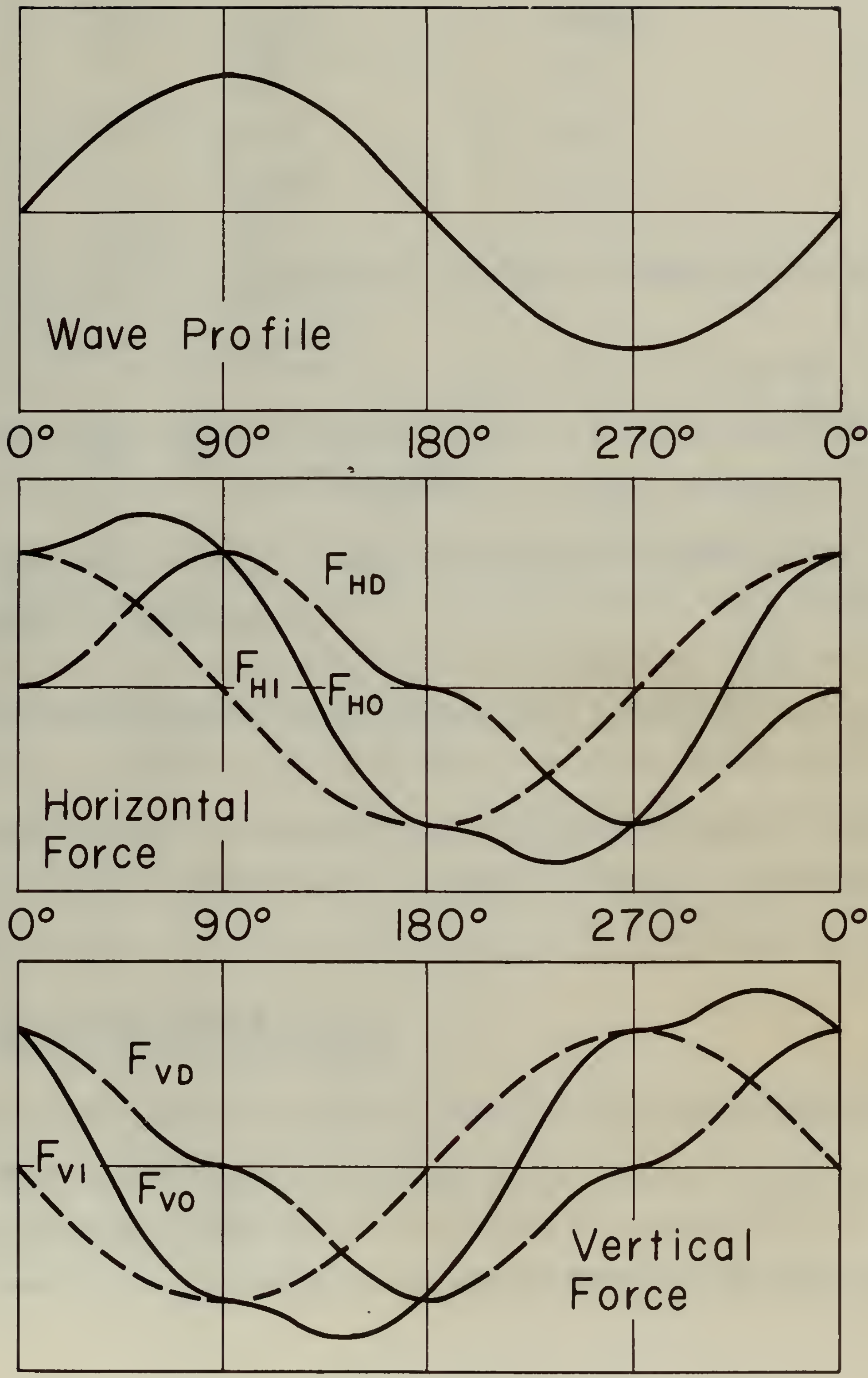

Figure 3. Superposition of Inertia and Drag to Give Total Wave Force

TABLE II PERIOD PARAMETER
VALUES FOR ELLIPSOID TESTS

Runs	Um T/D	Vm T/D
1-12	5.62	2.30
13-23	5.15	2.11
24-35	4.57	1.87

In Table II the period parameter is found by substitution from equation (1) and (2) for Um and Vm.

$$\frac{U_m T}{D} = \frac{\pi H}{D} \frac{\cosh \frac{2\pi}{L}(h+z)}{\sinh \frac{2\pi}{L} h} \qquad (10)$$

The maximum cross sectional diameter of the body is employed as the characteristic body dimension.

The preceding discussion has equal validity for both the horizontal and vertical components of the total force. In the following development, the particular component under consideration will be identified in an equation by the subscript $_H$ for horizontal component, $_V$ for vertical component.

4. Theory of Mechanical Vibrations

Only those aspects of vibration theory which have direct application to the present problem will be considered.

The submerged buoyant body may be treated as a single degree of freedom system with a sinusoidally varying driving force and non-linear damping.

TABLE II PERIOD PARAMETER
VALUES FOR ELLIPSOID TESTS

Runs	$U_m T/D$	$V_m T/D$
1-12	5.62	2.30
13-23	5.15	2.11
24-35	4.57	1.87

In Table II the period parameter is found by substitution from equation (1) and (2) for Um and Vm.

$$\frac{U_m T}{D} = \frac{\pi H}{D} \frac{\text{Cosh}\ \frac{2\pi}{L}(h+z)}{\text{Sinh}\ \frac{2\pi}{L} h} \qquad (10)$$

The maximum cross sectional diameter of the body is employed as the characteristic body dimension.

The preceding discussion has equal validity for both the horizontal and vertical components of the total force. In the following development, the particular component under consideration will be identified in an equation by the subscript $_H$ for horizontal component, $_V$ for vertical component.

4. Theory of Mechanical Vibrations

Only those aspects of vibration theory which have direct application to the present problem will be considered.

The submerged buoyant body may be treated as a single degree of freedom system with a sinusoidally varying driving force and non-linear damping.

For the system thus described the differential equation of motion is given by Den Hartog (8) as

$$m\ddot{x} + c_2\dot{x}^2 + k\,x = Pom \sin \omega t \qquad (11)$$

where $k\,x$ = Spring force

$c_2\dot{x}^2$ = Non Linear Damping force

$m\ddot{x}$ = Inertia force

$Pom \sin \omega t$ = Driving force

It may be mentioned briefly that, for the case of creeping flow, the drag coefficient is inversely proportional to the Reynolds number, and for this case, the damping force becomes linear. The exact solution for the linearized equation is known (8) but applied to viscous damping only at very low Reynolds numbers. At moderate Reynolds numbers, which obtain in the present study, the drag force becomes proportional to the square of the velocity and the non-linear equation (11) must be employed to describe the motion.

By substituting an equivalent linear damping coefficient, c_1, for the square low damping coefficient, c_2, Jacobsen (9) was able to develop an approximate solution to the non-linear equation (11). With this substitution equation (11) reduces to

$$m\ddot{x} + c_1\dot{x} + kx = Pom \sin \omega t \qquad (12)$$

The determination of the damping coefficient, c_1, will permit the solution of equation (12) by methods analagous to the solution of the linear differential vibrations equation.

For the system thus described the differential equation of motion is given by Den Hartog (9) as

$$m\ddot{x} + c_2\dot{x}^2 + k\,x = F_o \sin \omega t \qquad (11)$$

where $k\,x$ = Spring force

$c_2\dot{x}^2$ = Non linear damping force

$m\ddot{x}$ = Inertia force

$F_o \sin \omega t$ = Driving force

It may be mentioned briefly that, for the case of creeping flow, the drag coefficient is inversely proportional to the Reynolds number, and for this case, the damping force becomes linear. The exact solution for the linearized equation is known (9) but applied to viscous damping only at very low Reynolds numbers. At moderate Reynolds numbers, which obtain in the present study, the drag force becomes proportional to the square of the velocity and the non-linear equation (11) must be employed to describe the motion.

By substituting an equivalent linear damping coefficient, c_1, for the square law damping coefficient, c_2, Jacobsen (9) was able to develop an approximate solution to the non-linear equation (11). With this substitution equation (11) reduces to

$$m\ddot{x} + c_1\dot{x} + kx = F_o \sin \omega t \qquad (12)$$

The determination of the damping coefficient, c_1, will permit the solution of equation (12) by methods analogous to the solution of the linear differential vibrations equation.

Jacobsen evaluated the equivalent damping coefficient by the criterion of equivalent dissipative work done during a cycle, assuming the oscillation of the mass to be sinusoidal. The equation relating c_2 and c_1 is

$$\text{Work} = 4c_2 \int_0^{X_m} \left(\frac{dx}{dt}\right)^2 dx = 4c_1 \int_0^{X_m} \left(\frac{dx}{dt}\right) dx \tag{13}$$

where Xm is the maximum amplitude of motion. The solution of equation (13 is

$$c_1 = c_2 \frac{8}{3\pi} X_m \omega \tag{14}$$

The particular solution of interest for equation (12) with c_1 defined by equation (14) is

$$X = X_m \cos(\omega t - \phi) \tag{15}$$

where now

$$\frac{X_m}{X_{om}} = \frac{P_m}{P_{om}} = \frac{1}{\sqrt{2}\, n_2 \left(\frac{f}{f_n}\right)^2} \left[\left\{\left(1 - \left(\frac{f}{f_n}\right)^2\right)^4 + 4 n_2^2 \left(\frac{f}{f_n}\right)^4\right\}^{\frac{1}{2}} - \left(1 - \left(\frac{f}{f_n}\right)^2\right)\right]^{\frac{1}{2}} \tag{16}$$

$$\text{and} \quad n_2 = \frac{2}{3} \frac{c_2}{\pi\, 3_m} \frac{P_{om}}{2 f_n^2} \tag{17}$$

The phase shift ϕ is given by

$$\tan\phi = \frac{1}{\sqrt{2}} \left[\left\{\frac{1 + 4 n_2^2 \left(f/f_n\right)^4}{\left(1 - \left(f/f_n\right)^2\right)^4}\right\}^{\frac{1}{2}} - 1\right]^{\frac{1}{2}} \tag{18}$$

where ϕ is the angle by which the oscillations are out of phase with the driving force.

Figure 4 is a plot of the multiplication factor versus frequency ratio

Jacobsen evaluated the equivalent damping coefficient by the criterion of equivalent dissipative work done during a cycle, assuming the oscillation of the mass to be sinusoidal. The equation relating c_2 and c_1 is

$$\text{Work} = 4c_2 \int_0^{X_m} \left(\frac{dx}{dt}\right)^2 dx = 4c_1 \int_0^{X_m} \left(\frac{dx}{dt}\right) dx \qquad (13)$$

where X_m is the maximum amplitude of motion. The solution of equation (13 is

$$c_1 = c_2 \frac{8}{3\pi} X_m \omega \qquad (14)$$

The particular solution of interest for equation (12) with c_1 defined by equation (14) is

$$X = X_m \cos(\omega t - \phi) \qquad (15)$$

where now

$$\frac{X_m}{X_{st}} = \frac{P_m}{P_{om}} = \frac{1}{\sqrt{2}\, n_2 \left(\frac{f}{f_n}\right)^2} \left[\left\{ \left(1 - \left(\frac{f}{f_n}\right)^2\right)^2 + 4 n_2^2 \left(\frac{f}{f_n}\right)^4 \right\}^{\frac{1}{2}} - \left(1 - \left(\frac{f}{f_n}\right)^2\right) \right]^{\frac{1}{2}} \qquad (16)$$

and $n_2 = \frac{8}{3} \frac{c_2}{\pi m} \frac{P_{om}}{2k}$ (17)

The phase angle ϕ is given by

$$\tan \phi = \frac{1}{\sqrt{2}} \left[\left\{ 1 + 4 n_2^2 \frac{\left(\frac{f}{f_n}\right)^4}{\left(1 - \left(\frac{f}{f_n}\right)^2\right)^2} \right\}^{\frac{1}{2}} - 1 \right]^{\frac{1}{2}} \qquad (18)$$

where ϕ is the angle by which the oscillations are out of phase with the driving force.

Figure 4 is a plot of the multiplication factor versus frequency ratio

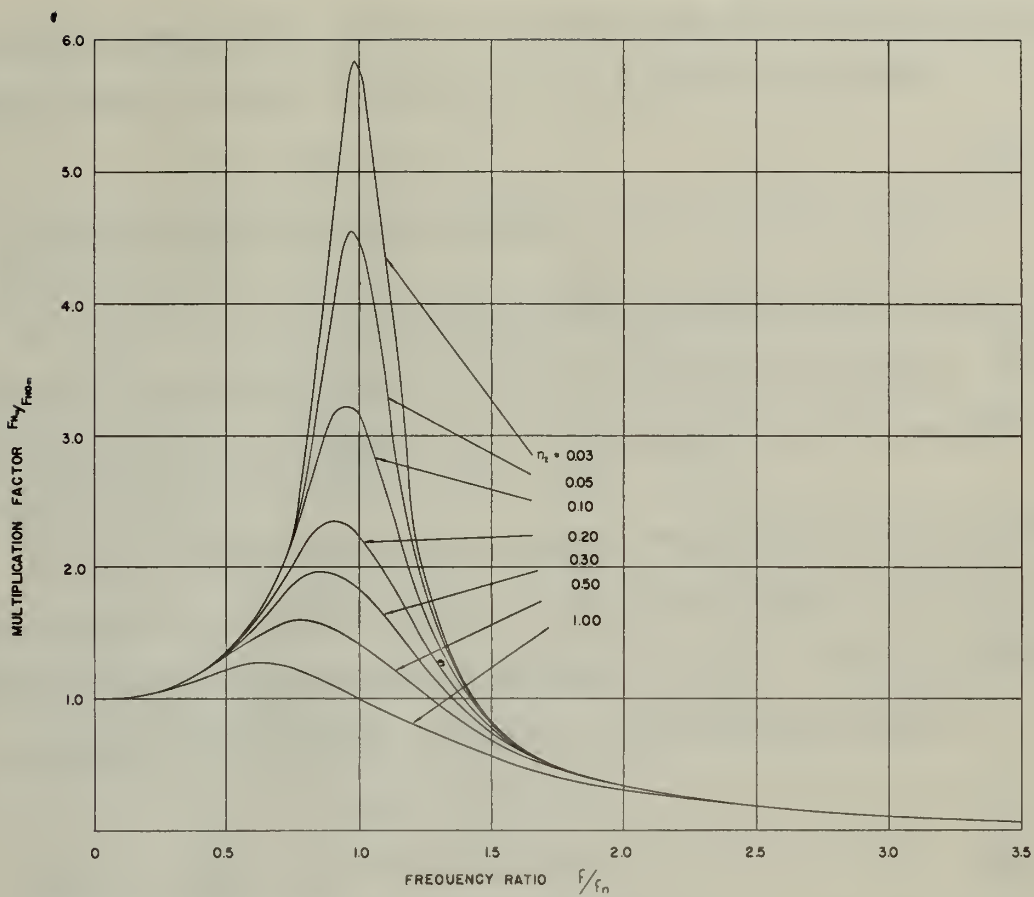

Figure 4. Multiplication Factor for Square Law Damping

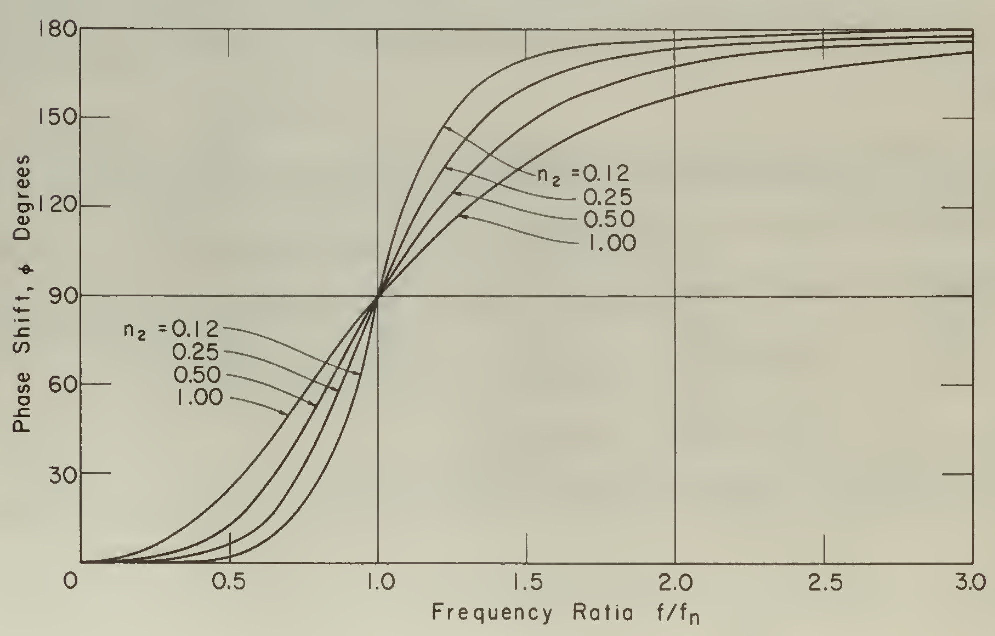

Figure 5. Phase Shift for Square Law Damping

as computed from equation (16) for various values of the parameter n_2.
The phase shift as given by equation (18) is plotted in Figure 5.

5. Analysis of the Ellipsoidal Problem

The analysis of the buoyant ellipsoid will be treated essentially as a problem of vibrations dynamics subjected to quadratic damping. This method was used successfully by Shapiro (1) in the sphere analysis problem.

a. Free Oscillation

It is necessary first to consider free oscillations of the submerged object in order to identify forces acting on the system. Figure 6 is a definition sketch for the submerged ellipsoid analysis. Newton's second law is written in the tangential direction for the element of mass dm

$$d\ \text{Force} = dm\ \ddot{\psi}\lambda$$

where $\ddot{\psi}$ is the angular acceleration.

Multiplying both sides of the equation by λ gives

$$d\ \text{Torque} = \lambda^2\ dm\ \ddot{\psi}$$

Noting that $\iiint \lambda^2 dm = I$, moment of inertia of the body about point O, integration over the volume of the body yields

$$\tau = I\ \ddot{\psi} \qquad (19)$$

which is an expression of Newton's second law for rotating bodies. The torque, τ, is the summation of the torques due to all the forces acting on the object. In order these are the buoyant force torque or "spring torque"

$$\text{Spring Torque} = -(N_t)\,\ell = -N\,\ell\sin\psi$$
$$= -(\text{Vol}\ \rho g - mg)\,\ell\sin\psi \qquad (20)$$

and the virtual mass torque which accounts for a body of fluid the same size as computed from equation (16) for various values of the parameter n_2. The phase shift as given by equation (18) is plotted in Figure 5.

5. Analysis of the Ellipsoidal Problem

The analysis of the buoyant ellipsoid will be treated essentially as a problem of vibrations dynamics subjected to quadratic damping. This method was used successfully by Shapiro (1) in the sphere analysis problem.

a. Free Oscillation

It is necessary first to consider free oscillations of the submerged object in order to identify forces acting on the system. Figure 6 is a definition sketch for the submerged ellipsoid analysis. Newton's second law is written in the tangential direction for the element of mass dm

$$d\,\text{Force} = dm\,\ddot{\psi}\,\lambda$$

where $\ddot{\psi}$ is the angular acceleration.

Multiplying both sides of the equation by λ gives

$$d\,\text{Torque} = \lambda^2\,dm\,\ddot{\psi}$$

Noting that $\iiint \lambda^2 dm = I$, moment of inertia of the body about point O, integration over the volume of the body yields

$$\tau = I\,\ddot{\psi} \qquad (19)$$

which is an expression of Newton's second law for rotating bodies. The torque, τ, is the summation of the torques due to all the forces acting on the object. In order these are the buoyant force torque or "spring torque"

$$\text{Spring Torque} = -(N_t)\,\ell = -N\,\ell \sin\psi$$

$$= -(\text{Vol}\,\rho g - mg)\,\ell \sin\psi \qquad (20)$$

and the virtual mass torque which accounts for a body of fluid the same size and shape as the actual body but having a mass equal to κ times the mass of the fluid.

$$\text{Virtual Mass Torque} = -I'\ddot{\psi} \tag{21}$$

where I' is the moment of inertia of the fluid body about point 0.

Summing these two torques equation (19) becomes

$$-I'\ddot{\psi} - (\text{Vol}\,\rho g - mg)\,\ell \sin\psi = I\ddot{\psi}$$

$$\text{or}\quad (I + I')\ddot{\psi} + (\text{Vol}\,\rho g - mg)\,\ell \sin\psi = 0 \tag{22}$$

If the angle ψ is assumed to be small, then

$$\left.\begin{array}{l} \sin\psi \approx \tan\psi \approx \psi \text{ in radians} \\ \cos\psi \approx 1 \end{array}\right\} \text{Small } \psi \tag{23}$$

which permits equation (22) to be written as

$$(I + I')\ddot{\psi} + (\text{Vol}\,\rho g - mg)\,\ell\,\psi = 0$$

$$\text{or}\quad A\ddot{\psi} + B\psi = 0 \tag{24}$$

$$\text{where } A = I + I' \tag{25}$$

$$\text{and}\quad B = (\text{Vol}\,\rho g - mg)\,\ell \tag{26}$$

The solution for an equation identical in form to equation (23) is given by Den Hartog (8) and is applied here to equation (24).

$$\psi = \psi_m \cos\left[\frac{B}{A}\right]^{1/2} t \tag{27}$$

The motion is sinusoidal with amplitude or maximum angle ψ_m and frequency

$$f_n = \frac{1}{2\pi}\left[\frac{B}{A}\right]^{1/2} \tag{28}$$

and shape as the vessel body but having a mass equal to K times the mass of the fluid.

$$\text{Virtual Mass Torque} = -I'\ddot{\psi} \qquad (21)$$

where I' is the moment of inertia of the fluid body about point O.

Summing these two torques equation (19) becomes

$$-I'\ddot{\psi} - (\text{Vol}\,\rho g - mg)\,l \sin\psi = I\ddot{\psi}$$

$$\text{or} \quad (I + I')\ddot{\psi} + (\text{Vol}\,\rho g - mg)\,l \sin\psi = 0 \qquad (22)$$

If the angle ψ is assumed to be small, then

$$\left.\begin{array}{l} \sin\psi \approx \tan\psi \approx \psi \text{ in radians} \\ \cos\psi \approx 1 \end{array}\right\} \text{Small } \psi \qquad (23)$$

which permits equation (22) to be written as

$$(I + I')\ddot{\psi} + (\text{Vol}\,\rho g - mg)\,l\,\psi = 0$$

$$\text{or} \quad A\ddot{\psi} + B\psi = 0 \qquad (24)$$

$$\text{where } A = I + I' \qquad (25)$$

$$\text{and } B = (\text{Vol}\,\rho g - mg)\,l \qquad (26)$$

The solution for an equation identical in form to equation (23) is given by Den Hartog (8) and is applied here to equation (24).

$$\psi = \psi_m \cos\left[\frac{B}{A}\right]^{1/2} t \qquad (27)$$

The motion is sinusoidal with amplitude or maximum angle ψ_m and frequency

$$f_n = \frac{1}{2\pi}\left[\frac{B}{A}\right]^{1/2} \qquad (28)$$

Equation (28) will be the basis for the predicted natural frequency of the object. This is an approximation since the freely vibrating object is subject to damping, and the natural frequency, f_q, depends on the ratio of the damping coefficient to the critical damping coefficient. However, for small damping ($C/C_c < 0.2$), which prevails for the conditions of the present study, the damped natural frequency very nearly equals the undamped natural frequency, this constitutes the justification for the use of equation (28) even though damping is present.

A sample calculation of the undamped natural frequency from equation (28) including the evaluation of the constant A is presented in Appendix A.

b. Forced Oscillation

The forced oscillation of a buoyant submerged object with quadratic damping is a complicated problem and requires a systematic approach. The flow field in waves is described by equations (1) through (4). All the torques which act on the system must be considered. The technique will be to evaluate these torques and substitute their sum into equation (19). An additional condition to be kept in mind is that the object will have relative motion with respect to the fluid and a fixed reference point.

1) Spring Torque

This is given by equation (20)

Spring Torque $= -(\text{Vol}\,\rho g - mg)\,\ell \sin\psi$

2) Pressure Gradient Torque

This torque depends on the acceleration and the mass of the displaced fluid. The total torque is the sum of the horizontal and vertical pressure gradient force components in the tangential direction.

$$\text{Pressure gradient torque} = \text{Vol}\,\rho \left[\frac{du}{dt} \cos\psi - \frac{dv}{dt} \sin\psi\right)\ell \qquad (29)$$

Equation (30) will be the basis for the predicted natural frequency of the object. This is an approximation since the freely vibrating object is subject to damping, and the natural frequency, f_d depends on the ratio of the damping coefficient to the critical damping coefficient. However, for small damping ($C/C_c < 0.2$), which prevails for the conditions of the present study, the damped natural frequency very nearly equals the undamped natural frequency, this constitutes the justification for the use of equation (30) even though damping is present.

A sample calculation of the undamped natural frequency from equation (28) including the evaluation of the constant A is presented in Appendix A.

b. Forced Oscillation

The forced oscillation of a buoyant submerged object with quadratic damping is a complicated problem and requires a systematic approach. The flow field in waves is described by equations (1) through (4). All the torques which act on the system must be considered. The technique will be to evaluate these torques and substitute their sum into equation (19). An additional condition to be kept in mind is that the object will have relative motion with respect to the fluid and a fixed reference point.

1) Spring Torque

This is given by equation (20)

$$\text{Spring Torque} = -(\text{Vol}\,\rho g - mg)\,\ell \sin\psi$$

2) Pressure Gradient Torque

This torque depends on the acceleration and the mass of the displaced fluid. The total torque is the sum of the horizontal and vertical pressure gradient force components in the tangential direction.

$$\text{Pressure gradient torque} = \text{Vol}\,\rho\left[\frac{du}{dt}\cos\psi - \frac{dv}{dt}\sin\psi\right]\ell \qquad (29)$$

Involved in the equation is the implicit assumption that the fluid acceleration is constant over the cross section of the body and is equal to the value at the center when $\psi = 0$

3) <u>Virtual Mass Torque</u>

The virtual mass torque depends upon the relative acceleration between the fluid and the object and is written

$$\text{Virtual mass torque} = I'\ddot{\psi} + K \,\text{vol}\, \rho \left(\frac{du}{dt} \cos\psi - \frac{dv}{dt} \sin\psi\right) \ell \quad (30)$$

where I' is as defined in connection with equation (21)

4) <u>Damping Torque</u>

The damping torque depends on the relative velocity of object and fluid in the tangential direction

$$\text{Damping torque} = C_2 \ell \left\{ \left[-\dot{\psi}\ell + (u\cos\psi - v\sin\psi) \right] \left| -\dot{\psi}\ell + (u\cos\psi - v\sin\psi) \right| \right\} \quad (31)$$

The four torques described above may now be added and the result equated to $I\ddot{\psi}$ in equation (19)

$$\Sigma \mathcal{T} = I\ddot{\psi}$$

However, in order to simplify this summation the following assumptions are made.

<u>Assumption 1.</u> The vertical component of the mooring line force is equal to the net buoyancy N. This is valid if the vertical dynamic wave force F_y is small with respect to net buoyancy. By this device terms containing vertical components of velocity and acceleration may be neglected.

<u>Assumption 2.</u> The drag wave force component is small with respect to the inertia wave force component. This has been shown to be valid for small values of the period parameter. Period parameters for the ex-

Involved in the equation is the implicit assumption that the fluid acceleration is constant over the cross section of the body and is equal to the value at the center when $\psi = 0$

3) Virtual Mass Torque

The virtual mass torque depends upon the relative acceleration between the fluid and the object and is written

$$\text{Virtual mass torque} = I'\ddot{\psi} + K \,\text{vol}\, \rho \left(\frac{du}{dt}\cos\psi - \frac{dv}{dt}\sin\psi\right)\ell \quad (30)$$

where I' is as defined in connection with equation (21)

4) Damping Torque

The damping torque depends on the relative velocity of object and fluid in the tangential direction

$$\text{Damping torque} = C\rho\ell^2 \left\{ \left[-\dot{\psi}\ell + (u\cos\psi - v\sin\psi)\right] \left|-\dot{\psi}\ell + (u\cos\psi - v\sin\psi)\right| \right\} \quad (31)$$

The four torques described above may now be added and the result equated to $I\ddot{\psi}$ in equation (19)

$$\Sigma T = I\ddot{\psi}$$

However, in order to simplify this summation the following assumptions are made.

Assumption 1. The vertical component of the mooring line force is equal to the net buoyancy N. This is valid if the vertical dynamic wave force F_y is small with respect to net buoyancy. By this device terms containing vertical components of velocity and acceleration may be neglected.

Assumption 2. The drag wave force component is small with respect to the inertia wave force component. This has been shown to be valid for small values of the period parameter. Period parameters for the experimental runs in this report, as seen from Table II, are less than 15 and may be treated, approximately, as "small."

Assumption 3. The mooring line angle ψ, is small. This allows use of the small angle approximations for $\sin\psi$ and $\cos\psi$

Making use of the foregoing assumptions the result of the addition of torques and subsequent substitution into equation (19) is

$$(I + I')\ddot{\psi} + C_2 (\psi \ell)^2 \ell + \left[(\text{Vol}\, \rho g - mg\right] \ell \psi = \left((K + 1)\, \text{Vol}\, \rho \frac{du}{dt}\right) \ell \quad (32)$$

In equation (32) the term on the right hand side represents the product of the horizontal sinusoidally varying forcing function on the object and the radius of oscillation and is the exciting torque.

Therefore equation (32), the differential equation of motion, becomes

$$A \ddot{\psi} + C_2 \dot{\psi}^2 + B \psi = F_{hom} \ell \cos\theta \quad (33)$$

where

$$A = I + I'$$

$$B = (\text{Vol}\, \rho g - mg)\, \ell$$

$$C_2 = c_2 \ell^3$$

$$F_{hom} = \left[(K + 1)\, \text{Vol}\, \rho \frac{du}{dt}\right]_m$$

$$\theta = \frac{2\pi t}{T} = 2\pi f t = \omega t$$

In the previous equations, the subscript "o" denotes rigidly restrained values and the subscript "m" denotes maximum values.

Equation (33) is identical in form to equation (11) with the substitution of parameters of the present problem, therefore, Jacobsen's solution may be applied.

perimental runs in this report, as seen from Table II, are less than 15 and may be treated, approximately, as "small."

<u>Assumption 3</u>. The mooring line angle ψ, is small. This allows use of the small angle approximations for $\sin \psi$ and $\cos \psi$

Making use of the foregoing assumptions the result of the addition of torques and subsequent substitution into equation (19) is

$$(I + I')\ddot{\psi} + C_2 (\dot{\psi} \ell)^2 \ell + \left[(Vol\, \rho g - mg\right] \ell \psi - \left((K + 1)\, Vol\, \rho \frac{du}{dt}\right) \ell \quad (32)$$

In equation (32) the term on the right hand side represents the product of the horizontal sinusoidally varying forcing function on the object and the radius of oscillation and is the exciting torque.

Therefore equation (32), the differential equation of motion, becomes

$$A \ddot{\psi} + C_2 \dot{\psi}^2 + B \psi = F_{hom} \ell \cos \theta \quad (33)$$

where

$$A = I + I'$$

$$B = (Vol\, \rho g - mg)\, \ell$$

$$C_2 = c_2 \ell^3$$

$$F_{hom} = \left[(K + 1)\, Vol\, \rho \frac{du}{dt}\right]_m$$

$$\theta = \frac{2 \pi t}{T} = 2 \pi f t = \omega t$$

In the previous equations, the subscript "o" denotes rigidly restrained values and the subscript "m" denotes maximum values.

Equation (33) is identical in form to equation (11) with the substitution of parameters of the present problem, therefore, Jacobsen's solution may be applied.

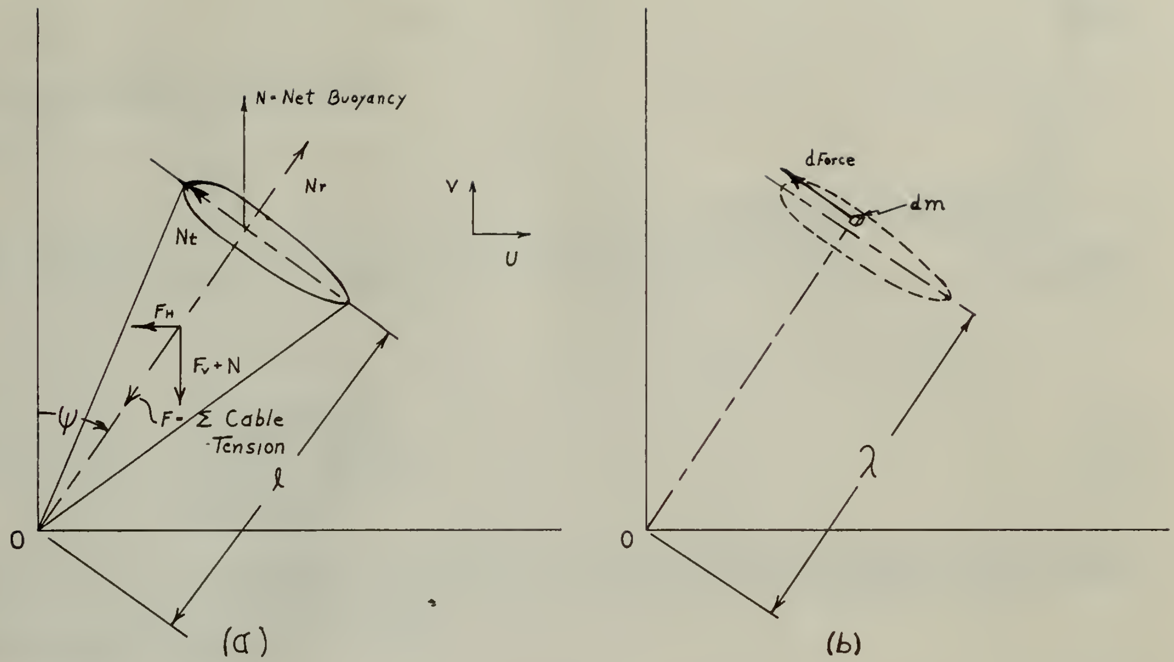

Figure 6. Definition Sketch - Submerged Object

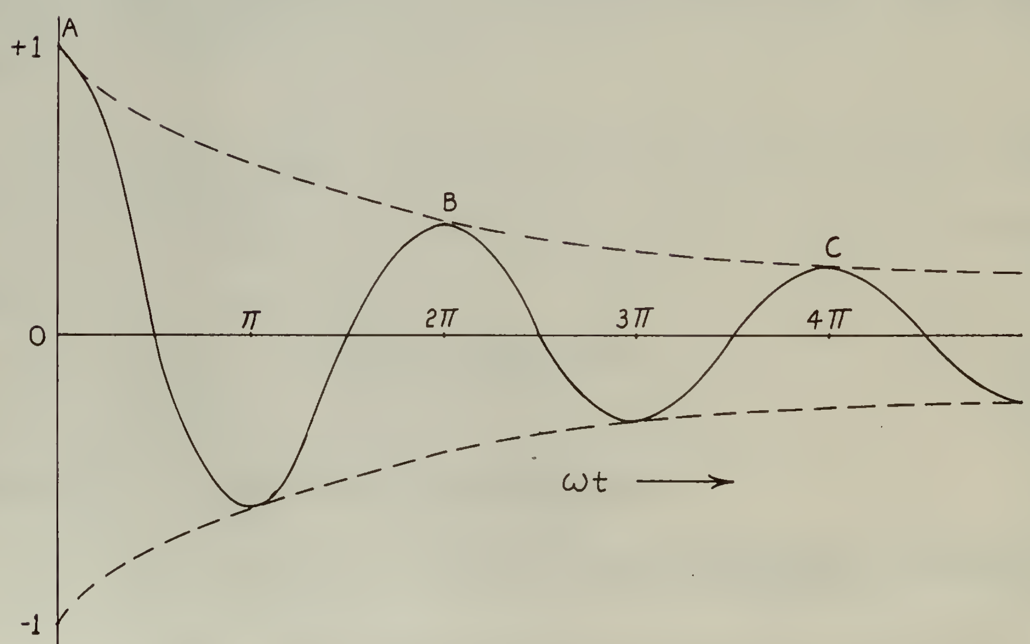

Figure 7. Free Vibration of a System with Damping Less than the Critical Damping Value

The solution is

$$\psi = \psi_m \cos(\theta - \phi) \tag{34}$$

by analogy with equation (15)

where

$$\frac{\psi_m}{\psi^o_m} = \frac{F_{Hm}}{F_{Hom}} = \frac{1}{\sqrt{2}\, n_2 \,(f/f_n)^2} \left[\left\{ \left(1 - \left(\frac{f}{f_n}\right)^2\right)^4 - 4n_2^2 \left(\frac{f}{f_n}\right)^4 \right\}^{\frac{1}{2}} - \left(1 - (f/f_n)^2\right)^2 \right]^{\frac{1}{2}} \tag{35}$$

and

$$\tan\phi = \frac{1}{\sqrt{2}} \left[\left\{ 1 + \frac{4\, n_2^2\, (f/f_n)^4}{\left(1 - (f/f_n)^2\right)^4} \right\}^{\frac{1}{2}} - 1 \right]^{\frac{1}{2}} \tag{36}$$

Figures 4 and 5 graphically represent equations (35) and (36) respectively.

By comparison with equation (17)

$$n_2 = \frac{2}{3} \frac{C_2 F_{Hom} \ell}{3 A^2 f_n^2}$$

where C_2 is defined as presented in equation (33). The constant C_2 is found from the drag force equation (8) with the cross sectional area of the object inserted.

$$F_{HD} = \underbrace{C_D \frac{\rho}{2} \frac{\pi D^2}{4}}_{C_2} \; |u| \; u \tag{37}$$

Therefore

$$n_2 = \frac{1}{12 \pi^2} \frac{C_D\, \rho\, D^2 \ell^4 F_{Hom}}{A^2 f_n^2} \tag{38}$$

6. Determination of Test Object Drag Coefficient

It is necessary to obtain as accurate a determination for the drag coefficient, C_D, as possible. The data presented by Rouse do not extend to the range of Reynolds numbers in this study and further inaccuracy is involved, in attempt-

The solution is

$$\psi = \psi_m \cos(\theta - \phi) \qquad (34)$$

by analogy with equation (15)

where

$$\frac{\psi_m}{\psi_{0m}} = \frac{F_{Tm}}{F_{T0m}} = \frac{1}{\sqrt{2}\, n^{\frac{1}{2}} (f/f_n)^2} \left[\left\{ \left(1 - \left(\frac{f}{f_n}\right)^2\right)^4 + 4n^2 \left(\frac{f}{f_n}\right)^4 \right\}^{\frac{1}{2}} - \left(1 - (f/f_n)^2\right)^2 \right]^{\frac{1}{2}} \qquad (35)$$

and

$$\tan\phi = \frac{1}{\sqrt{2}} \left[\left\{ 1 + \frac{4 n^2 (f/f_n)^4}{\left(1 - (f/f_n)^2\right)^4} \right\}^{\frac{1}{2}} - 1 \right]^{\frac{1}{2}} \qquad (36)$$

Figures 4 and 5 graphically represent equations (35) and (36) respectively.

By comparison with equation (17)

$$n^2 = \frac{2}{3} \frac{C_2\, F_{Tom}\, \ell}{A^2 f_n^2}$$

where C_2 is defined as presented in equation (13). The constant C_2 is found from the drag force equation (8) with the cross sectional area of the object inserted.

$$FTD = \underbrace{C_D \frac{\rho}{2} \frac{\pi D^2}{4}}_{C_2} |u|\, u \qquad (37)$$

Therefore

$$n^2 = \frac{1}{12\pi^2} \frac{C_D\, \rho\, D^2 \ell^4\, F_{Tom}}{A^2 f_n^2} \qquad (38)$$

6. Determination of Test Object Drag Coefficient

It is necessary to obtain as accurate a determination for the drag coefficient, C_D, as possible. The data presented by Rouse do not extend to the range of Reynolds numbers in this study and further inaccuracy is involved, in attempt-ing to make use of this data, due to the presence of stabilizing fins and mooring appendages on the test object. Also it was shown earlier that for low values of the period parameter, as obtained in these tests, the steady state drag coefficient became increasingly inaccurate.

However, consideration of the experimentally observed free vibrations of the test object offer a means for obtaining reasonably accurate values for the drag coefficient. The steady flow hydrodynamic drag force is given by equation (37)

$$F_{HD} = C_D \frac{\rho}{2} \frac{\pi D^2}{4} |u| u \qquad (37)$$

For the case of linear damping, which will occur at very low Reynolds numbers,

$$C_D = \frac{\text{Constant}}{N_r} \qquad (39)$$

where CD $= C_D$ (Reynolds number, shape) and Reynolds number is defined as

$$N_r = \frac{u D}{\nu} \qquad (40)$$

Substitution of these expressions into (37) yields

$$FHD = \underbrace{\frac{\text{Constant}\ \nu \rho \pi D u}{8}}_{c_1} \qquad (41)$$

The bracketed expression is defined as the linear damping coefficient.

For the case of torsional free vibrations with linear damping the differential equation of motion becomes

$$A \ddot{\psi} + C_1 \dot{\psi} + B \psi = 0 \qquad (42)$$

where A, and B are defined as in equation (33) and

$$C_1 = c_1 \ell^2$$

The solution for an equation of this form, with damping less than critical, is given by Den Hartog (8)

$$\psi = e^{-\frac{C' t}{2 A}} (C_1' \cos q t + C_2' \sin q t) \qquad (43)$$

ing to make use of this data, due to the presence of stabilizing fins and mooring appendages on the test object. Also it was shown earlier that for low values of the period parameter, as obtained in these tests, the steady state drag coefficient becomes increasingly inaccurate.

However, consideration of the experimentally observed free vibrations of the test object offer a means for obtaining reasonably accurate values for the drag coefficient. The steady flow hydrodynamic drag force is given by equation (37)

$$F_D = C_D \frac{\rho}{2} \frac{\pi D^2}{4} |u| u \qquad (37)$$

For the case of linear damping, which will occur at very low Reynolds numbers,

$$C_D = \frac{\text{Constant}}{N_r} \qquad (39)$$

where $C_D = C_D$ (Reynolds number, shape) and Reynolds number is defined as

$$N_r = \frac{u D}{\nu} \qquad (40)$$

Substitution of these expressions into (37) yields

$$F_D = \underbrace{\frac{\text{Constant}\ \nu \rho \pi D}{8}}_{c_1} u \qquad (41)$$

The bracketed expression is defined as the linear damping coefficient.

For the case of torsional free vibrations with linear damping the differential equation of motion becomes

$$A \ddot{\psi} + C_1' \dot{\psi} + B \psi = 0 \qquad (42)$$

where A, and B are defined as in equation (33) and

$$C_1' = c_1 \ell^2$$

The solution for an equation of this form, with damping less than critical, is given by Den Hartog (8)

$$\psi = e^{-\frac{C_1' t}{2A}} (C_1' \cos q t + C_2' \sin q t) \qquad (43)$$

where C_1' and C_2' are arbitrary complex constants and

$$q = 2\pi f_q = \left[\frac{B}{A} - \frac{C_1^{\,2}}{4A^2}\right]^{\frac{1}{2}} \tag{44}$$

This is the solution for a damping smaller than C_c. It consists of two factors, the first a decreasing exponential and the second a sine wave. The combined result is a "damped sine wave" lying in the space between the exponential curve and its mirrored image as shown in Figure 7 after Den Hartog.

The rate of this dying down is of interest and can be calculated in a simple manner by considering any two consecutive maxima of the curve A-B, B-C, etc. During the time interval between two such maxima, i.e. during $\frac{2\pi}{q}$ seconds, the amplitude of the vibration diminishes from $e^{-C_1/2A\,t}$ to $e^{\frac{-C_1}{2A}\left(t + \frac{2\pi}{q}\right)}$. The latter of these two expressions is seen to be equal to the first one multiplied by the constant factor $e^{\frac{-\pi C_1}{A q}}$, which factor naturally is smaller than unity. This factor is the same for any two consecutive maxima, independent of the amplitude of vibration or of the time. The ratio between two consecutive maxima is constant, the amplitude decreases in a geometric series.

If ψ_n is the n th maximum amplitude during a vibration and ψ_{n+1} is the next maximum then

$$\psi_{n+1} = \psi_n \, e^{\frac{-\pi C_1}{A q}} \tag{45}$$

or

$$\ln \frac{\psi_n}{\psi_{n+1}} = \frac{\pi C_1}{A q} = \delta \tag{46}$$

where δ is known as the logarithmic decrement.

Equation (46) may be evaluated for C_1

$$C_1 = 2\,A\,fq \ln \frac{\psi_n}{\psi_{n+1}} \tag{47}$$

There remains to be established a relation between C_1, the linear coefficient of damping and C_2, the quadratic coefficient of damping from which the coefficient of drag, C_D, may be evaluated. For the case of linear vibration where C_1' and C_2' are arbitrary complex constants and

$$q = 2\pi f = \left[\frac{g}{A} - \frac{C_1^2}{4A^2}\right]^{\frac{1}{2}} \tag{44}$$

This is the solution for a damping smaller than C_c. It consists of two factors, the first a decreasing exponential and the second a sine wave. The combined result is a "damped sine wave" lying in the space between the exponential curve and its mirrored image as shown in Figure 7 after Den Hartog.

The rate of this dying down is of interest and can be calculated in a simple manner by considering any two consecutive maxima of the curve A-B, B-C, etc. During the time interval between two such maxima, i.e. during $\frac{2\pi}{q}$ seconds, the amplitude of the vibration diminishes from $e^{-C_1 t/2A}$ to $e^{-\frac{C_1}{2A}\left(t + \frac{2\pi}{q}\right)}$. The latter of these two expressions is seen to be equal to the first one multiplied by the constant factor $e^{-\frac{\pi C_1}{Aq}}$, which factor naturally is smaller than unity. This factor is the same for any two consecutive maxima, independent of the amplitude of vibration or of the time. The ratio between two consecutive maxima is constant, the amplitude decreases in a geometric series.

If ψ_n is the n th maximum amplitude during a vibration and ψ_{n+1} is the next maximum then

$$\psi_{n+1} = \psi_n e^{-\frac{\pi C_1}{qA}} \tag{45}$$

or

$$\ln \frac{\psi_n}{\psi_{n+1}} = \frac{\pi C_1}{qA} = \delta \tag{46}$$

where δ is known as the logarithmic decrement.

Equation (46) may be evaluated for C_1

$$C_1 = 2 A q \ln \frac{\psi_n}{\psi_{n+1}} \tag{47}$$

There remains to be established a relation between C_1, the linear coefficient of damping and C_2, the quadratic coefficient of damping from which the coefficient of drag, C_D, may be evaluated. For the case of linear vibration this relation was presented in section 3 equation (14). Following Jacobsen's criterion of equivalent dissipative work done during a cycle, an analogous expression can be derived for the condition of torsional vibration.

For the case of angular velocity

$$u = \dot{\psi}\, l = l\, \psi_{max}\ \omega \cos\ \omega t \qquad (48)$$

Substituting this expression into equation (41) yields

$$F_{HD} = \frac{\text{Constant}\ \nu\ \rho\ \Pi\ D\ l}{8}\, \psi_{max}\ \ \omega \cos\ \omega t \qquad (49)$$

The damping torque for this motion can now be expressed as

$$\tau = F_{HD}\ l = \underbrace{\left[\frac{\text{Constant}\ \nu\ \rho \pi\ \ \ D\, l^2}{8}\right]}_{C_1} \psi_{max}\ \ \omega \cos\ \ \omega t \qquad (50)$$

where the expression in brackets is the coefficient C_1 modifying $\dot{\psi}$ in equation (42).

The work over one cycle is

$$\text{Work} = 4 \int_0^{\psi_{max}} \tau\, d\psi \qquad (51)$$

but $d\,\psi = \psi_{max}\ \omega\ \cos\ \omega t\ \ dt \qquad (52)$

The limits are

at $\quad \psi = 0 \quad , \quad t = 0$

$\quad \psi = \psi_{max}\ ,\ \omega t = \frac{\pi}{2} \qquad , \quad t = \frac{\pi}{2\omega}$

Therefore the work over one cycle for linear damping is

$$\text{Work} = 4 \int_0^{\pi/2\omega} C_1\ \psi^2_{max}\ \omega^2\ \ \cos^2 \omega t\ dt = \pi C_1\ \psi^2_{max}\ \omega \qquad (53)$$

For the case of quadratic damping the torque may be expressed as

$$\tau = F_{HD}\ l = \underbrace{\left[C_d\ \frac{\rho}{8}\ \ \ D^2\ l^3\right]}_{C_2} |\dot{\psi}|\ \dot{\psi} \qquad (54)$$

where the expression in brackets is the coefficient C_2 modifying $\dot{\psi}^2$ in equation (33)

The work over one cycle is

this relation was presented in section 3 equation (14). Following Jacobsen's criterion of equivalent dissipative work done during a cycle, an analogous expression can be derived for the condition of torsional vibration.

For the case of angular velocity

$$u = \dot{\psi}\, l = l\, \psi_{max}\, \omega \cos \omega t \qquad (48)$$

Substituting this expression into equation (41) yields

$$F_{HD} = \frac{\text{Constant}\ \nu\, \rho\, \Pi\, D\, l}{\delta}\, \psi_{max}\, \omega \cos \omega t \qquad (49)$$

The damping torque for this motion can now be expressed as

$$\tau = F_{HD}\, l = \underbrace{\left[\frac{\text{Constant}\ \nu\, \rho\, \pi\, D\, l^2}{\delta}\right]}_{C_1} \psi_{max}\, \omega \cos \omega t \qquad (50)$$

where the expression in brackets is the coefficient C_1 modifying $\dot{\psi}$ in equation (42).

The work over one cycle is

$$\text{Work} = 4 \int_0^{\psi_{max}} \tau\, d\psi \qquad (51)$$

$$\text{but } d\psi = \psi_{max}\, \omega \cos \omega t\, dt \qquad (52)$$

The limits are

at $\psi = 0$, $t = 0$

$\psi = \psi_{max}$, $\omega t = \frac{\pi}{2}$, $t = \frac{\pi}{2\omega}$

Therefore the work over one cycle for linear damping is

$$\text{Work} = 4 \int_0^{\pi/2\omega} C_1\, \psi^2_{max}\, \omega^2 \cos^2 \omega t\, dt = \pi C_1\, \psi^2_{max}\, \omega \qquad (53)$$

For the case of quadratic damping the torque may be expressed as

$$\tau = F_{HD}\, l = \underbrace{\left[C_d\, \frac{\rho}{2}\, D^2\, l^3\right]}_{C_2} |\dot{\psi}|\, \dot{\psi} \qquad (54)$$

where the expression in brackets is the coefficient C_2 modifying $\dot{\psi}^2$ in equation (53).

The work over one cycle is

$$\text{Work} = 4\int_{0}^{\pi/2\omega} C_2\, \psi^3_{max}\, \omega^3 \cos^3 \omega t \;\; dt = \frac{8}{3} C_2\, \psi^3_{max}\, \omega^2 \tag{55}$$

Equating (53) and (55)

$$C_1 = \frac{8}{3\pi}\, \omega\, \psi_{max}\, C_2 \tag{56}$$

which is similar to equation (14).

Substituting this expression into equation (47) and re-arranging terms yields

$$C_D = \frac{3\, C_1}{\omega\, \psi_{max}\, \rho\, D^2\, \ell^3} = \frac{3\, A}{\pi\, \rho\, D^2\, \ell^3\, \psi_{max}} \ln \frac{\psi_n}{\psi_{n+1}} \tag{57}$$

where A is defined as in equation (33) and from Figure 6

$$\psi_{max} = \tan^{-1} \frac{F_H}{F_V + N} \tag{58}$$

From Assumption 1, $F_V + N$ is approximately equal to the net buoyancy of the object and F_H may be measured from experimental results.

A sample calculation for the coefficient of drag from equation (57) is presented in Appendix B.

Over limited ranges of Reynolds numbers C_D may be considered a constant. It will be of value to establish the order of Reynolds numbers based on maximum object velocity for a range of angles of oscillation. In this computation the ellipsoid is assumed to be oscillating sinusoidally at a frequency of 0.5 cycles per second which is the wave frequency for all test runs. The radius of oscillation is as indicated. The angular displacement of the body is

$$\psi = \psi_m \sin 2\pi ft \tag{59}$$

By differentiation, the angular velocity is

$$\dot{\psi} = \psi_m\, 2\pi f \cos 2\pi ft \tag{60}$$

and $\dot{\psi} = \dot{\psi}_m$ at $\cos 2\pi ft = 1$

$$\text{Work} = 4\int_0^{\pi/2\omega} C_2 \psi^3_{max}\,\omega^3 \cos^3 \omega t \; dt = \frac{8}{3} C_2 \psi^3_{max}\,\omega^2 \qquad (55)$$

Equating (53) and (55)

$$C_1 = \frac{8}{3\pi}\,\omega\,\psi_{max}\,C_2 \qquad (56)$$

which is similar to equation (14).

Substituting this expression into equation (47) and re-arranging terms yields

$$C_D = \frac{3C_1}{\omega\,\psi_{max}\,\rho D^2 \ell^3} = \frac{3A}{\pi\,\rho D^2 \ell^3\,\psi_{max}} \ln \frac{\psi_n}{\psi_{n+1}} \qquad (57)$$

where A is defined as in equation (33) and from Figure 6

$$\psi_{max} = \tan^{-1} \frac{F_H}{F_V + W} \qquad (58)$$

From assumption 1, $F_V + W$ is approximately equal to the net buoyancy of the object and F_H may be measured from experimental results.

A sample calculation for the coefficient of drag from equation (57) is presented in Appendix B.

Over limited ranges of Reynolds numbers C_D may be considered a constant. It will be of value to establish the order of Reynolds numbers based on maximum object velocity for a range of angles of oscillation. In this computation the ellipsoid is assumed to be oscillating sinusoidally at a frequency of 0.5 cycles per second which is the wave frequency for all test runs. The radius of oscillation is as indicated. The angular displacement of the body is $\psi = \psi_m \sin 2\pi ft$ (59)

By differentiation, the angular velocity is

$$\dot{\psi} = \psi_m \, 2\pi f \cos 2\pi ft \qquad (60)$$

and $\dot{\psi} = \dot{\psi}_m$ at $\cos 2\pi ft = 1$

The maximum tangential velocity is therefore

$$U_m = \dot{\psi}_m \ell = 2\pi f \psi_m \ell \tag{61}$$

The Reynolds number based on the maximum velocity is

$$N_r = \frac{U_m D}{\nu} = \frac{2\pi f \psi_m \ell D}{\nu} \tag{62}$$

The kinematic viscosity ν is taken to be 10^{-5} ft ^{2}/sec.

The Reynolds numbers computed on the above basis are presented in Table III

TABLE III REYNOLDS NUMBERS FOR TYPICAL TEST CONDITIONS

Diameter = 0.208 ft $\nu = 10^{-5}$ ft^2/sec $f = 0.5$ cps

Maximum angle of motion, ψ_m	ℓ	Reynolds No. Eq. (62)	C_D -Rouse (7)
5°	0.479 ft	2.725×10^3	0.100
10°	0.479	5.450×10^3	0.095
20°	0.479	1.090×10^4	0.095
5°	1.112	6.350×10^3	0.095
10°	1.112	1.270×10^4	0.095
20°	1.112	2.540×10^4	0.090
5°	1.540	8.790×10^3	0.095
10°	1.540	1.758×10^4	0.090
20°	1.540	3.516×10^4	0.085

Values of C_D corresponding to the computed Reynolds numbers in Table III were obtained from Rouse (7)/ However, as has been previously demonstrated, for the period parameters of the experimental work, steady state values for the coefficient of drag are not reliable. These have been included to permit comparison with values for the drag coefficient obtained from equation (57).

Two conclusions may be drawn from Table III, the possibility of linear viscous damping being present is eliminated at the expected Reynolds numbers and, over the range of Reynolds numbers involved, C_D is fairly constant.

The maximum tangential velocity is therefore

$$U_m = \dot{\psi}_m \ell = 2\pi f \psi_m \ell \qquad (61)$$

The Reynolds number based on the maximum velocity is

$$R_r = \frac{U_m D}{\nu} = \frac{2\pi f \psi_m \ell D}{\nu} \qquad (62)$$

The kinematic viscosity ν is taken to be 10^{-5} ft ^{2}/sec.

The Reynolds numbers computed on the above basis are presented in Table III below.

TABLE III REYNOLDS NUMBERS FOR TYPICAL TEST CONDITIONS

Diameter = 0.208 ft $\nu = 10^{-5}$ ft ^{2}/sec f = 0.5 cps

Maximum angle of motion, ψ_m	ℓ	Reynolds No. Eq.(62)	C_D -Rouse (7)
5°	0.479 ft	2.725×10^3	0.100
10°	0.479	5.450×10^3	0.095
20°	0.479	1.090×10^4	0.095
5°	1.112	6.350×10^3	0.095
10°	1.112	1.270×10^4	0.095
20°	1.112	2.540×10^4	0.090
5°	1.540	8.790×10^3	0.095
10°	1.540	1.758×10^4	0.090
20°	1.540	3.515×10^4	0.085

Values of C_D corresponding to the computed Reynolds numbers in Table III were obtained from Rouse (7). However, as has been previously demonstrated, for the period parameters of the experimental work, steady state values for the coefficient of drag are not reliable. These have been included to permit comparison with values for the drag coefficient obtained from equation (57). Two conclusions may be drawn from Table III, the possibility of linear viscous damping being present is eliminated at the expected Reynolds numbers and, over the range of Reynolds numbers involved, C_D is fairly constant.

7 Effect of Variation of Mooring Line Length

The length of the test object mooring line is an important parameter affecting the damping factor, coefficient of drag and natural frequency of the object

With increasing centerline depth the fixed object will encounter reduced water particle velocities and less interaction with the fluid - air interface, these two factors will act to reduce total hydrodynamic force. In the partially restrained condition, shortening the length of the mooring line will lead to higher natural frequencies. The effect on the damping factor, N_2, includes an affect arising from a change in the coefficient of drag since N_2 is a function of C_D as well as "ℓ". Equation (57) indicates that C_D will increase as "ℓ" decreases therefore these two variables will have a conflicting influence on the damping factor. At some depth it may be expected that one of the two will become the controlling influence.

The objective of this portion of the test program will be to determine an optimum centerline depth for the location of the object with respect to actual maximum hydrodynamic force.

The theoretical development, as previously presented, will lead to a predicted value of $\left.\frac{F_{Hm}}{F_{Hom}}\right|_{max}$ for each test depth. On this and the basis of the measured rigidly restrained force the maximum hydrodynamic force at each depth can be predicted and the relation of F_{Hm} and depth constructed.

III EXPERIMENTAL EQUIPMENT

1. Wave Tank and Wave Generator

The M.I.T. Hydrodynamics wave channel, which was used in this study, is a steel framed structure with a working section 30 inches wide, 36 inches deep and 90 feet long. The side walls of the channel consist of 1/2 inch plate glass over the whole 90 feet. The bottom is horizontal with a 40 foot section of 1/2 inch plate glass beginning 16 feet from the generator end and with the remaining section of 1/4 inch steel plate. A model beach made of transite plates occupies the last 35 feet of the tank and is supported on a steel framework at a slope of 15 horizontal to 1 vertical. The beach serves as an energy absorber and limits undesirable wave reflections. Figure 8 is a photograph of the wave tank

The channel is equipped with a hydraulically controlled piston-type wave generator, Figures 9 and 10, for generating shallow water waves. The generator proper consists of a horizontal aluminum piston with a vertical face, rigidly suspended from a rail-mounted carriage on top of the entrance box. The carriage-piston assembly is actuated by a cam-operated hydraulic servomechanism providing variation in frequency and stroke and thus wave length and height during operation of the generator.

Use of a servomechanism permits a choice of the displacement - time curve for the generator piston. Wave heights are controlled by varying the position of the cam contact point on the follower. Wave periods are

III EXPERIMENTAL EQUIPMENT

1. Wave Tank and Wave Generator

The M.I.T. Hydrodynamics wave channel, which was used in this study, is a steel framed structure with a working section 30 inches wide, 36 inches deep and 90 feet long. The side walls of the channel consist of 1/2 inch plate glass over the whole 90 feet. The bottom is horizontal with a 40 foot section of 1/2 inch plate glass beginning 10 feet from the generator end and with the remaining section of 1/4 inch steel plate. A model beach made of transite plates occupies the last 35 feet of the tank and is supported on a steel framework at a slope of 15 horizontal to 1 vertical. The beach serves as an energy absorber and limits undesirable wave reflections. Figure 8 is a photograph of the wave tank

The channel is equipped with a hydraulically controlled piston-type wave generator, Figures 9 and 10, for generating shallow water waves. The generator proper consists of a horizontal aluminum piston with a vertical face, rigidly suspended from a rail-mounted carriage on top of the entrance box. The carriage-piston assembly is actuated by a cam-operated hydraulic servomechanism providing variation in frequency and stroke and thus wave length and height during operation of the generator.

Use of a servomechanism permits a choice of the displacement - time curve for the generator piston. Wave heights are controlled by varying the position of the cam contact point on the follower. Wave periods are controlled by varying the speed of the cam motor.

An expanded Aluminum wave filter, Figure 11, 4 feet long, is used to dampen the minor surface disturbances on the generated waves.

2. Wave Tank Equipment

The wave channel is equipped with a shock-mounted movable test stand containing a dynamic balance for measurement of lift, drag and moment on immersed bodies. Strain gage bridges are used as transducers in moment gages while differential transformers are used in the lift and drag gages. Measurement of wave profile is accomplished by means of resistance probes.

A multichannel Sanborn Model 150, direct recording oscillograph, equipped with 2400 cps, 6 volt output pre-amplifiers was used for the study. The recorder is shown in Figure 12. It is equipped with heated stylii and records four traces simultaneously on plastic coated heat sensitive paper. A fifth stylus is provided which records one second pulses along one margin. A wide choice of paper speeds are available, from 0.25 to 100 mm/sec by use of a clutch and gear shift lever arrangement. Attenuation of the amplifier output signal is provided in steps of 2 and 5 from full signal to 1/200 of full output.

3. Experimental Model

A cross section of the model is shown in Figure 13. The model was constructed in three sections. The fore and after sections being constructed of white pine and the middle body consisting of $2\frac{1}{2}$ inch outside diameter lucite tubing fitted with a drilled and tapped 1/2 inch diameter hole which was used for filling this section with a weighting substance or for attachcontrolled by varying the speed of the cam motor.

An expanded Aluminum wave filter, Figure 11, 4 feet long, is used to dampen the minor surface disturbances on the generated waves.

2. Wave Tank Equipment

The wave channel is equipped with a shore-mounted movable test stand containing a dynamic balance for measurement of lift, drag and moment on immersed bodies. Strain gage bridges are used as transducers in moment gages
gages while differential transformers are used in the lift and drag. Measurement of wave profile is accomplished by means of resistance probes.

A multichannel Sanborn model 150, direct recording oscillograph, equipped with 2400 cps, 6 volt output pre-amplifiers was used for the study. The recorder is shown in Figure 12. It is equipped with heated styli and records four traces simultaneously on plastic coated heat sensitive paper. A fifth stylus is provided which records one second pulses along one margin. A wide choice of paper speeds are available, from 0.25 to 100 mm/sec by use of a clutch and gear shift lever arrangement. Attenuation of the amplifier output signal is provided in steps of 2 and 5 from full signal to 1/200 of full output.

3. Experimental Model

A cross section of the model is shown in Figure 13. The model was constructed in three sections. The fore and after sections being constructed of white pine and the middle body consisting of 6½ inch outside diameter lucite tubing fitted with a drilled and tapped 1/2 inch diameter hole which was used for filling thissection with a weighting substance or for attach-

Figure 8. Wave tank.

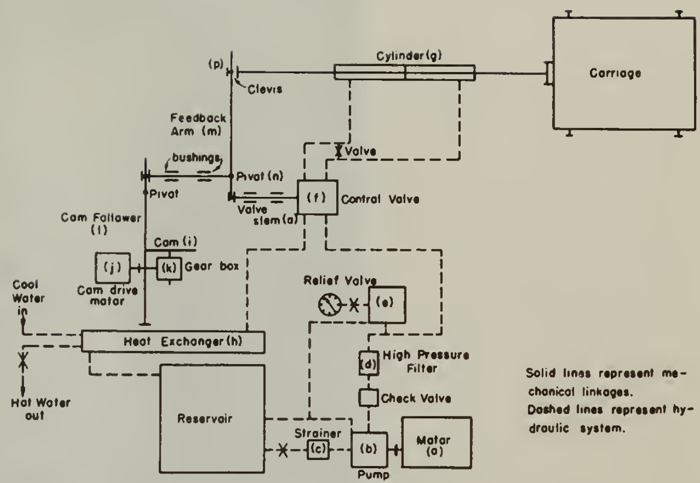

Figure 10. Schematic of wave generator.

Figure 9. Wave generator.

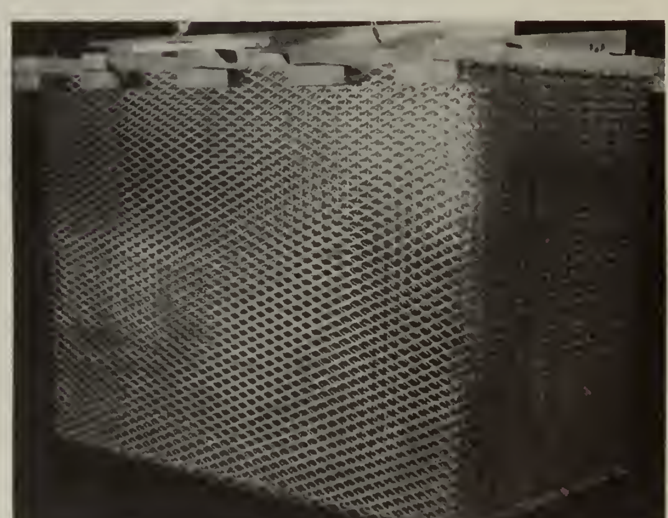

Figure 11. Wave filter.

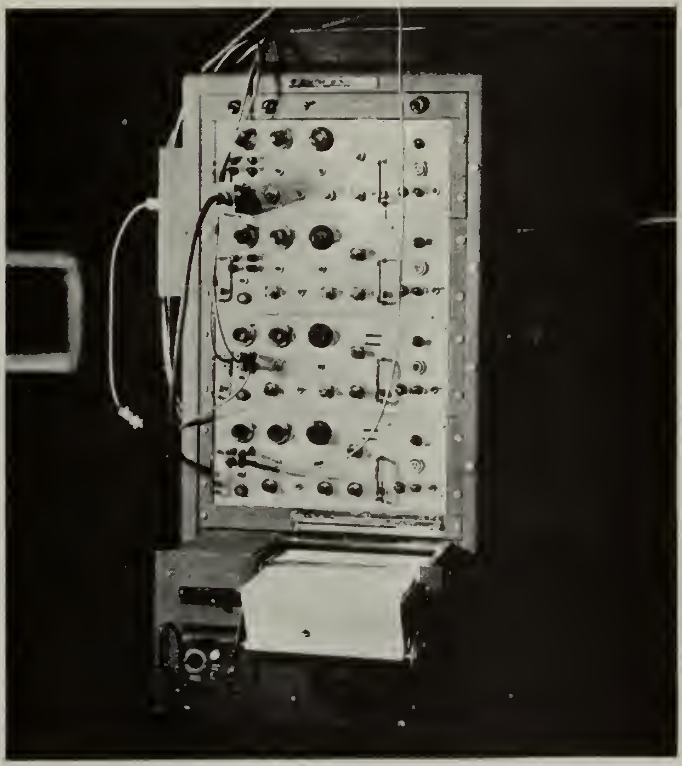

Figure 12. Test Stand and Recorder

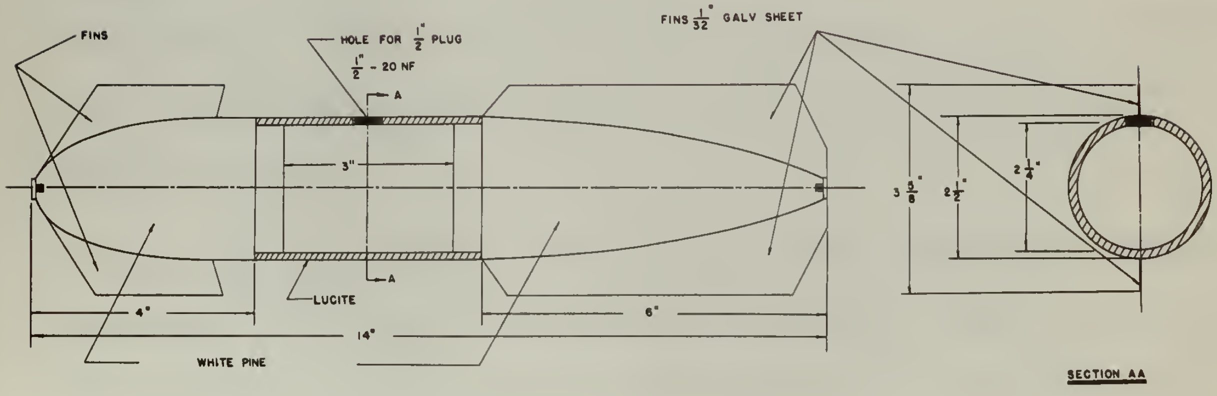

Figure 13. Test Model

ing the model to a rod for the rigidly restrained test. The three sections were joined together by press fitting. The joints were sufficiently tight to withstand testing stresses but had to be sealed with modeling clay in order to maintain water tightness. The wood fore and aft sections were fitted with mooring line attachments consisting of brass screws, fishing swivels and fishing clips. In order to reduce undesired transverse motion of the test object it was found necessary to utilize stablilizing fins. These consisted of 1/32 inch thick galvanized sheet metal shaped to conform to the contour of the body.

As stated in the introduction, it was desired to change the natural frequency of the test object by varying the weight. This was accomplished by filling the hollow lucite middle section with materials of various densities. The filler densities required to give an even gradiation of weight through eleven increments, from the model weight empty to the weight which corresponded to a condition of neutral buoyancy, were calculated. It was determined that eleven different densities varying from 0.1583 to 1.745 gms/cc would be required. To provide these mixtures of sawdust (density = 0.160 gms/cc), a commercially available dry detergent (density = 0.345 gms/cc) granulated salt (density = 1.218 gms/cc) and sand (density 1.610 gms/cc)were used. Buckshot (density 6.415 gms/cc) was added to sand to produce the highest densities.

Wire fish leader lines were used in the mooring arrangement. These are attached by fishing clips and swivels to the brass screws secured to each end of the body. A brass bolt with swivels soldered to one end served to secure the mooring lines to the mooring force balance.

ing the model to a rod for the rigidly restrained test. The three sections were joined together by press fitting. The joints were sufficiently tight to withstand bending stresses but had to be sealed with modeling clay in order to maintain water tightness. The wood fore and aft sections were fitted with mooring line attachments consisting of brass screws, fishing swivels and fishing clips. In order to reduce undesired transverse motion of the test object it was found necessary to utilize stabilizing fins. These consisted of 1/32 inch thick galvanized sheet metal shaped to conform to the contour of the body.

As stated in the introduction, it was desired to change the natural frequency of the test object by varying the weight. This was accomplished by filling the hollow lucite middle section with materials of various densities. The filler densities required to give an even gradation of weight through eleven increments, from the model weight empty to the weight which corresponded to a condition of neutral buoyancy, were calculated. It was determined that eleven different densities varying from 0.1583 to 1.745 gms/cc would be required. To provide these mixtures of sawdust (density = 0.150 gms/cc), a commercially available dry detergent (density = 0.345 gms/cc) granulated salt (density = 1.218 gms/cc) and sand (density 1.610 gms/cc) were used. Buckshot (density 6.415 gms/cc) was added to sand to produce the highest densities.

Wire fish leader lines were used in the mooring arrangement. These are attached by fishing clips and swivels to the brass screws secured to each end of the body. A brass bolt with swivels soldered to one end served to secure the mooring lines to the mooring force balance.

For the rigidly restrained tests, the body was supported from the test stand as shown in Figures 14 and 15. The 3/4 inch support rod was not shielded and separate "tare" runs for each restrained test were made in order to determine both horizontal and vertical forces due to the rod alone so that these could be deducted from the net force measured with the body attached.

4. Instrumentation

a. Wave Characteristics

The wave characteristics of primary importance in this study were the wave height and period. A complete wave profile was also required to relate the experimental force histories to the wave phase angle. Wave characteristics were measured electronically by a resistance type wave gage shown schematically in Figure 16. The active elements of the gage are two vertical platinum wires, insulated from each other. When they are partially immersed in water a flow of current occurs between them which is proportional to the depth of immersion. The wave gage was calibrated before each series of test runs.

b. Forces on Rigidly Restrained Objects

Horizontal wave force components on the model were measured by means of a shear balance hereafter referred to as the portal gage. Figures 17 and 18 show the portal gage which consists of two vertical parallel webs clamped between two rigid horizontal plates. The horizontal component of the force on the object is transmitted in shear to the lower plate of the portal gage, which moves horizontally an amount directly proportional to the force on the object. A Schaevitz Linear Variable Differential Transformer is used to convert the displacement of the bottom gage plate relative to the top plate into an electrical signal which is amplified and recorded.

For the rigidly restrained tests, the body was supported from the test stand as shown in Figures 14 and 15. The 3/4 inch support rod was not shielded and appropriate "tare" runs for each restrained test were made in order to determine both horizontal and vertical forces due to the rod alone so that these could be deducted from the net force measured with the body attached.

4. Instrumentation

a. Wave Characteristics

The wave characteristics of primary importance in this study were the wave height and period. A complete wave profile was also required to relate the experimental force histories to the wave phase angle. Wave characteristics were measured electronically by a resistance type wave gage shown schematically in Figure 16. The active elements of the gage are two vertical platinum wires, insulated from each other. When they are partially immersed in water a flow of current occurs between them which is proportional to the depth of immersion. The wave gage was calibrated before each series of test runs.

b. Forces on Rigidly Restrained Objects

Horizontal wave force components on the model were measured by means of a shear balance transducer referred to as the portal gage. Figures 17 and 18 show the portal gage which consists of two vertical parallel webs clamped between two rigid horizontal plates. The horizontal component of the force on the object is transmitted in shear to the lower plate of the portal gage, which moves horizontally an amount directly proportional to the force on the object. A Schaevitz Linear Variable Differential Transformer is used to convert the displacement of the bottom gage plate relative to the top plate into an electrical signal which is amplified and recorded.

Figure 14. Rigidly Restrained Test Arrangement

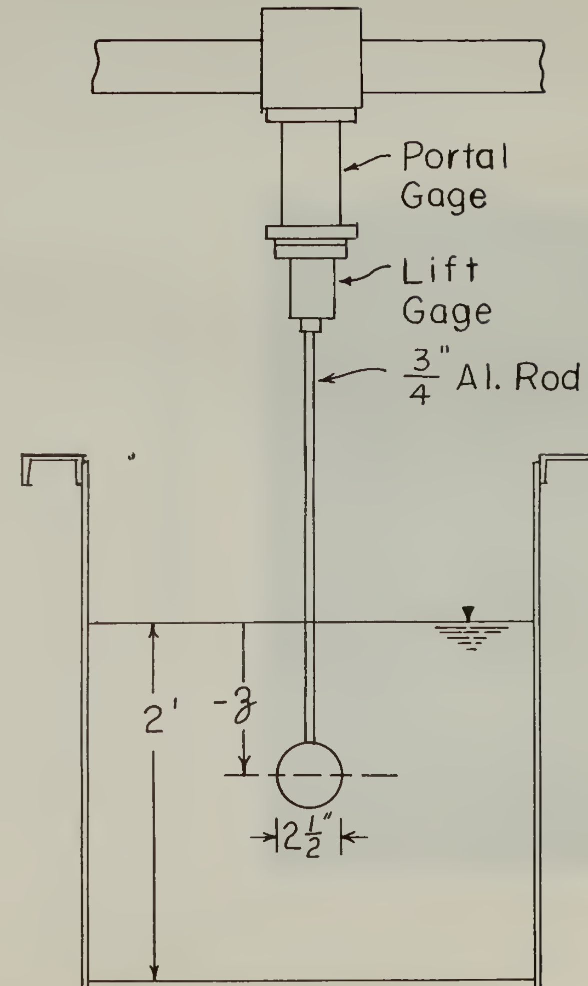

Figure 15. Schematic of Rigidly Restrained Test Arrangement

a) Photograph

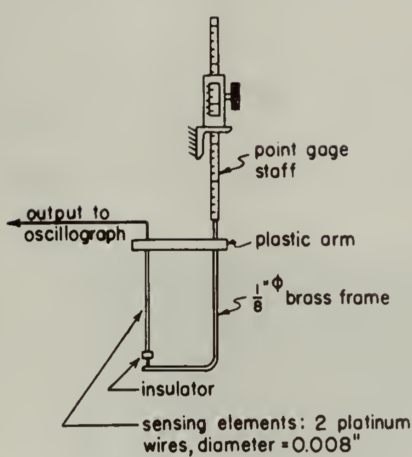

b) Schematic of Wave Gage

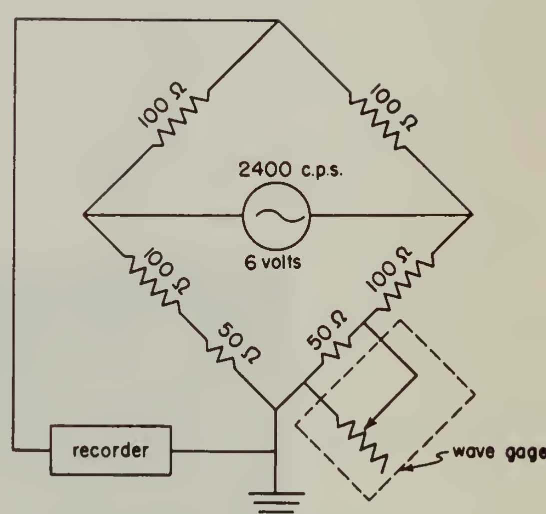

c) Circuit Diagram

Fig.16. Resistance Wave Gage.

Figure 17. Portal Gage

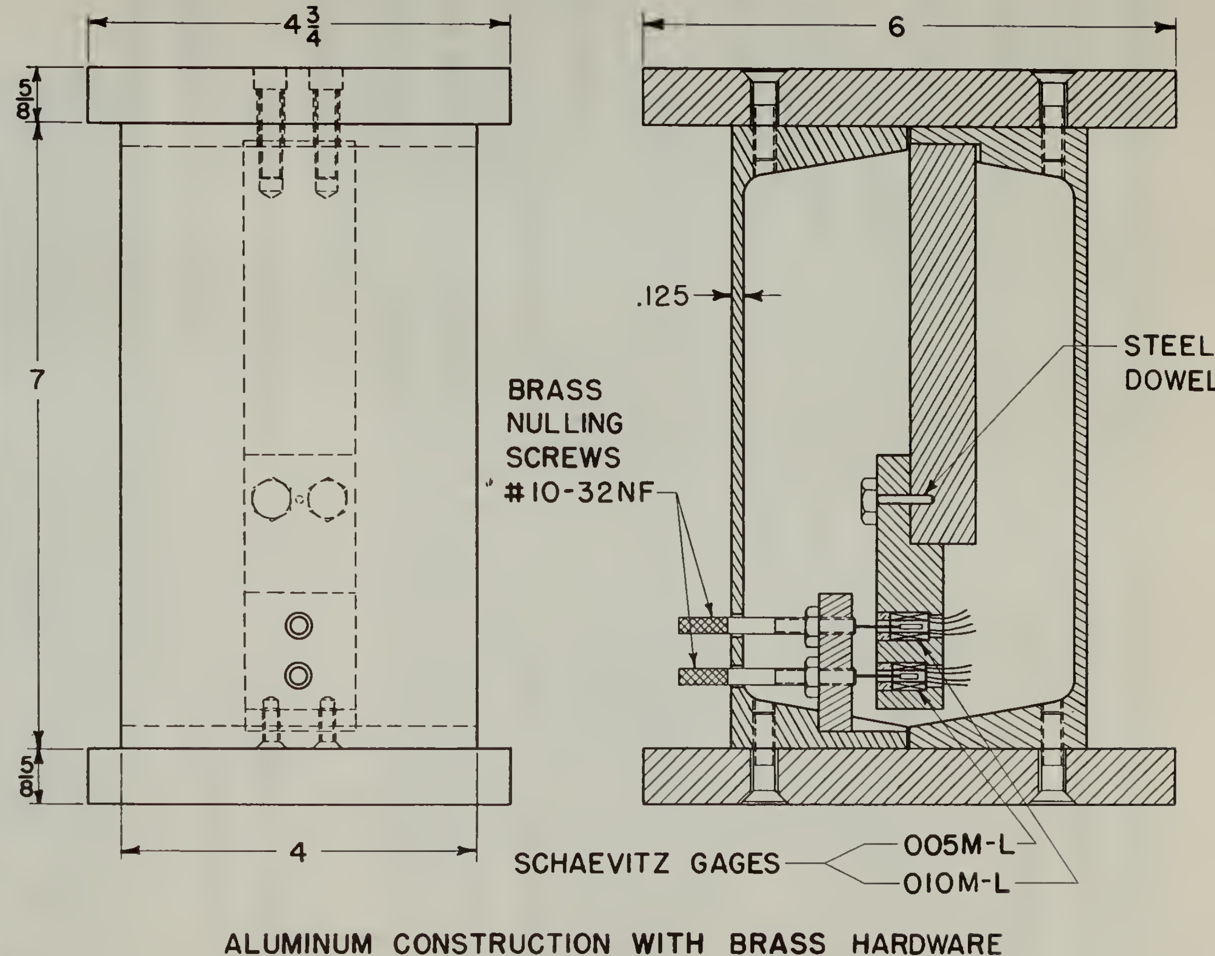

Figure 18. Portal Gage Schematic

This design of the portal gage results in a high resistance to bending deflections. Thus, the gage is for all practical purposes insensitive to bending moment and produces an output independent of the distance between the gage and the point of application of the force.

The gage was calibrated statically by means of a pulley system and has a sensitivity of 21 mm/lb at an attenuation of x20 referred to the Sanborn recorderfor which full scale is $\pm$25 mm.

Vertical wave force components were measured by a Lift Gage. Figures 19 and 20. The force on the object is transmitted to the gage by an aluminum rod clamped rigidly to the body of the gage. The vertical force causes the center part of the gage to move vertically with respect to the gage body This motion is converted to an electrical output by means of a Type 0.005M-L Schaevitz L.V.D.T.

The gage was calibrated statically by attaching weights to the object support rod installed below it. It has a sensitivity referred to the recorder of 21 mm/lb at an attenuation of x10.

c. Forces on Partially Restrained Objects

A two component force balance, Figures 21 and 22, was used in the experiments to measure both the horizontal and vertical components of mooring line tension. This balance was constructed on the force beam principle. It consists of two force beams perpendicular to one another, each with its own four active arm strain gage bridge. The horizontal outer beam is sensitive to the vertical component and the inner vertical beam is sensitive to the horizontal component of force.

This design of the portal gage results in a high resistance to bending deflections. Thus, the gage is for all practical purposes insensitive to bending moment and produces an output independent of the distance between the gage and the point of application of the force.

The gage was calibrated statically by means of a pulley system and has a sensitivity of 21 mm/lb at an attenuation of x20 referred to the Sanborn recorder for which full scale is ±25 mm.

Vertical wave force components were measured by a Lift Gage. Figures 19 and 20. The force on the object is transmitted to the gage by an aluminum rod clamped rigidly to the body of the gage. The vertical force causes the center part of the gage to move vertically with respect to the gage body This motion is converted to an electrical output by means of a Type 0.005M-L Schaevitz L.V.D.T.

The gage was calibrated statically by attaching weights to the object support rod installed below it. It has a sensitivity referred to the recorder of 21 mm/lb at an attenuation of x10.

c. Forces on Partially Restrained Objects

A two component force balance, Figures 21 and 22, was used in the experiments to measure both the horizontal and vertical components of mooring line tension. This balance was constructed on the force beam principle. It consists of two force beams perpendicular to one another, each with its own four active arm strain gage bridge. The horizontal outer beam is sensitive to the vertical component and the inner vertical beam is sensitive to the horizontal component of force.

Figure 19. Lift Gage

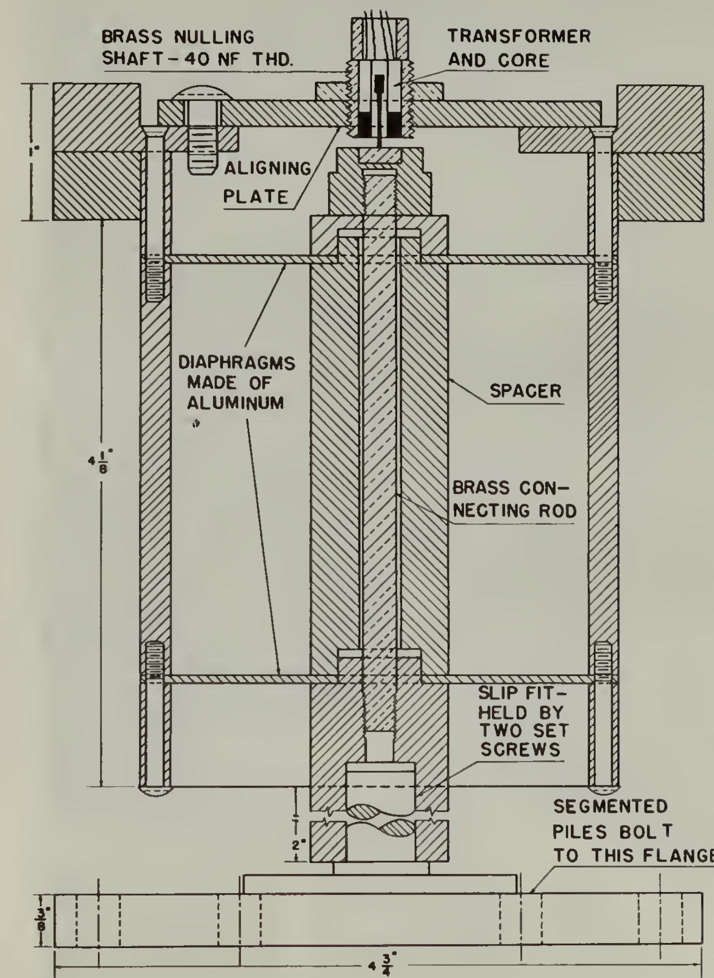

Figure 20. Lift Gage Schematic

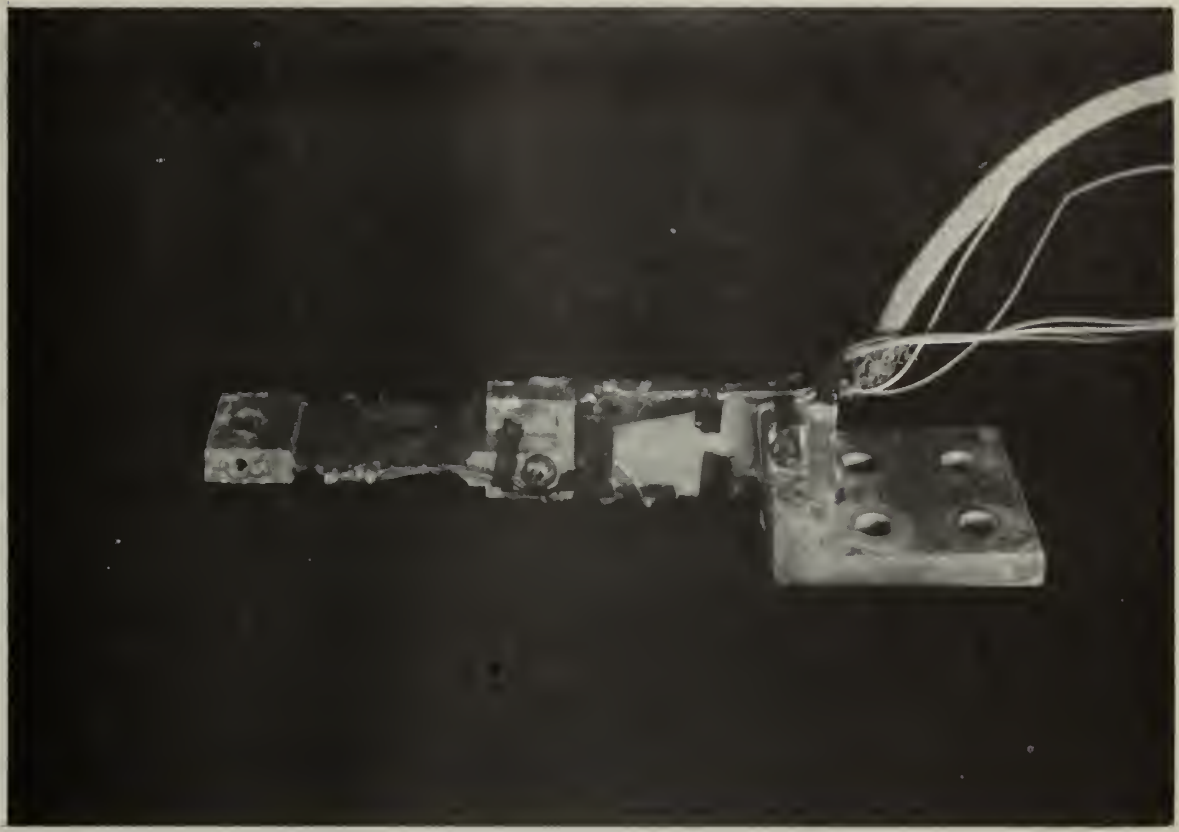

Figure 21. Two Component Balance

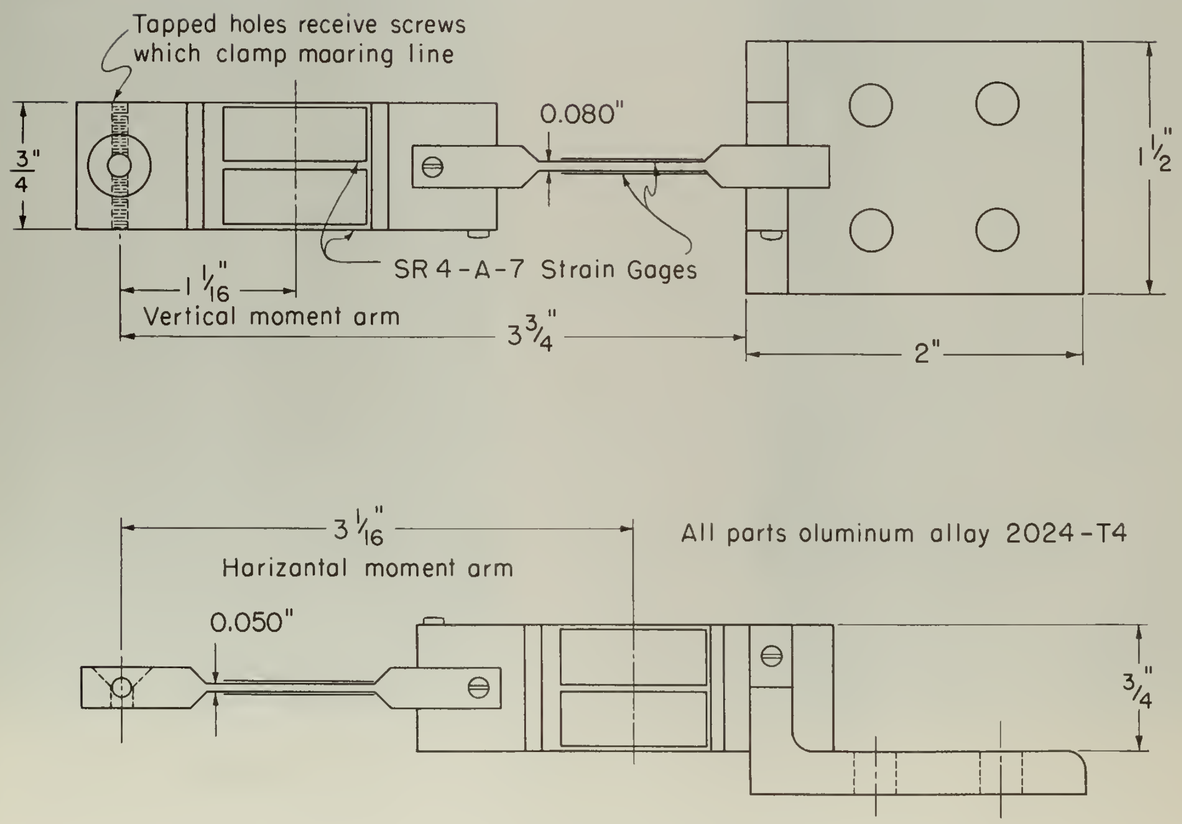

Figure 22. Two Component Balance Schematic

The sensitivity and deflection characteristics of the two component balance are as follows:

Horizontal:	Sensitivity	27 mm/lb at x 20
	Deflection	0.07 in/lb
Vertical:	Sensitivity	24 mm/lb at x 10
	Deflection	0.019 in/lb

The two component force balance was calibrated using a pulley system with the calibration line at an angle of 45^o. In this way, the two portions of the gage were calibrated simultaneously, the force applied to each being equal to $1/\sqrt{2}$ times the applied load. Sample calibrations are given in Figure 23.

The two component balance was attached to an aluminum bar, Figure 24, which in turn was bolted to the bottom of the flume.

The sensitivity and deflection characteristics of the two component balance are as follows:

Horizontal:	Sensitivity	27 mm/lb at x 20
	Deflection	0.07 in/lb
Vertical:	Sensitivity	24 mm/lb at x 10
	Deflection	0.019 in/lb

The two component force balance was calibrated using a pulley system with the calibration line at an angle of 45°. In this way, the two portions of the gage were calibrated simultaneously, the force applied to each being equal to $\sqrt{2}$ times the applied load. Sample calibrations are given in Figure 23.

The two component balance was attached to an aluminum bar, Figure 24, which in turn was bolted to the bottom of the flume.

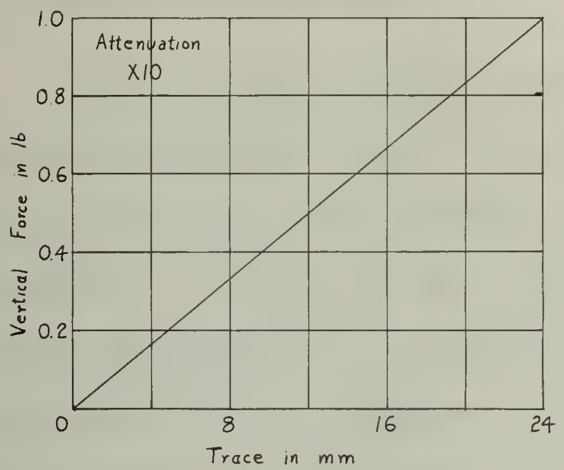

Figure 23. Two Component Balance, Sample Calibration Curve

Figure 24. Two Component Balance Holder

Figure 25. Test in Progress

IV TEST PROCEDURE

1. Rigidly Restrained Tests

For each series of runs at a specified object centerline depth a corresponding rigidly restrained test was conducted. The water level in the wave tank was maintained at two feet for all tests. By using various combinations of sections of the 3/4" aluminum support rod the object was located at the proper depth with respect to the free surface. The force gages were calibrated prior to each run at the expected attenuations. Two resistance type wave gages were used in all tests, one at the test stand and the other one wavelength downstream. The wave generator control settings, necessary to produce waves of the desired dimensions, had been previously established by experiment, minor adjustments were made as necessary prior to each run. The wave height was checked by a wave gage which was calibrated prior to each series of runs. Wave period was checked from the wave gage trace by counting the number of waves in 50^{mm} of record at a paper speed of 1^{mm} per second. Proper wave period and wavemaker stroke established proper wave height - and length.

The electronic gage circuits were balanced and zeroed with the test object in place and the wave generator was started. The test was run after a final check of the wave height and period. A test consisted of ten consecutive waves with the recorder run at 50^{mm} per second. Upon completion of the test, the wave generator was stopped but data recording was continued at a reduced paper speed until the water in the flume became calm. This was done to see if any shift in the force trace zero readings had occurred in the course of the test. A tare run was made in connection with each

rigidly restrained test in order to measure forces on the support alone so that these could later be subtracted from the net force measured during the test.

2. Partially Restrained Tests

In preparation for the partially restrained tests, the two component mooring force balance holder was fixed in place in the wave tank and was calibrated. A resistance wave gage was secured at the same channel location as the force balance and another wave gage was located one wave length downstream. The hollow middle section of the test object was filled with the proper filler mixture, weighed, and connected to the force balance.

Prior to each run, a natural frequency determination was made. This was done by manually displacing the test object from its equilibrium position in still water and releasing it. As the object oscillated, a record was made of the horizontal mooring force component at slow paper speed. The natural frequency was determined from the number of oscillations in a given length of record.

The wave height and period were adjusted before each run and the test was then conducted in a manner similar to the rigidly restrained tests. Preliminary data reduction was conducted during the course of each run to detect errors and insure an even spacing of the experimental data points. A test in progress is shown in Figure 25.

As in the rigidly restrained tests, the depth of water in the tank was maintained at two feet for all runs. There were twelve runs at each of the three separate mooring depths. The use of fishing clips facilitated changing of the mooring lines.

rigidly restrained test in order to measure forces on the support alone so that these could later be subtracted from the net force measured during the test.

2. Partially Restrained Tests

In preparation for the partially restrained tests, the two component mooring force balance holder was fixed in place in the wave tank and was calibrated. A resistance wave gage was secured at the same channel location as the force balance and another wave gage was located one wave length downstream. The hollow middle section of the test object was filled with the proper filler mixture, weighed and connected to the force balance.

Prior to each run, a natural frequency determination was made. This was done by manually displacing the test object from its equilibrium position in still water and releasing it. As the object oscillated, a record was made of the horizontal mooring force component at slow paper speed. The natural frequency was determined from the number of oscillations in a given length of record.

The wave height and period were adjusted before each run and the test was then conducted in a manner similar to the rigidly restrained tests. Preliminary data reduction was conducted during the course of each run to detect errors and insure an even spacing of the experimental data points. A test in progress is shown in Figure 25.

As in the rigidly restrained tests, the depth of water in the tank was maintained at two feet for all runs. There were twelve runs at each of the three separate mooring depths. The use of fishing clips facilitated changing of the mooring lines.

V EVALUATION OF DATA

1. Primary Data Reduction

a. Natural Frequency Data

Natural frequencies were determined from horizontal mooring line tension component traces made with the test object in free oscillation. A sample free oscillation record is presented in Figure 26. The average natural frequency of 20 or more oscillations was obtained by the use of the following formula:

$$\text{Natural Frequency} = \frac{\text{No. of oscillations in } 50^{mm} \times \text{Paper Speed}(mm/_{sec})}{50}$$

Application of the above formula to different portions of the free oscillation record showed the natural frequency to be independent of the amplitude of free oscillation but less reliance was placed on the measurements as the amplitude of the oscillations became small and died out.

b. Wave and Force Data

Most of the experimental data in this study were obtained in the form of oscillograph records. Figure 27 is a portion of an oscillograph test record. The data recorded are the wave traces at the object and one wave length downstream from the object, and the horizontal and vertical mooring line tension components.

Primary reduction of the test records consisted of determining the wave period and maximum force component values. Where required, the complete force component histories were obtained from the records. The wave period was determined from the portion of the record run at slow speed using the following formulae.

$$\text{Wave Frequency} = \frac{\text{Number of waves in } 50^{mm} \times \text{paper speed (mm/sec)}}{50}$$

$$\text{Period} = \frac{1}{\text{frequency}}$$

V EVALUATION OF DATA

1. Primary Data Reduction

a. Natural Frequency Data

Natural frequencies were determined from horizontal mooring line tension component traces made with the test object in free oscillation. A sample free oscillation record is presented in Figure 26. The average natural frequency of 20 or more oscillations was obtained by the use of the following formula:

$$\text{Natural Frequency} = \frac{\text{No. of oscillations in } 50^{mm} \times \text{Paper Speed}(mm/sec)}{50}$$

Application of the above formula to different portions of the free oscillation record showed the natural frequency to be independent of the amplitude of free oscillation but less reliance was placed on the measurements as the amplitude of the oscillations became small and died out.

b. Wave and Force Data

Most of the experimental data in this study were obtained in the form of oscillograph records. Figure 27 is a portion of an oscillograph test record. The data recorded are the wave traces at the object and one wave length downstream from the object, and the horizontal and vertical mooring line tension components.

Primary reduction of the test records consisted of determining the wave period and maximum force component values. Where required, the complete force component histories were obtained from the records. The wave period was determined from the portion of the record run at slow speed using the following formulae.

$$\text{Wave Frequency} = \frac{\text{Number of waves in } 50^{mm} \times \text{paper speed } (mm/sec)}{50}$$

$$\text{Period} = \frac{1}{\text{Frequency}}$$

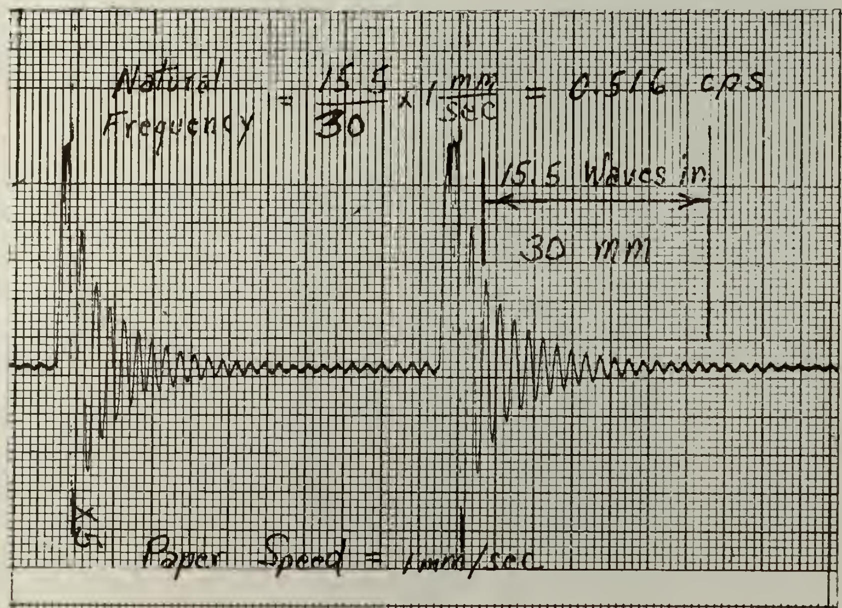

Figure 26. Free Oscillation Record

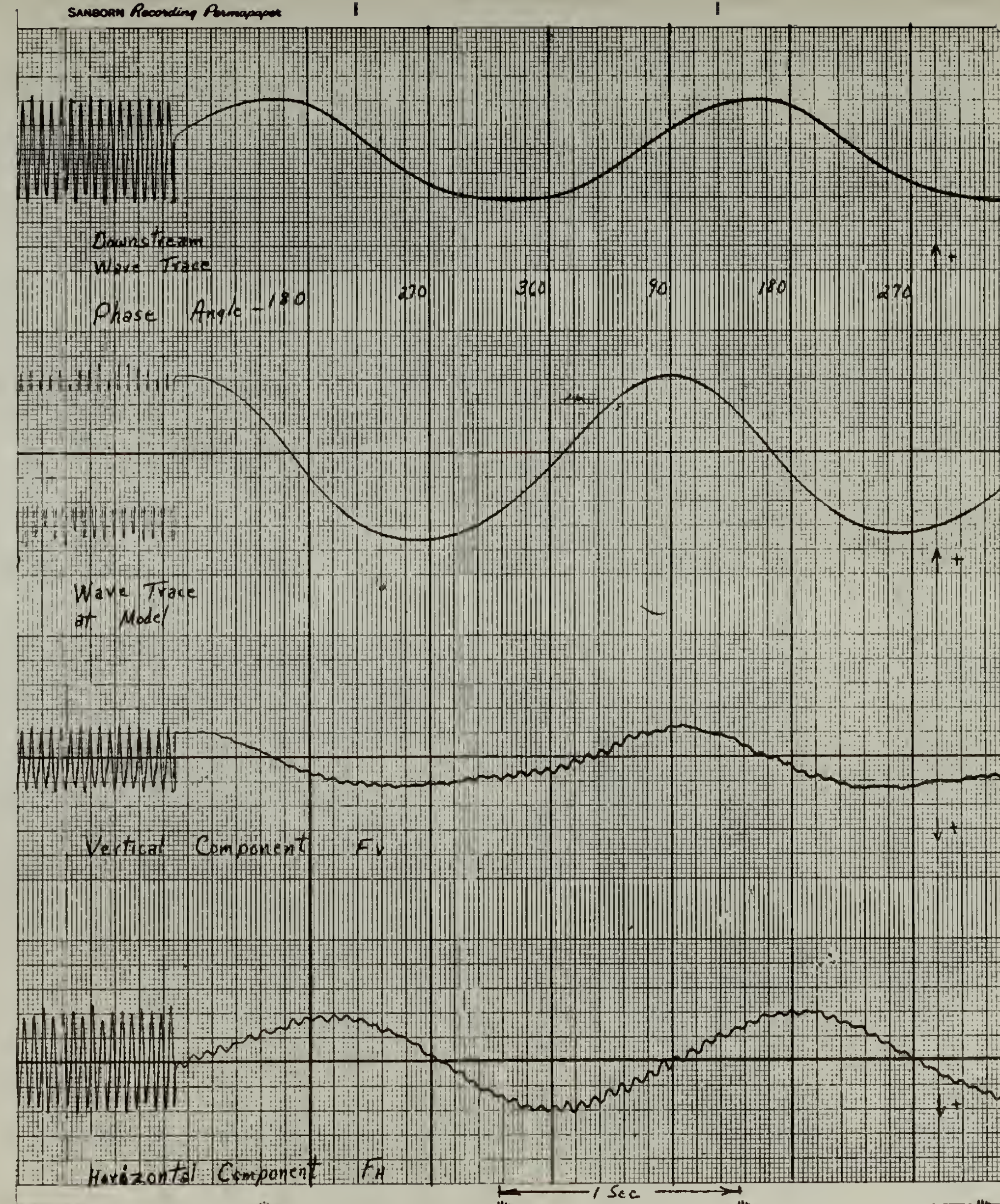

Figure 27. Sample Test Record

The wave period desired for all runs was 2 seconds per cycle. This value was maintained to within ± 2% by careful measurement in accordance with the above formulae before each run.

The maximum force values for each run were determined by averaging the maxima for a number of waves and converting the resulting value to force units by means of the force balance calibration curve. In order to obtain the entire force history from the test record, it was first necessary to construct a wave phase angle scale on the force record. This was done by locating successive crests on the trace and dividing the distance between them into even increments, usually 90^{o} increments were sufficient. The forces corresponding to a desired phase angle could then be read from the trace at each location. For a desired force history the average of several waves was employed to compensate for small differences between successive waves resulting from unevenness in the wave generator operation. The final step in the procedure was the conversion of the average trace readings to force units by means of the force balance calibration curves.

2. Secondary Data Reduction

a. Rigidly Restrained Tests

The rigidly restrained tests yielded oscillograph records similar to the ones shown in Figure 27. The data recorded included wave traces at the object and one wavelength downstream, and the total horizontal and vertical wave force components on test object and support rod. Tare tests on the support rod alone provided the necessary data to reduce, from the gross measured force, the net wave force component history due to the presence of the body.

The wave period desired for all runs was 2 seconds per cycle. This value was maintained to within $\pm 2\%$ by careful measurement in accordance with the above formulae before each run.

The maximum force values for each run were determined by averaging the maxima for a number of waves and converting the resulting value to force units by means of the force balance calibration curve. In order to obtain the entire force history from the test record, it was first necessary to construct a wave phase angle scale on the force record. This was done by locating successive crests on the trace and dividing the distance between them into even increments, usually 90° increments were sufficient. The forces corresponding to a desired phase angle could then be read from the trace at each location. For a desired force history the average of several waves was employed to compensate for small differences between successive waves resulting from unevenness in the wave generator operation. The final step in the procedure was the conversion of the average trace readings to force units by means of the force balance calibration curves.

2. Secondary Data Reduction

a. Rigidly Restrained Tests

The rigidly restrained tests yielded oscillograph records similar to the ones shown in Figure 27. The data recorded included wave traces at the object and one wavelength downstream, and the total horizontal and vertical wave force components on test object and support rod. Tare tests on the support rod alone provided the necessary data to reduce, from the gross measured force, the net wave force component history due to the presence of the body.

From the horizontal wave force component history on the stationary object experimental inertia and drag force coefficients were determined making use of equations presented in the theoretical development. These are repeated for convenience.

$$FHo = FHI + FHD \tag{6}$$

or as given by equation (9)

$$FHo = Cm \; \rho \, Vol \left(\frac{du}{dt}\right)_m \cos \sigma t + C_D \; \frac{\rho}{2} \, Area \; U_m^2 \left| \sin \sigma t \right| \sin \sigma t \tag{9}$$

Equations (1) and (3) define u and $\left(\frac{du}{dt}\right)$ respectively.

At $\sigma t = 0^{\circ}$ and 180° FH_D is zero by equation (9)

and the quantity C_m may be expressed in terms of FH_o which can be read directly from the force trace history. At $\sigma t = 90^{\circ}$ and 270° FHi is zero and equation (9) can be solved for C_D in terms of FH_o. These calculations were performed in order to provide values for comparison with the potential flow theory inertia coefficient and steady state drag coefficient as determined by the means outlined in the following paragraph.

Values for the drag coefficient were also found by measurement of the decremental decay of the natural frequency tests and application of equation (57) of the theoretical development.

b. Partially Restrained Tests

By using the average of at least ten waves the maximum total force components, both vertical and horizontal, were obtained from the oscillograph records for each run.

For several of the partially restrained tests the mooring line angle was determined from the experimental data. As seen in Figure 6, the angle

From the horizontal wave force component history on the stationary object experimental inertia and drag force coefficients were determined making use of equations presented in the theoretical development. These are repeated for convenience.

$$FHo = FHI + FHD \qquad (6)$$

or as given by equation (9)

$$FHo = Cm\,\rho\,Vol\left(\frac{du}{dt}\right)_m \cos\sigma t + C_D\,\frac{\rho}{2}\,Area\,U_m^2\,|\sin\sigma t|\,\sin\sigma t \qquad (9)$$

Equations (1) and (3) define u and $\left(\frac{du}{dt}\right)$ respectively.

At $\sigma t = 0^\circ$ and 180° FH_D is zero by equation (9) and the quantity C_m may be expressed in terms of FH_o which can be read directly from the force trace history. At $\sigma t = 90^\circ$ and 270° FHI is zero and equation (9) can be solved for C_D in terms of FH_o. These calculations were performed in order to provide values for comparison with the potential flow theory inertia coefficient and steady state drag coefficient as determined by the means outlined in the following paragraph.

Values for the drag coefficient were also found by measurement of the decremental decay of the natural frequency tests and application of equation (57) of the theoretical development.

b. <u>Partially Restrained Tests</u>

By taking the average of at least ten waves the maximum total force components, both vertical and horizontal, were obtained from the oscillograph records for each run.

For several of the partially restrained tests the mooring line angle was determined from the experimental data. As seen in Figure 6, the angle is related to the mooring line tension components by the equation

$$\psi = \tan^{-1} \left(\frac{F_H}{F_V + N}\right) \tag{58}$$

where FH can be measured from the experimental record and $F_v + N$ is approximately equal to the net buoyancy of the object for a given run.

VI PRESENTATION AND DISCUSSION OF RESULTS

1. Rigidly Restrained Tests

The purpose of the rigidly restrained tests is to establish the theoretical condition of force for the ratio $f/f_h = 0$. The maximum rigidly restrained force is, in addition, a parameter in the determination of the damping factor η_2, equation (38)

The maximum positive and negative experimental net forces on the body are not equal although the theoretical force equation (9), and the equivalent expression for vertical force, yield equal positive and negative maxima. The results, in this case however, are not surprising in view of the unsymmetrical fore and aft shape of the body. The difference will be taken into account in the formation of experimental force multiplication factors for the dynamic tests where both positive and negative factors will be calculated using the appropriate static test results.

The principal results of the rigidly restrained tests, the horizontal and vertical component maxima, both positive and negative, are presented in Table IV. For later use in theoretical calculations, the average maximum values were computed and are also tabulated.

VI PRESENTATION AND DISCUSSION OF RESULTS

1. Rigidly Restrained Tests

The purpose of the rigidly restrained tests is to establish the theoretical condition of force for the ratio $f/f_n = 0$. The maximum rigidly restrained force is, in addition, a parameter in the determination of the damping factor η_e, equation (35).

The maximum positive and negative experimental net forces on the body are not equal although the theoretical force equation (9), and the equivalent expression for vertical force, yield equal positive and negative maxima. The results, in this case however, are not surprising in view of the unsymmetrical fore and aft shape of the body. The difference will be taken into account in the formation of experimental force multiplication factors for the dynamic tests where both positive and negative factors will be calculated using the appropriate static test results.

The principal results of the rigidly restrained tests, the horizontal and vertical component maxima, both positive and negative, are presented in Table IV. For later use in theoretical calculations, the average maximum values were computed and are also tabulated.

TABLE IV MAXIMUM RIGIDLY RESTRAINED FORCES

	Horizontal			Vertical		
Test	Pos (lbs)	Neg (lbs)	Ave (lbs)	Pos (lbs)	Neg (lbs)	Ave (lbs)
1-12	0.1142	0.1100	0.1121	0.0968	0.0859	0.0914
13-23	0.1133	0.1102	0.1118	0.0484	0.0386	0.0435
24-35	0.1102	0.0882	0.0992	0.0242	0.0198	0.0220

From the experimental horizontal force component histories inertia and drag coefficients were calculated, through the use of equation (9) and the method outlined in Chapter V. The values for the inertia coefficients agree favorably with the value predicted by potential theory, that is $C_m = 1.053$. As previously noted, however, drag coefficients computed in this manner may be subject to excessive error due to the low drag conditions indicated by the period parameters; they were in fact, found to be much higher than would appear reasonable. The average value will be compared to the average drag coefficient computed from the decremental decay found in the observation of natural frequencies.

The results of these calculations are presented in Table V along with the period parameters and the effective Reynolds number of each series of tests.

TABLE IV MAXIMUM RIGIDLY RESTRAINED FORCES

Test	Horizontal Pos (lbs)	Neg (lbs)	Ave (lbs)	Vertical Pos (lbs)	Neg (lbs)	Ave (lbs)
1-12	0.1142	0.1100	0.1121	0.0968	0.0859	0.0914
13-23	0.1133	0.1102	0.1118	0.0484	0.0386	0.0435
24-35	0.1102	0.0882	0.0992	0.0242	0.0198	0.0220

From the experimental horizontal force component histories inertia and drag coefficients were calculated, through the use of equation (9) and the method outlined in Chapter V. The values for the inertia coefficients agree favorably with the value predicted by potential theory, that is $C_m = 1.053$. As previously noted, however, drag coefficients computed in this manner may be subject to excessive error due to the low drag conditions indicated by the period parameters; they were in fact, found to be much higher than would appear reasonable. The average value will be compared to the average drag coefficient computed from the decremental decay found in the observation of natural frequencies.

The results of these calculations are presented in Table V along with the period parameters and the effective Reynolds number of each series of tests.

TABLE V EXPERIMENTAL COEFFICIENTS OF INERTIA AND DRAG

Test	Um T/D	$N_{R\,mean}$	Cm Eq (9) ave value	C_D Eq (9) ave value
1-12	5.62	1.758×10^4	1.077	1.830
13-23	5.15	1.270×10^4	1.070	1.460
24-35	4.57	5.450×10^3	1.073	1.004

2. Partially Restrained Tests

a. Natural Frequencies

For each partially restrained test, a natural frequency measurement was made. The experimental natural frequencies are plotted against total weight for each of the three series of test runs in Figure 28. Also shown are the theoretical undamped natural frequencies computed from equation (28) as shown in Appendix A. For these computations an added mass coefficient of 0.05, the potential flow value was used. Good agreement between theory and experiment was obtained.

b. Coefficients of Drag from Natural Frequency

A persistent problem in this investigation was the establishment of an accurate value for the drag coefficient of the test body. The data presented by Rouse, which has been previously cited, is for a body of similar shape but is of dubious value, except for comparative purposes, since it is for the case of steady translational flow past the object. When moored and subject to wave motion the body continually presents a different orientation with respect to the direction of flow. In addition the test object was equipped with mooring appendages and rather large fins which undoubtedly acted to

TABLE V EXPERIMENTAL COEFFICIENTS OF INERTIA AND DRAG

Test	$U_m T/D$	$R_{e\,max}$	Cm Eq (9) ave value	CD Eq (9) ave value
1-12	5.62	1.758×10^4	1.077	1.830
13-23	5.15	1.270×10^4	1.070	1.460
24-35	4.57	5.450×10^3	1.073	1.004

2. Partially Restrained Tests

a. Natural Frequencies

For each partially restrained test, a natural frequency measurement was made. The experimental natural frequencies are plotted against total weight for each of the three series of test runs in Figure 28. Also shown are the theoretical undamped natural frequencies computed from equation (28) as shown in Appendix A. For these computations an added mass coefficient of 0.05, the potential flow value was used. Good agreement between theory and experiment was obtained.

b. Coefficients of Drag from Natural Frequency

A persistent problem in this investigation was the establishment of an accurate value for the drag coefficient of the test body. The data presented by Rouse, which has been previously cited, is for a body of similar shape but is of dubious value, except for comparative purposes, since it is for the case of steady translational flow past the object. When moored and subject to wave motion the body continually presents a different orientation with respect to the direction of flow. In addition the test object was equipped with mooring appendages and rather large fins which undoubtedly acted to increase the drag effect.

To aid in establishing as accurate as possible a value for the coefficient of drag the data from several natural frequency observations were applied in equation (57). Only those runs at the lighter test object weights were used since the assumption that the vertical component of mooring line force is equal to the net buoyancy N, becomes less valid as the test object becomes heavier.

The results of these calculations are given in Table VI. A sample calculation is presented in Appendix B.

TABLE VI EXPERIMENTAL COEFFICIENTS OF DRAG FROM NATURAL FREQUENCY AMPLITUDE DECAY

Run	Centerline Depth ft.	Radius of Oscillation (ft)	Object Weight (lbs)	C_D Eq (57)
1	0.291	1.540	.988	.385
2	0.291	1.540	1.100	.335
3	0.291	1.540	1.139	.280
13	0.720	1.112	.966	.506
14	0.720	1.112	1.070	.480
15	0.720	1.112	1.125	.399
Extra Run	1.020	0.813	1.503	.546
24	1.352	0.479	.988	1.66
25	1.352	0.479	1.100	1.66
26	1.352	0.479	1.139	1.55

The coefficient of drag obtained from the above calculations shows marked dependence on the radius of oscillation and to a less extent on the weight of the body as seen in Figure 29. The latter effect may be explained as a result increase the drag effect.

To aid in establishing as accurate as possible a value for the coefficient of drag the data from several natural frequency observations were applied in equation (57). Only those runs at the lighter test object weights were used since the assumption that the vertical component of mooring line force is equal to the net buoyancy B, becomes less valid as the test object becomes heavier.

The results of these calculations are given in Table VI. A sample calculation is presented in Appendix E.

TABLE VI EXPERIMENTAL COEFFICIENTS OF DRAG FROM NATURAL FREQUENCY AMPLITUDE DECAY

Run	Centerline Depth Ft.	Radius of Oscillation (ft)	Object Weight (lbs)	C_d Eq (57)
1	0.291	1.540	.963	.285
2	0.291	1.540	1.100	.335
3	0.291	1.540	1.139	.280
13	0.720	1.112	.956	.506
14	0.720	1.112	1.070	.480
15	0.720	1.112	1.125	.399
Extra Run	1.020	0.813	1.503	.546
24	1.352	0.479	.988	1.66
25	1.352	0.479	1.100	1.66
26	1.352	0.479	1.139	1.55

The coefficient of drag obtained from the above calculations shows marked dependence on the radius of oscillation and to a less extent on the weight of the body as seen in Figure 29. The latter effect may be explained as a result of the assumption that vertical component of mooring line force is equal to net buoyancy becoming less valid as the test object becomes heavier. The average value of C_D for the rigidly restrained body from Table V is 1.432 but there is no apparent relation between this value and C_D for the partially restrained oscillating body. The agreement between C_D in Table VI and the average steady state value of 0.095 from Table III is best at the largest radius becoming poor as "ℓ" diminishes. It appears that for very large radii of oscillation the coefficient of drag for the oscillating body will tend to approach the steady state value as a limit. An attempt will be made to account for this phenomena in the following chapter. The average value for C_D associated with each centerline depth from Table VI was used in the calculations which follow and provided good correlation between theory and experimental data.

c. Force Multiplication Factors

For each test made in this study, horizontal and vertical force multiplication factors were computed from the maximum experimental force components and are tabulated in Appendix C. The horizontal multiplication factors are plotted against frequency ratio in Figures 30 through 32. There is a separate plot for each length of mooring line. In each of these figures, the experimental points define resonance curves of the form of Figure 4. The theoretical curve, computed from equations (16) and (17), is presented as a solid line in each of these Figures. A sample calculation is shown in Appendix A. In all computations an inertial coefficient $C_m \doteq 1.05$ was used. The theoretical curves do not fall on a single line in Figure 4 since these curves are drawn for constant values of damping factor n_2 and this factor varies with the frequency ratio due to the method of conducting tests.

of the assumption that vertical component of mooring line force is equal to net buoyancy becoming less valid as the test object becomes heavier. The average value of C_D for the rigidly restrained body from Table V is 1.432 but there is no apparent relation between this value and C_D for the partially restrained oscillating body. The agreement between C_D in Table VI and the average steady state value of 0.955 from Table III is best at the largest radius becoming poor as ℓ'' diminishes. It appears that for very large radii of oscillation the coefficient of drag for the oscillating body will tend to approach the steady state value as a limit. An attempt will be made to account for this phenomena in the following chapter. The average value for C_D associated with each centerline depth from Table VI was used in the calculations which follow and provided good correlation between theory and experimental data.

c. Force Multiplication Factors

For each test made in this study, horizontal and vertical force multiplication factors were computed from the maximum experimental force components and are tabulated in Appendix C. The horizontal multiplication factors are plotted against frequency ratio in Figures 30 through 32. There is a separate plot for each length of mooring line. In each of these figures, the experimental points define resonance curves of the form of Figure 4. The theoretical curve, computed from equations (16) and (17), is presented as a solid line in each of these figures. A sample calculation is shown in Appendix A. In all computations an inertial coefficient $C_M = 1.05$ was used. The theoretical curves do not fall on a single line in Figure 4 since these curves are drawn for constant values of damping factor n_T and this factor varies with the frequency ratio due to the method of conducting tests.

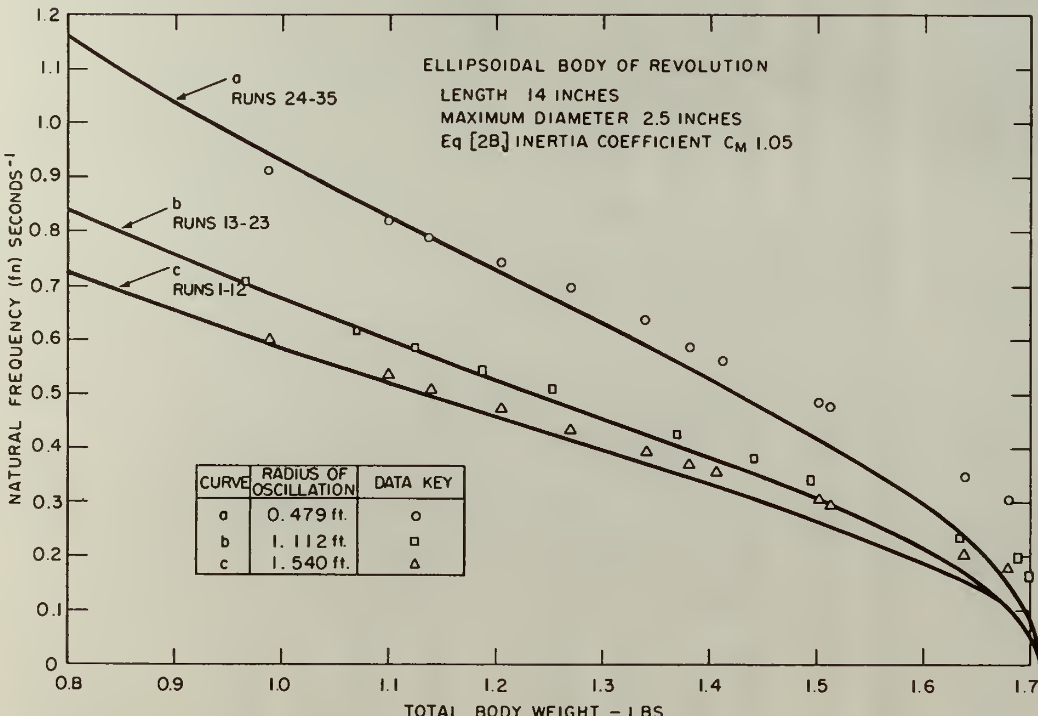

FIG 28 NATURAL FREQUENCY VARIATION WITH BODY WEIGHT

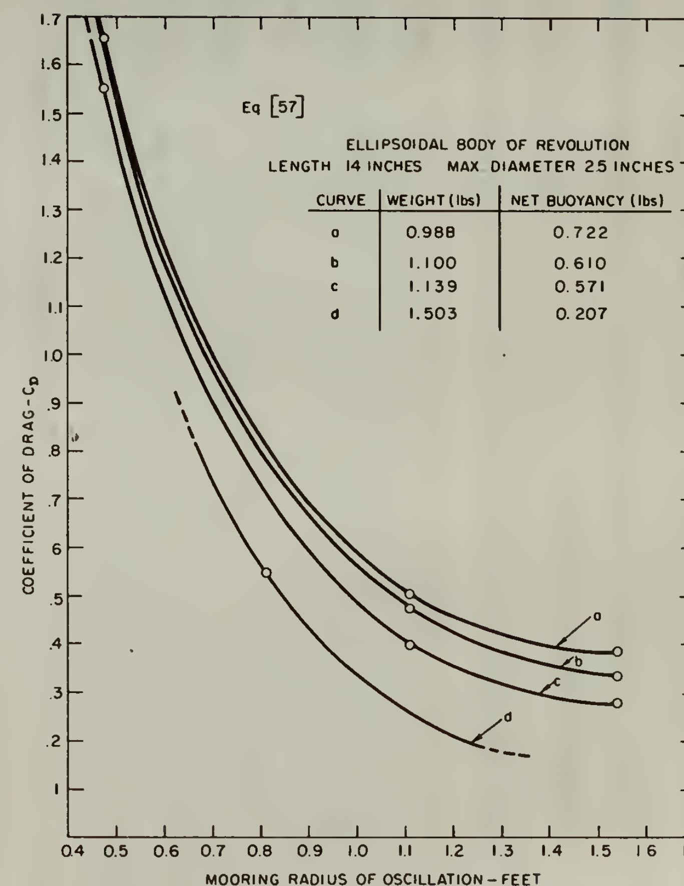

FIG. 29 COEFFICIENT OF DRAG VARIATION WITH RADIUS OF OSCILLATION.

The agreement between theory and experiment is best for the longer lengths of mooring line. For the shortest length of mooring line, test runs 24-35, the agreement is poor however the trend is evident. In this series of runs the resonant frequency occurred at the heavier body weights when the net buoyant force was relatively low. For this condition the assumption that the vertical component of mooring line force is equal to the net buoyancy is much less valid since the wave force is no longer small with respect to the net buoyancy. The actual measured forces in runs number 32 and 33, which are at frequency ratios greater than unity, and well beyond the theoretical resonant frequency are not considered valid since the test object was oscillating so vigorously it struck the bottom of the tank. These runs do indicate that the mooring lines should be long enough to insure that the moored body will not strike bottom even at the greatest anticipated angle of oscillation in order to avoid subjecting a mooring to such relatively large forces.

It is possible that an improved method of evaluating the coefficient of drag for the test object would lead to better agreement between predicted and observed results since the damping factor is proportional to C_D. The effect of damping on theoretical force magnification is indicated in Figure 4. The greatest effect of damping factor occurs between frequency ratios of about 0.75 to 1.4. An improved value for the drag coefficient would have little effect on the results beyond a frequency ratio of 1.4. But in the region of frequency ratios 0.75 to 1.4 the value used for the coefficient drag is of great importance. The accuracy of the coefficient of drag found as indicated in section b is considered reasonably accurate for the purpose of this study in view of the agreement between predicted and experimental results shown in Figures 30 through 32.

The agreement between theory and experiment is best for the longer lengths of mooring line. For the shortest length of mooring line, test runs 24-35, the agreement is poor however the trend is evident. In this series of runs the resonant frequency occurred at the heavier body weights when the net buoyant force was relatively low. For this condition the assumption that the vertical component of mooring line force is equal to the net buoyancy is much less valid since the wave force is no longer small with respect to the net buoyancy. The actual measured forces in runs number 32 and 33, which are at frequency ratios greater than unity, and well beyond the theoretical resonant frequency are not considered valid since the test object was oscillating so vigorously it struck the bottom of the tank. These runs do indicate that the mooring lines should be long enough to insure that the moored body will not strike bottom even at the greatest anticipated angle of oscillation in order to avoid subjecting a mooring to such relatively large forces.

It is possible that an improved method of evaluating the coefficient of drag for the test object would lead to better agreement between predicted and observed results since the damping factor is proportional to C_D. The effect of damping on theoretical force magnification is indicated in Figure 4. The greatest effect of damping factor occurs between frequency ratios of about 0.75 to 1.4. An improved value for the drag coefficient would have little effect on the results beyond a frequency ratio of 1.4. But in the region of frequency ratios 0.75 to 1.4 the value used for the coefficient drag is of great importance. The accuracy of the coefficient of drag found as indicated in section b is considered reasonably accurate for the purpose of this study in view of the agreement between predicted and experimental results shown in Figures 30 through 32.

The experimental vertical multiplication factors are listed in Appendix C and are plotted in Figures 33 through 35. The dashed lines in these Figures do not represent theory. They serve to connect the positive and negative experimental points to show the trend of data.

The results presented in Figures 30 through 35 indicate the validity of analyzing the present problem by applying vibration theory with square law damping. This is not surprising in view of the good agreement achieved by Shapiro in his investigation (1). They also establish a basis for evaluating the effect of shape on the wave forced oscillations of a submerged moored buoyant object.

d. Slacking of Mooring Lines

When the maximum dynamic negative mooring force is greater than the net buoyancy, one or both of the test object mooring lines will slacken. Expressing this criterion in terms of the ratio

$N/\bar{F}_{vm}$ -, slacking will occur when $N/\bar{F}_{vm} < 1$

This occurred during a portion of the wave cycle at the heavier body weights as noted in the compilation of data in Appendix C. The results of the tests show a decrease in mooring line force with increasing frequency ratio, produced by increasing the test object weight. This desirable trend is limited by the net buoyancy becoming so small that slacking occurs. When slacking occurs over any portion of the wave cycle it is followed by a severe jerk as the mooring lines again become taut. The magnitude of forces imposed by this jerk may be seen by referring to Figures 29 through 34. The last two experimental points on each curve were obtained when the test object mooring lines were slackening and tightening during a portion of the cycle. This effect must be considered undesirable and severely limits the available range of

The experimental vertical multiplication factors are listed in Appendix C and are plotted in Figures 33 through 35. The dashed lines in these Figures do not represent theory. They serve to connect the positive and negative experimental points to show the trend of data.

The results presented in Figures 30 through 35 indicate the validity of analyzing the present problem by applying vibration theory with square law damping. This is not surprising in view of the good agreement achieved by Shapiro in his investigation (1). They also establish a basis for evaluating the effect of shape on the wave forced oscillations of a submerged moored buoyant object.

d. <u>Slacking of Mooring Lines</u>

When the maximum dynamic negative mooring force is greater than the net buoyancy, one or both of the test object mooring lines will slacken. Expressing this criterion in terms of the ratio $\frac{N/F_{vm}}{S/F_{vm}}$, slacking will occur when < 1

This occurred during a portion of the wave cycle at the heavier body weights as noted in the compilation of data in Appendix C. The results of the tests show a decrease in mooring line force with increasing frequency ratio, produced by increasing the test object weight. This desirable trend is limited by the net buoyancy becoming so small that slacking occurs. When slacking occurs over any portion of the wave cycle it is followed by a severe jerk as the mooring line again become taut. The magnitude of forces imposed by this jerk may be seen by referring to Figures 29 through 34. The last two experimental points on each curve were obtained when the test object mooring lines were slackening and tightening during a portion of the cycle. This effect must be considered undesirable and severely limits the available range of frequency ratios for a given design condition wave. In the present study the wave selected was on the basis of convenience to allow a comparison of effects and did not necessarily represent an expected design condition.

In still water both mooring lines were taut for all test conditions. Slacking occurred only when the object was subjected to wave forces.

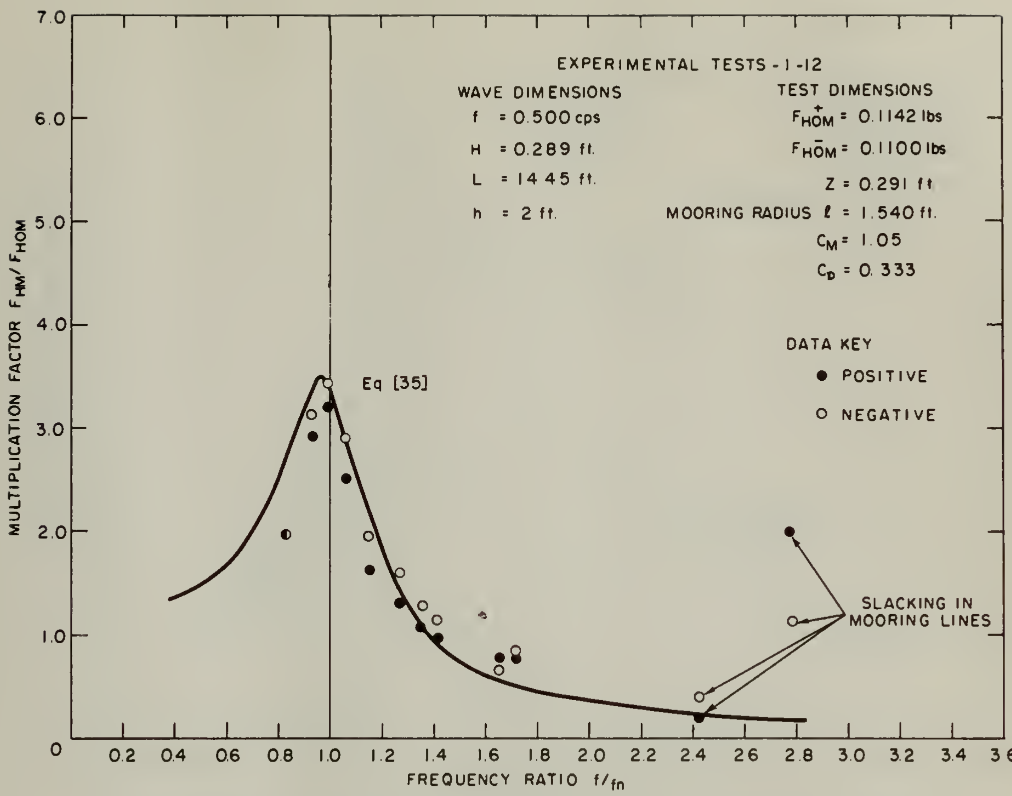

FIG 30 VARIATION OF HORIZONTAL MULTIPLICATION FACTOR WITH FREQUENCY RATIO

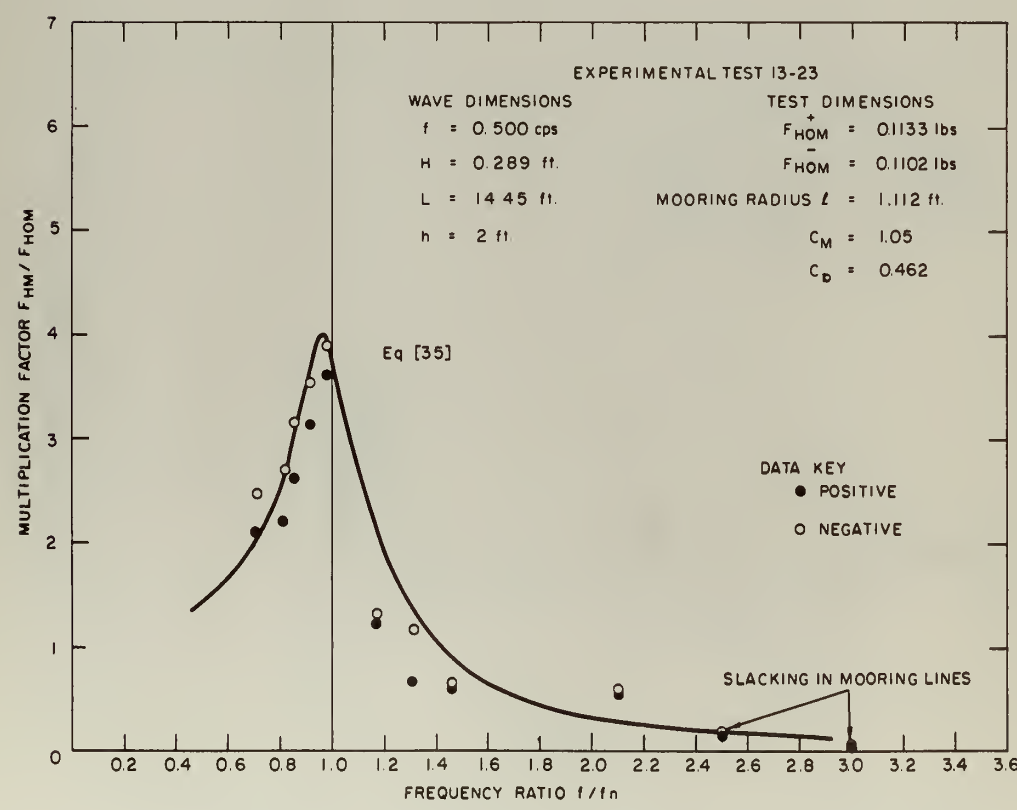

FIG. 31 VARIATION OF HORIZONTAL MULTIPLICATION FACTOR WITH FREQUENCY RATIO

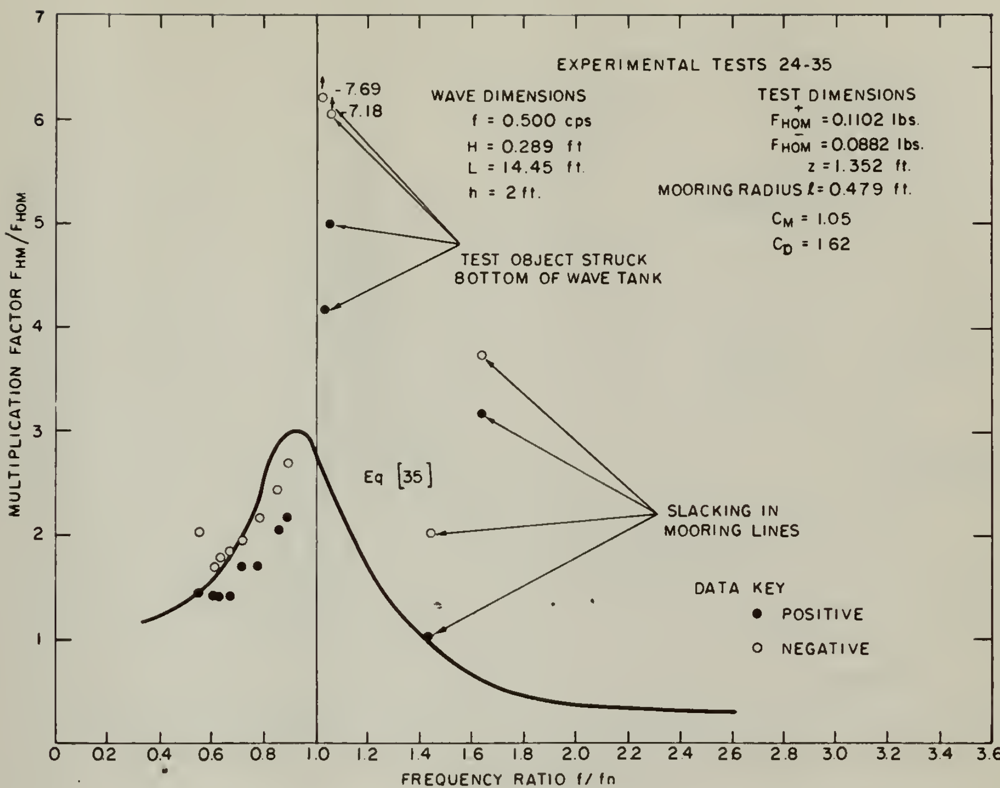

FIG 32 VARIATION OF HORIZONTAL MULTIPLICATION FACTOR WITH FREQUENCY RATIO

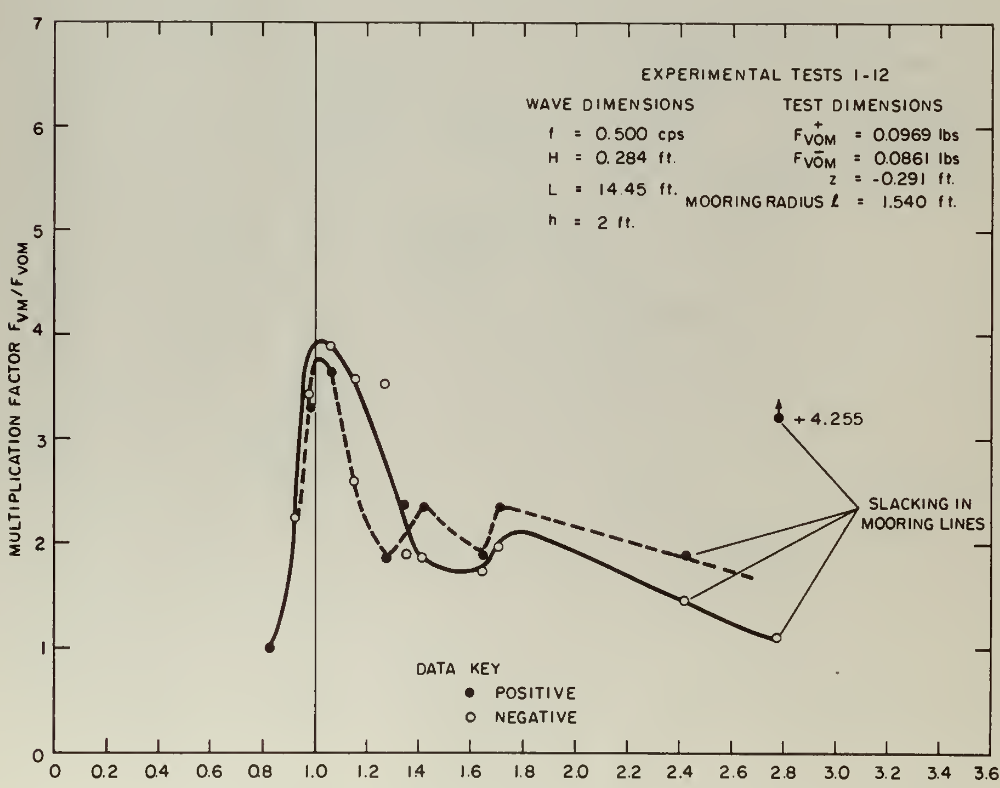

FIG. 33 VARIATION OF VERTICAL VARIATION FACTOR WITH FREQUENCY RATIO

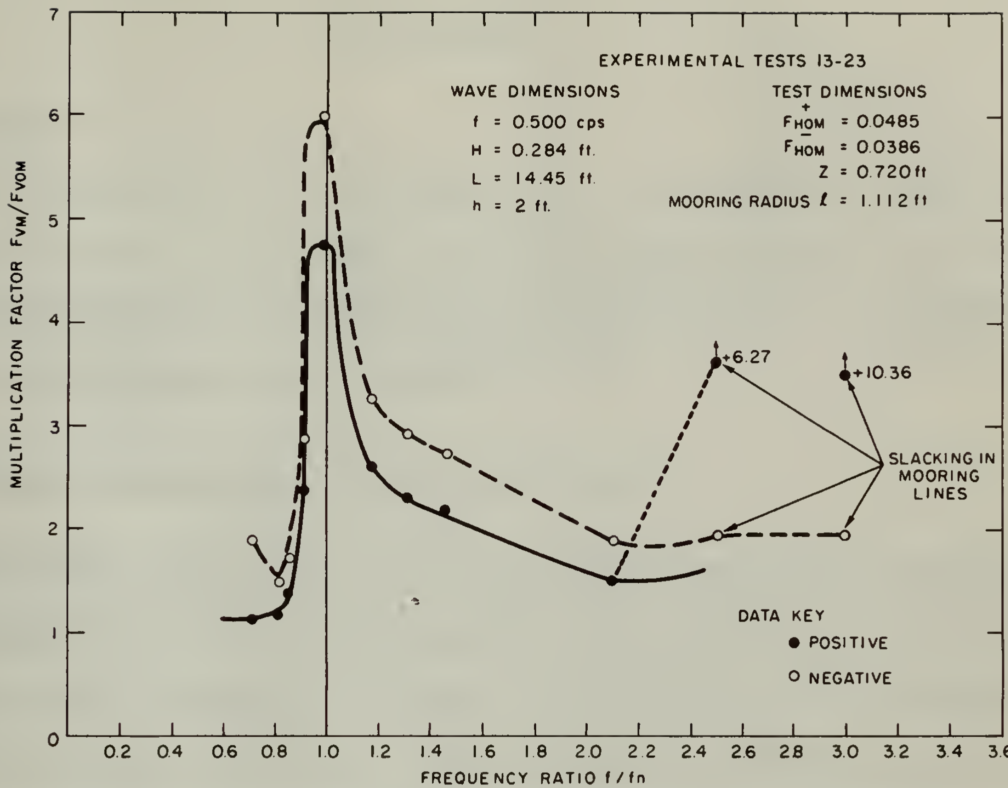

FIG 34 VARIATION OF VERTICAL MULTIPLICATION FACTOR WITH FREQUENCY RATIO

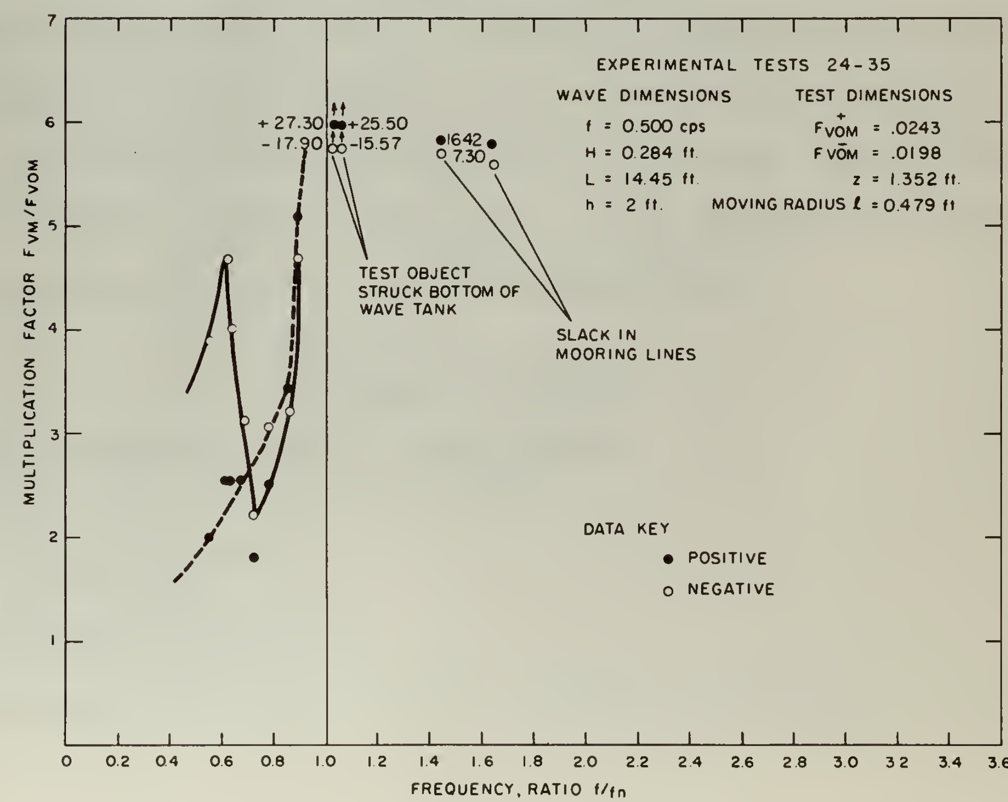

FIG 35 VARIATION OF VERTICAL MULTIPLICATION FACTOR WITH FREQUENCY RATIO

VII CONCLUSIONS

1. General

This study gives further demonstration of the validity of describing the behavior of moored submerged buoyant objects in oscillating waves by vibration theory with square law damping provided there is no radical departure from the assumptions listed in Chapter II.

2. Effect of Shape on Forced Oscillatory Motion

The effect of shape can be most readily demonstrated by comparing two differently shaped objects restrained by mooring systems having equal radii of oscillation and subjected to forced oscillatory motion in identical wave systems. The streamlined shape of the present study will be compared to a sphere of equal volume since the payload capacity would appear to be one of the most important considerations in a prototype installation.

An arbitrary volume of 38.2 cubic feet for both the ellipsoid and sphere will be employed in order to permit utilization of data presented in Shapiro's study. The approximate solution of the non linear equation of motion, equation (35) will be applied to both objects. Weight and wave characteristics were selected on the basis of realism and convenience.

COMPARISON OF SYSTEMS

Sphere and Mooring system characteristics

$D = 4.18$ ft

$\ell = 9.27$ ft

Total Weight = 735 lbs

Added Mass Coefficient $K = 0.5$, potential flow theory

VII CONCLUSIONS

1. General

This study gives further demonstration of the validity of describing the behavior of moored submerged buoyant objects in oscillating waves by vibration theory with square law damping provided there is no radical departure from the assumptions listed in Chapter II.

2. Effect of Shape on Forced Oscillatory Motion

The effect of shape can be most readily demonstrated by comparing two differently shaped objects restrained by mooring systems having equal radii of oscillation and subjected to forced oscillatory motion in identical wave systems. The streamlined shape of the present study will be compared to a sphere of equal volume since the payload capacity would appear to be one of the most important considerations in a prototype installation.

An arbitrary volume of 38.2 cubic feet for both the ellipsoid and sphere will be employed in order to permit utilization of data presented in Shapiro's study. The approximate solution of the non linear equation of motion, equation (35) will be applied to both objects. Weight and wave characteristics were selected on the basis of realism and convenience.

COMPARISON OF SYSTEMS

Sphere and Mooring system characteristics

$D = 4.18$ ft

$l = 9.27$ ft

Total Weight = 735 lbs

Added Mass Coefficient $K = 0.5$, potential flow theory

Drag Coefficient, $C_D = 0.42$, steady state value

$B = 15850$ ft lbs Eq (26)

$A = 5939$ slug ft^2 Eq (25)

$f_n = 0.259$ cps Eq (28)

Streamlined Body and Mooring system characteristics

$D = 2.32$ ft Maximum Diameter

$\ell = 9.27$ ft

Total Weight = 1270 lbs

Added Mass Coefficient, K = 0.05 , potential flow theory

Drag Coefficient, $C_D = 0.69$ Average Value, Figure 29, for model at similar "ℓ" $/D_{max}$ ratio

$B = 10870$ ft lbs Eq (26)

$A = 4100$ slug ft^2 Eq (25)

$fn = 0.259$ cps Eq (28)

Wave Characteristics

$H = 1.434$ ft

$L = 71.70$ ft

$h = 20$ ft Shallow water conditions

$T = 3.86$ seconds

$f_\pi = 0.259$ cps

Density of Water $\rho = 1.99$ slugs / cu ft

Forces on the systems

Sphere $F_{Hom} = 110$ lbs Eq (9)

Drag Coefficient, $C_D = 0.42$, steady state value

$B = 15850$ ft lbs Eq (26)

$A = 5939$ slug ft^2 Eq (25)

$f_n = 0.259$ cps Eq (28)

Streamlined Body and Mooring system characteristics

$D = 2.32$ ft Maximum Diameter

$l = 9.27$ ft

Total Weight = 1270 lbs

Added Mass Coefficient, $K = 0.05$, potential flow theory

Drag Coefficient, $C_D = 0.69$ Average Value, Figure 29, for model at similar "l"/D_{max} ratio

$B = 10870$ ft lbs Eq (26)

$A = 4100$ slug ft^2 Eq (25)

$f_n = 0.259$ cps Eq (28)

Wave Characteristics

$H = 1.434$ ft

$L = 71.70$ ft

$h = 20$ ft Shallow water conditions

$T = 3.86$ seconds

$f_w = 0.259$ cps

Density of Water $\rho = 1.95$ slugs / cu ft

Forces on the system

Sphere $F_{Dm} = 110$ lbs Eq (9)

$N_2 = .0422$ Eq (38)

$f/f_n = 1$

$\frac{F_{Hm}}{F_{Hom}} = 4.87$ Eq (35)

$F_{Hm} = 536$ lbs

<u>Streamlined Body</u> $F_{Hom} = 77$ lbs Eq (9)

$N_2 = .0314$ Eq (25)

$f/f_n = 1$

$\frac{F_{Hm}}{F_{Hom}} = 5.64$ Eq (35)

$F_{Hm} = 434$ lbs

The theoretical results, therefore, predict that the streamlined body will be the superior shape in hydrodynamic performance for the conditions described in the comparison. The degree of difference is on the order of 23% in favor of the streamlined body, however it should be emphasized that these results are valid only for the particular cases chosen.

The most important condition to be noted is the radius of oscillation ; "ℓ", and the variation of the coefficient of drag as indicated in Figure 29. It is possible that for large values of "ℓ" the force on the sphere may become less than that on the streamlined body due to reduction in the coefficient of drag for the latter shape as "ℓ" increases. However for both shapes the limiting value of "ℓ" will be reached just prior to the object breaking the water surface. The present theory would no longer apply if the objects were not completely immersed, since surface effects and loss of buoyant force would enter the problem.

For the sphere the coefficient of drag as a function of mooring radius

N_2 = .0422 Eq (38)

f/f_n = 1

$\frac{F_{HM}}{F_{HOM}}$ = 4.87 Eq (35)

F_{HM} = 596 lbs

Streamlined body F_{HOM} = 77 lbs Eq (9)

N_2 = .0514 Eq (25)

f/f_n = 1

$\frac{F_{HM}}{F_{HOM}}$ = 5.64 Eq (35)

F_{HM} = 434 lbs

The theoretical results, therefore, predict that the streamlined body will be the superior shape in hydrodynamic performance for the conditions described in the comparison. The degree of difference is on the order of 23% in favor of the streamlined body, however it should be emphasized that these results are valid only for the particular cases chosen.

The most important condition to be noted is the radius of oscillation "ℓ", and the variation of the coefficient of drag as indicated in Figure 29. It is possible that for large values of "ℓ" the force on the sphere may become less than that on the streamlined body due to reduction in the coefficient of drag for the latter shape as "ℓ" increases. However for both shapes the limiting value of "ℓ" will be reached just prior to the object breaking the water surface. The present theory would no longer apply if the objects were not completely immersed, since surface effects and loss of buoyant force would enter the problem.

For the sphere the coefficient of drag as a function of mooring radius is not known but it seems reasonable to believe that it would be less dependent on this parameter than the streamlined body since its cross sectional area normal to the flow is constant as orientation with respect to the stream flow changes.

Provided this assumption is correct the advantage of the streamlined body over the spherical body would increase as the radius of oscillation decreased since the coefficient of drag and therefore damping factor, increases significantly in the case of the former shape as "ℓ" diminishes.

3. Effect of Centerline Depth on Forced Oscillatory Motion

Increasing centerline depth is accomplished by decreasing the radius of oscillation of the moored body and it is this parameter which appears to have the most important influence on the damping factor for the streamlined body.

The damping factor is a function of C_D "ℓ" and other characteristics of the body but as indicated by equation (57) the coefficient of drag is also a function of "ℓ". As seen in Figure 29 at large radii of oscillation C_D is less sensitive to changes in "ℓ", this represents shallow centerline depths. Therefore for large radii of oscillation the damping factor varies approximately as

$$N_2 \propto \ell^{\frac{1}{2}}$$

At smaller radii of oscillation C_D increases rapidly as "ℓ" decreases and the damping factor is more strongly influenced by this parameter. This may be expressed approximately as

$$N_2 \propto C_D$$

indicating, therefore, increase in N_2 as "ℓ" decreases.

Figure 36 shows the variation of the theoretical maximum partially restrained force on the object as a function of centerline depth. This Figure is not known but it seems reasonable to believe that it would be less dependent on this parameter than the streamlined body since its cross sectional area normal to the flow is constant as orientation with respect to the stream flow changes.

Provided this assumption is correct the advantage of the streamlined body over the spherical body would increase as the radius of oscillation decreased since the coefficient of drag and therefore damping factor, increases significantly in the case of the former shape as "l" diminishes.

3. Effect of Centerline Depth on Forced Oscillatory Motion

Increasing centerline depth is accomplished by decreasing the radius of oscillation of the moved body and it is this parameter which appears to have the most important influence on the damping factor for the streamlined body.

The damping factor is a function of C_D "l" and other characteristics of the body but as indicated by equation (57) the coefficient of drag is also a function of "l". As seen in Figure 29 at large radii of oscillation C_D is less sensitive to changes in "l", this represents shallow centerline depths. Therefore for large radii of oscillation the damping factor varies approximately as

$$N_2 \propto l^{\frac{1}{2}}$$

At smaller radii of oscillation C_D increases rapidly as "l" decreases and the damping factor is more strongly influenced by this parameter. This may be expressed approximately as

$$N_2 \propto C_D$$

indicating, therefore, increase in N_2 as "l" decreases.

Figure 35 shows the variation of the theoretical maximum partially restrained force on the object as a function of centerline depth. This Figure is a combination of theory and experimental values. For each centerline depth $\frac{F_{Hm}}{F_{Hom_{max}}}$ was computed from equation (35). The value of F_{Hm} was then calculated on the basis of experimental values of F_{Hom} measured in rigidly restrained tests. Since both a positive and negative value for F_{Hom} were recorded at each depth, two values of F_{Hm} are shown in Figure 36 for each series of test runs. The curve connecting these points represents the theoretical variation of F_{H_m} as a function of centerline depth. It may be seen from the Figure that no optimum depth is indicated but a maximum force does occur near a centerline depth ratio of 3. In a prototype installation this depth should be avoided.

But of greater significance than ceterline depth in this consideration is the reduction in "ℓ" which produced greater centerline depth the most interesting aspect of this study proved to be the marked increase noted in the coefficient of drag as "ℓ" diminished. Several reasons are considered to be responsible for this phenomena, these are:

is a combination of theory and experimental values. For each centerline depth F_{pm} was computed from equation (35). The value of F_m was then calculated on the basis of experimental values of F_{pm} measured in rigidly restrained tests. Since both a positive and negative value for F_{pm} were recorded at each depth, two values of F_m are shown in Figure 36 for each series of test runs. The curve connecting these points represents the theoretical variation of F_m as a function of centerline depth. It may be seen from the Figure that no optimum depth is indicated but a maximum force does occur near a centerline depth ratio of 3. In a prototype installation this depth should be avoided.

But of greater significance than centerline depth in this consideration is the reduction in "ℓ" which produced greater centerline depth the most interesting aspect of this study proved to be the marked increase noted in the coefficient of drag as "ℓ" diminished. Several reasons are considered to be responsible for this phenomena, these are:

1) The possibility of earlier separation and greater energy loss as the mooring radius decreases. This appears to be the most important effect causing the increase in the coefficient of drag. This is not surprising when consideration is given to the flow of streamlines around the body. Figure 37 is intended to depict the possible separation that may result as the body causes greater disturbance to the free flow of fluid around it at shorter radii of oscillations.

2) The assumptions which led to the derivation of equation (57) which defines C_D. It is based on the criterion of equivalent dissipative work done during a cycle. This approximation proved successful when applied to solve the quadratic damping equation of motion. The technique is to replace the quadratic damping coefficient with an equivalent linear damping coefficient. The observed decremental decay of the free vibrations which are in fact the result of quadratic damping, are then used to evaluate the coefficient of drag defined in terms of the equivalent linear damping coefficient.

3) The possibility of interference between the object and bottom of the tank as the radius of oscillation is shortened. Energy loss in this interaction would result probably in increased drag with decreasing mooring line length.

4) Change in projected area of the body normal to fluid streamlines. The projected area normal to the flow will increase as the radius is shortened. This would result in an increase in drag and would be more accurately reflected in the product of C_D and area. But since cross sectional area is treated as a constant any increase in drag would appear only as an increase in the drag coefficient.

1) The possibility of earlier separation and greater energy loss as the mooring radius decreases. This appears to be the most important effect causing the increase in the coefficient of drag. This is not surprising when consideration is given to the flow of streamlines around the body. Figure 37 is intended to depict the possible separation that may result as the body causes greater disturbance to the free flow of fluid around it at shorter radii of oscillations.

2) The assumptions which led to the derivation of equation (57) which defines C_D. It is based on the criterion of equivalent dissipative work done during a cycle. This approximation proved successful when applied to solve the quadratic damping equation of motion. The technique is to replace the quadratic damping coefficient with an equivalent linear damping coefficient. The observed decremental decay of the free vibrations which are in fact the result of quadratic damping, are then used to evaluate the coefficient of drag defined in terms of the equivalent linear damping coefficient.

3) The possibility of interference between the object and bottom of the tank as the radius of oscillation is shortened. Energy loss in this interaction would result probably in increased drag with decreasing mooring line length.

4) Change in projected area of the body normal to fluid streamlines. The projected area normal to the flow will increase as the radius is shortened. This would result in an increase in drag and would be more accurately reflected in the product of C_D and area. But since cross sectional area is treated as a constant any increase in drag would appear only as an increase in the drag coefficient.

The occurrence of any or all of the above, as the radius of oscillation is shortened, would account for the increase in the doefficient of drag. The results obtained from the application of equation (57) led to good agreement with experiment and provide a strong argument for the validity of this equation.

The occurrence of any or all of the above, as the radius of os-cillation is shortened, would account for the increase in the coefficient of drag. The results obtained from the application of equation (57) led to good agreement with experiment and provide a strong argument for the validity of this equation.

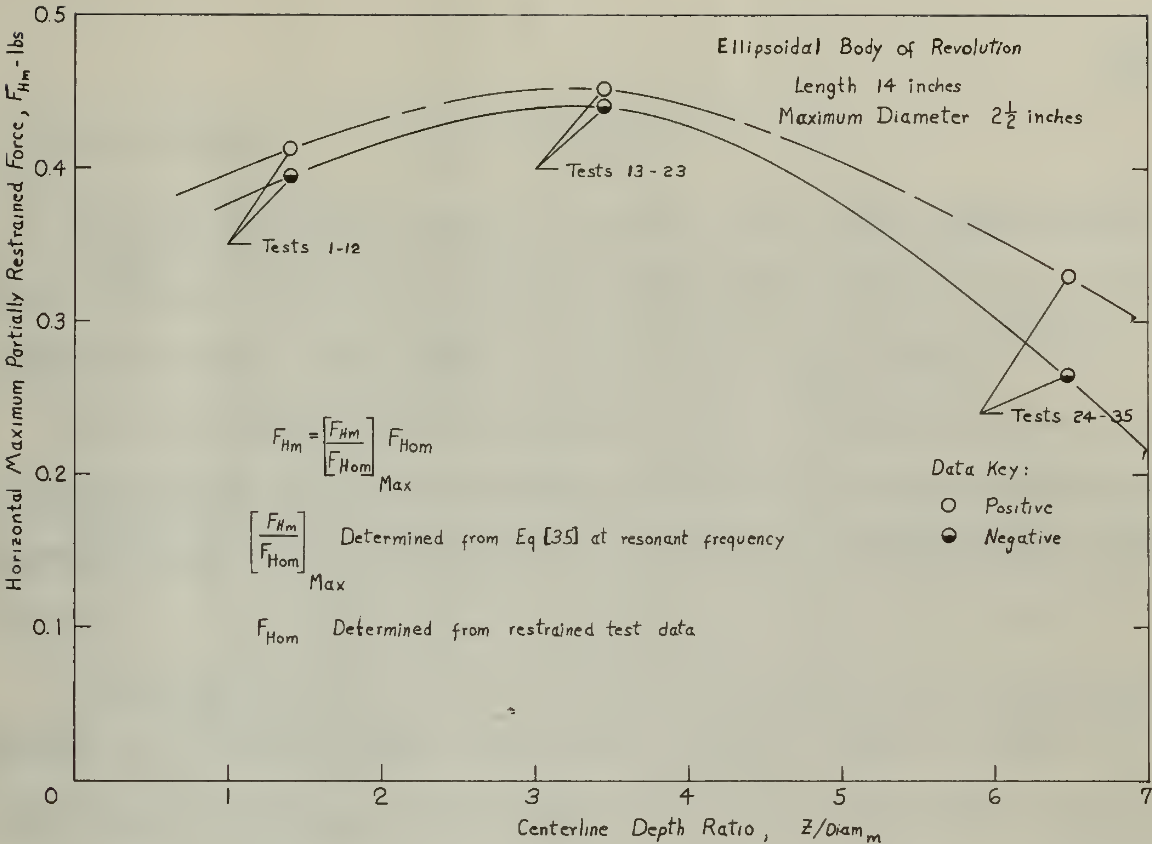

Figure 36. Variation of Theoretical Maximum Partially Restrained Force with Centerline Depth Ratio

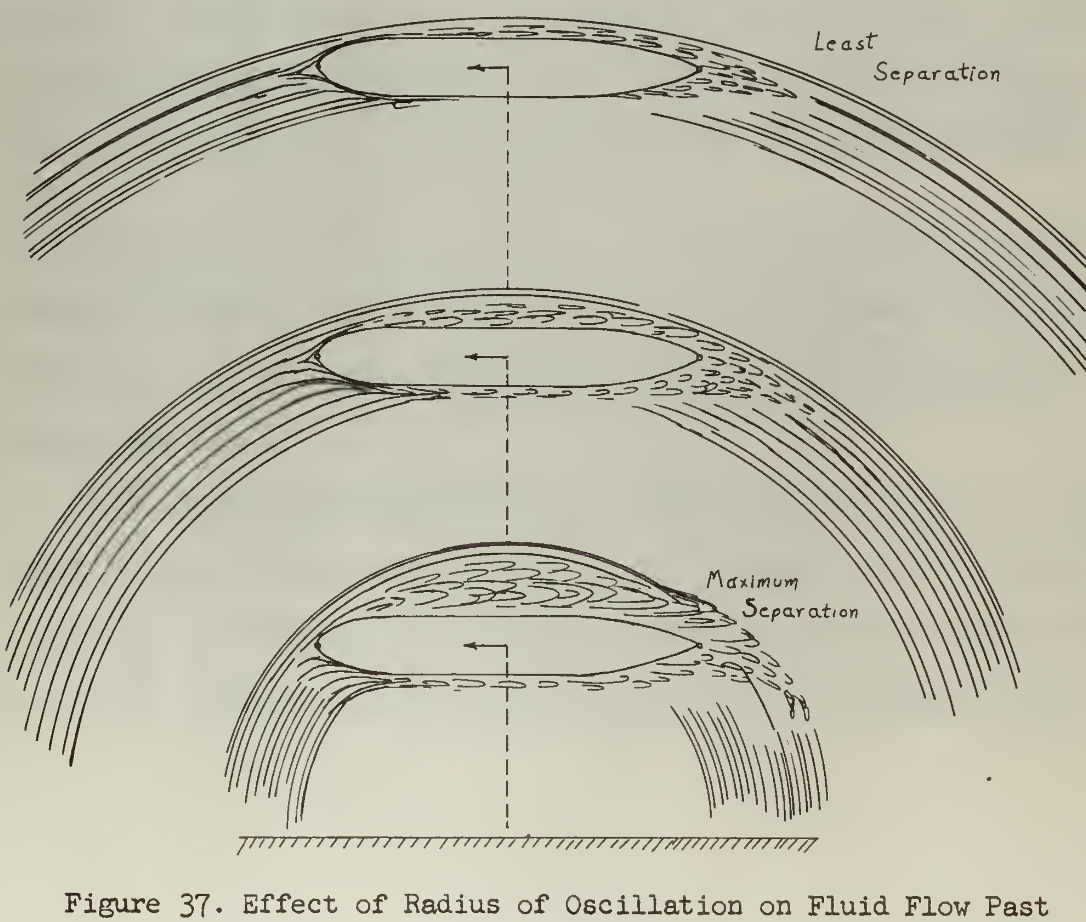

Figure 37. Effect of Radius of Oscillation on Fluid Flow Past a Body

4 Recommendations

The most difficult problem encountered in this study involved the accurate determination of the drag of the moored body, as reflected in the coefficient of drag, with changes in the radius of oscillation.

While the coefficient of drag appeared to be adequately defined by equation (57) several approximations were necessary to obtain this solution. These approximations could be avoided by utilizing more direct methods of measuring the drag.

As a possibility for further research and a more direct approach to the problem it is suggested that an arbitrary shape be caused to rotate with steady angular velocity, in still water and its drag measured at various radii of rotation. It would be possible in this manner to isolate the effect of separation, due to interference with streamlined flow, and bottom interaction effects. At very great radii of oscillation the body motion would tend to approach rectilinear translation, this trend is indicated in Figure 29 by flattening of the curve toward the steady state value at the longer radii.

At zero radius of oscillation the body would be rotating about its own center of gravity. For this condition it is perhaps most readily apparent that there will be a much larger drag coefficient than for the case of steady rectilinear flow.

Although it appears reasonable to expect that the increase in drag at shorter radii is more severe with elongated bodies than, for instance, spherical bodies, quantitative information on this aspect of the effect of shape is not now available and is suggested as a topic for further study.

4 Recommendations

The most difficult problem encountered in this study involved the accurate determination of the drag of the moored body, as reflected in the coefficient of drag, with changes in the radius of oscillation.

While the coefficient of drag appeared to be adequately defined by equation (57) several approximations were necessary to obtain this solution. These approximations could be avoided by utilizing more direct methods of measuring the drag.

As a possibility for further research and a more direct approach to the problem it is suggested that an arbitrary shape be caused to rotate with steady angular velocity, in still water and its drag measured at various radii of rotation. It would be possible in this manner to isolate the effect of separation, due to interference with streamlined flow, and bottom interaction effects. At very great radii of oscillation the body motion would tend to approach rectilinear translation, this trend is indicated in Figure 29 by flattening of the curve toward the steady state value at the longer radii.

At zero radius of oscillation the body would be rotating about its own center of gravity. For this condition it is perhaps most readily apparent that there will be a much larger drag coefficient than for the case of steady rectilinear flow.

Although it appears reasonable to expect that the increase in drag at shorter radii is more severe with elongated bodies than, for instance, spherical bodies, quantitative information on this aspect of the effect of shape is not now available and is suggested as a topic for further study.

VIII REFERENCES

1. Shapiro, W. C., "Forced Oscillations of Submerged Objects in Water Waves" (ScD. Thesis), M.I.T. Hydrodynamics Laboratory Cambridge, Mass., August 1958

2. Marlow, T. A. II, "An Experimental Determination of Particle Velocities in the Oscillatory Water Wave" (S. M. Thesis), M.I.T. Hydrodynamics Laboratory Cambridge, Mass. 1957

3. Lamb, H. "Hydrodynamics," Sixth Ed Dover Publications, New York, 1932

4. O'Brien, M.P. and Morison, J.R., "The Forces Exerted by Waves on Objects," Transactions, American Geophysical Union, Vol.33,No.1 , February 1952

5. Keulegan, G. H. and Carpenter, L. H., "Forces on Cylinders and Plates in an Oscillating Fluid," National Bureau of Standards Report 4821, 1956

6. Landweber, L. "A Comparison of the Added Masses of Streamlined Bodies and Prolate Spheroids" Experimental Towing Tank Stevens Institute of Technology, New Jersey Report No. 572, June 1955

VIII REFERENCES

1. Shapiro, W. C., "Forced Oscillations of Submerged Objects in Water Waves" (ScD. Thesis), M.I.T. Hydrodynamics Laboratory Cambridge, Mass., August 1958

2. Marlow, T. A. II, "An Experimental Determination of Particle Velocities in the Oscillatory Water Wave" (S. M. Thesis), M.I.T. Hydrodynamics Laboratory Cambridge, Mass. 1957

3. Lamb, H. "Hydrodynamics," Sixth Ed Dover Publications, New York, 1932

4. O'Brien, M.P. and Morison, J.R., "The Forces Exerted by Waves on Objects," Transactions, American Geophysical Union, Vol.33,No.1, February 1952

5. Keulegan, G. H. and Carpenter, L. H., "Forces on Cylinders and Plates in an Oscillating Fluid," National Bureau of Standards Report 4821, 1956

6. Landweber, L. "A Comparison of the Added Masses of Streamlined Bodies and Prolate Spheroids" Experimental Towing Tank Stevens Institute of Technology, New Jersey Report No. 572, June 1955

VIII REFERENCES (cont'd)

7. Rouse, H. "Elementary Mechanics of Fluids" Second Printing
John Wiley & Sons Inc. New York, 1946

8. Den Hartog, J.P. "Mechanical Vibrations" Third Edition
McGraw-Hill Book Co. Inc., New York, 1947

9. Jacobsen, L. S., "Steady Forced Vibrations as Influenced by Damping"
Transactions, American Society of Mechanical Engineers,
Vol. 52, No. APM 52-15, 1930

VIII REFERENCES (cont'd)

7. Rouse, H. "Elementary Mechanics of Fluids" Second Printing

John Wiley & Sons Inc. New York, 1946

8. Den Hartog, J.P. "Mechanical Vibrations" Third Edition

McGraw-Hill Book Co. Inc., New York, 1947

9. Jacobsen, L. S., "Steady Forced Vibrations as Influenced by Damping"

Transactions, American Society of Mechanical Engineers,

Vol. 52, No. APM 52-15, 1930

APPENDIX A - SAMPLE CALCULATIONS

NATURAL FREQUENCY AND FORCE MAGNIFICATION

Given: Test Model under conditions of test 14

Model and Mooring System Characteristics

$D_{max} = 0.208$ ft

Total Volume = 0.0274 cu.ft (Calculated)

$\ell = 1.112$ ft

Total Weight, $mg = 1.070$ lbs

Model Weight, $m_1 g = 0.966$ lbs

Filer Weight, $m_2 g = 0.104$ lbs

Wave Characteristics

$H = 0.289$ ft　　　　$T = 2.00$ secs

$L = 14.45$ ft　　　　$f = 0.500$ cps

$d = 2.00$ ft

Physical constants

Density of water, $\rho = 1.94$ slugs/cu.ft

Acceleration of gravity, $g = 32.2$ ft/sec^2

Added mass coefficient, $K = 0.05$, ($C_m = 1.05$)

Drag coefficient, $C_D = 0.46$ (Figure 29)

Average Maximum force on rigidly restrained model

$F_{Hom} = 0.1117$ lbs (experiment)

Required: Theoretical natural frequency and horizontal force multiplication

APPENDIX A (Cont'd)

Natural Frequency Calculation

$$f_n = \frac{1}{2\pi}\left[\frac{B}{A}\right]^{1/2} \quad (28)$$

where $A = I + I'$ (25)

and $B = (\mathrm{Vol}\,\rho g - mg)\,\ell$ (26)

I = moment of inertia of model about anchor point of mooring line.

By the parellel axis theorem

$$I = I_{oo} + m\ell^2$$

where I oo is the moment of inertia of the body about its own center of gravity.

In order to simplify the calculations Ioo will be found by treating the model shape as a solid ellipsoid of revolution of constant density. The error introduced will be of minor significance since the value of I oo is small compared to the value $M\ell^2$

For an equivalent ellipsoid

$$I_{oo} = \frac{M}{5}\frac{(a^2 + b^2)}{144} = 0.00234 \text{ slugs ft}^2$$

where, from Figure 13, a = major radius = 7"

b = minor radius = 1.25"

Therefore $I = I_{oo} + M\ell^2 = 0.00234 + 0.0412 = \underline{0.04354 \text{ slug ft}^2}$

I' = virtual mass moment of inertia

$$I' = I'_{oo} + m'\ell^2$$

$$M' = K\rho\,\mathrm{Vol} = 0.002655 \text{ slugs}$$

$$I'_{oo} = \frac{M'}{5}\frac{(a^2 + b^2)}{144} = 0.00182 \text{ slugs ft}^2$$

$$I' = I'_{oo} + m\ell^2 = 0.000182 + 0.003285 = 0.003467 \text{ slugs ft}^2$$

APPENDIX A (Cont'd)

Therefore $A = I + I' = 0.04354 \quad 0.003467 = 0.04700$ slug ft^2

$$fn = \frac{1}{2\pi}\left[\frac{B}{A}\right]^{1/2} = \underline{\underline{0.619 \text{ cps}}}$$

<u>Horizontal Multiplication Factor Calculation</u>

$$\frac{F_{Hm}}{F_{Hom}} = \frac{1}{\sqrt{2}\, N_2 \left(\frac{f}{f_n}\right)^2}\left[\left\{\left(1 - \left(\frac{f}{f_n}\right)^2\right)^4 - 4 N_2^2 \left(\frac{f}{f_n}\right)^4\right\}^{\frac{1}{2}} - \left(1 - \left(\frac{f}{f_n}\right)^2\right)^2\right]^{\frac{1}{2}} \qquad (35)$$

$$\text{where} \quad N_2 = \frac{C_D\, \rho\, D^2\, \ell^4\, F_{Hom}}{A^2\, f_n^2} \quad \frac{1}{12\pi^2} \qquad (38)$$

$$N_2 = .0658$$

$$\frac{f}{fn} = 0.807$$

Therefore, from equation (35) or Figure 4

$$\frac{FH_m}{FH_{om}} = \underline{2.53}$$

APPENDIX A (Cont'd)

Therefore $A = I + I' = 0.04354 \quad 0.003467 = 0.04700$ slug ft^2

$$f_n = \frac{1}{2\pi}\left[\frac{B}{A}\right]^{1/2} = \underline{0.619 \text{ cps}}$$

<u>Horizontal Multiplication Factor Calculation</u>

$$\frac{F_{Hm}}{F_{Hom}} = \frac{1}{\sqrt{2}\, N_2 \left(\frac{f}{f_n}\right)^2}\left[\left\{\left(1-\left(\frac{f}{f_n}\right)^2\right)^4 - 4N_2^2\left(\frac{f}{f_n}\right)^4\right\}^{\frac{1}{2}} - \left(1-\left(\frac{f}{f_n}\right)^2\right)^2\right]^{\frac{1}{2}} \qquad (35)$$

$$\text{where } N_2 = \frac{C_D\, \rho\, D^2\, \ell^4\, F_{Hom}}{A^2 f_n^2}\,\frac{1}{12\pi^2} \qquad (38)$$

$$N_2 = .0658$$

$$\frac{f}{f_n} = 0.807$$

Therefore, from equation (35) or Figure 4

$$\frac{F_{Hm}}{F_{Hom}} = \underline{2.53}$$

APPENDIX B - SAMPLE CALCULATION

COEFFICIENT OF DRAG

Given: Test Model Under conditions of test 14 free oscillation

Model and Mooring system characteristics

$D_{max} = 0.208$ ft.

Total Volume = 0.0274 cu ft (calculated)

$\ell = 1.112$ ft.

Total Weight $mg = 1.070$ lbs

Net Buoyancy $N = 0.640$ lbs

Experimental data from free oscillation record

Ratio of amplitudes of two successive cycles $= \dfrac{\psi_n}{\psi_{n+1}} = 1.421$

Maximum horizontal force component associated with ψ_n

$(F_H)_{\psi_n} = 0.185$ lbs

Coefficient of drag calculation

$$\psi_{max} = \tan^{-1} \frac{F_H}{F_V + N} \approx \tan^{-1} \frac{F_H}{N} \qquad (58)$$

Therefore $\psi_{max} = \tan^{-1} \dfrac{0.185}{0.640} = 0.2815$ radians

$$C_D = \frac{3}{\pi \rho D^2 \ell^3} \left[\frac{A}{\psi_{max}} \ln \frac{\psi_n}{\psi_{n+1}} \right] \qquad (57)$$

where $A = 0.0470$ slug ft^2 from Appendix A

Therefore $C_D = \underline{\underline{0.480}}$

APPENDIX B - SAMPLE CALCULATION

COEFFICIENT OF DRAG

Given: Test Model Under conditions of test 14 free oscillation

Model and Mooring system characteristics

$D_{max} = 0.288$ ft.

Total Volume = 0.0274 cu ft (calculated)

$\ell = 1.112$ ft.

Total Weight mg = 1.070 lbs

Net Buoyancy N = 0.640 lbs

Experimental data from free oscillation record

Ratio of amplitudes of two successive cycles = $\frac{\psi_n}{\psi_{n+1}} = 1.421$

Maximum horizontal force component associated with ψ_n

$(F_H)_{\psi_n} = 0.185$ lbs

Coefficient of drag calculation

$$\psi_{max} = \tan^{-1} \frac{F_H}{F_V + N} \approx \tan^{-1} \frac{F_H}{N} \qquad (58)$$

Therefore $\psi_{max} = \tan^{-1} \frac{0.185}{0.640} = 0.2815$ radians

$$C_D = \frac{3}{\pi \rho D^2 \ell^3} \left[\frac{A}{\psi_{max}} \ln \frac{\psi_n}{\psi_{n+1}} \right] \qquad (57)$$

where A = 0.0470 slug ft^2 from Appendix A

Therefore $C_D = \underline{\underline{0.860}}$

APPENDIX C - TEST RESULTS

Run Centerline Depth (1-12) 0.291 ft.	f/fn	Multiplication Factor Horizontal +	Horizontal −	Vertical +	Vertical −
1	0.833	1.985	1.963	1.022	1.000
2	0.937	2.935	3.150	2.520	2.260
3	0.985	3.230	3.440	3.290	3.440
4	1.061	2.510	2.900	3.660	3.900
5	1.154	1.640	1.950	2.620	3.590
6	1.269	1.300	1.360	1.875	3.530
7	1.350	1.080	1.260	2.385	1.872
8	1.412	0.983	1.130	2.385	1.860
9	1.649	0.770	0.650	1.910	1.730
10	1.717	0.770	0.840	2.362	1.950
11 *	2.425	0.193	0.400	1.910	1.450
12 *	2.780	1.987	1.120	1.255	1.090
Center line Depth (13-23) 0.720 ft.					
13	0.707	2.110	2.481	1.135	1.890
14	0.810	2.190	2.700	1.180	1.485
15	0.850	2.620	3.160	1.362	1.710
16	0.916	3.160	3.540	2.360	2.870
17	0.980	3.610	3.900	4.780	6.000
18	1.172	1.225	1.315	2.590	3.260
19	1.304	0.687	1.160	2.330	2.910
20	1.460	0.623	0.662	2.180	2.740
21	2.100	0.582	0.598	1.500	1.890
22 *	2.500	0.194	0.199	6.270	1.942
23 *	3.000	0.097	0.099	10.360	1.942
Center line Depth (24-35) 1.352 ft.					
24	0.548	1.438	2.025	2.000	3.900
25	0.611	1.420	1.675	2.550	4.670
26	0.634	1.420	1.768	2.550	4.000
27	0.675	1.420	1.850	2.550	3.120
28	0.720	1.700	1.950	1.820	2.225
29	0.784	1.700	2.150	2.505	3.060
30	0.859	2.060	2.435	3.460	3.230
31	0.893	2.180	2.700	5.100	4.670
32 **	1.032	4.190	7.690	27.300	17.900
33 **	1.057	5.000	7.180	25.500	15.570
34 *	1.440	1.020	2.020	16.420	7.500
35 *	1.640	3.190	3.740	16.420	6.290

* Slacking in mooring line

** Test Object Struck Botton of Wave Tank on Forward Swing

APPENDIX C - TEST RESULTS

Run	f/f_n	Multiplication Factor Horizontal +	Horizontal −	Vertical +	Vertical −
Centerline Depth (1-12) 0.291 ft.					
1	0.833	1.985	1.963	1.022	1.000
2	0.937	2.335	3.150	2.520	2.260
3	0.995	3.230	3.440	3.290	3.440
4	1.061	2.510	2.900	3.660	3.900
5	1.154	1.640	1.950	2.620	3.590
6	1.269	1.300	1.360	1.875	3.530
7	1.350	1.080	1.260	2.385	1.872
8	1.412	0.983	1.130	2.385	1.860
9	1.649	0.770	0.650	1.910	1.730
10	1.717	0.770	0.840	2.362	1.950
11 *	2.425	0.193	0.400	1.910	1.450
12 *	2.730	1.987	1.120	1.255	1.090
Center line Depth (13-23) 0.720 ft.					
13	0.707	2.113	2.481	1.135	1.390
14	0.810	2.190	2.730	1.180	1.435
15	0.850	2.620	3.160	1.362	1.710
16	0.916	3.160	3.540	2.360	2.870
17	0.980	3.610	3.990	4.780	6.000
18	1.172	1.225	1.315	2.590	3.260
19	1.304	0.587	1.160	2.330	2.910
20	1.460	0.623	0.662	2.180	2.740
21	2.100	0.582	0.598	1.500	1.890
22 *	2.500	0.194	0.199	6.270	1.942
23 *	3.000	0.097	0.099	10.360	1.942
Center line Depth (24-35) 1.352 ft.					
24	0.548	1.438	2.025	2.000	3.900
25	0.611	1.490	1.675	2.550	4.670
26	0.634	1.420	1.768	2.550	4.000
27	0.675	1.420	1.850	2.550	3.120
28	0.720	1.700	1.950	1.820	2.225
29	0.784	1.700	2.150	2.505	3.060
30	0.859	2.060	2.435	3.460	3.230
31	0.893	2.120	2.700	5.100	4.670
32 **	1.032	4.150	7.690	27.300	17.900
33 **	1.057	5.000	7.130	25.500	15.570
34 *	1.440	1.020	2.020	16.420	7.500
35 *	1.640	3.150	3.740	16.420	6.290

* Slacking in Mooring Line

** Test Object Struck Bottom of Wave Tank on Forward Swing